Exploration of Graded Indium Gallium Nitride Heterojunction Solar Cells for Laterally Integrated, Spectrally-Split Solar Cell Arrays

A THESIS
SUBMITTED TO THE FACULTY OF THE GRADUATE SCHOOL
OF THE UNIVERSITY OF MINNESOTA
BY

Jennifer Jo Krohn

IN PARTIAL FULFILLMENT OF THE REQUIREMENTS
FOR THE DEGREE OF
MASTER OF SCIENCE

Paul Ruden, Advisor

December 2011

© Jennifer Jo Krohn 2011

Acknowledgements

Thank you Professor Ruden for providing me with this exciting opportunity to grow academically and to further develop a research oriented and scientifically innovative mind. I am grateful for your guidance, encouragement, and patience while I learned to lead myself on this research project.

Many academic teachers impacted my education and life in some way. Specifically, thank you to Dr. Gu, Dr. Pfieffer, Professor Campbell, and Professor Stadler. Also, thank you Professor Cohen and Professor Frisbie for your participation on my academic committee. A very early teacher influenced my excitement for learning; thank you Ms. Reynolds for your great mentorship at such an early stage in my life.

I am thankful to nature for providing a beautiful world in which to strive to understand better and for providing me with those I love. To my loving family whose strength and love is unparalleled, thank you. Thank you Grandma Helen Johnson for being an ever present positive influence in my life. Thank you Emmett for always supporting and loving my family. Thank you Steve for all your help, encouragement, and love. Thank you Mom Pamela Jo Krohn for your unconditional love, encouragement, support, and for making math fun – teaching me algebra at five with chocolate chips. I love you so much.

Most importantly, thank you Dad Howard Emil Krohn, for providing me the footsteps to follow as best I can. Thank you for your tenacity in teaching me, your guidance, and your incredible strength. You taught me to "Work hard and play hard," showed me what winning was all about, and how to live passionately. I can still remember the conversation on electricity that instigated my desire to pursue electrical engineering. You knew such a change would be hard work, but you believed in my abilities and knew I would succeed. I know your biggest wish for me was to always be happy and you showed me, through your life, how to achieve this. I could write an endless list of all the ways you inspire me.

For my entire family, my gratitude and love are endless and I will always carry a full heart because of you.

Dedication

I dedicate this thesis in honor and loving memory of my hero, Dr. Howard Emil Krohn whose heart and passion for nature, math, and life in general will always comfort, strengthen, and guide me. This is for you.

Abstract

The ternary group III/group V direct bandgap semiconductor alloy system of indium gallium nitride is emerging as a material with great potential for the production of highly efficient, low cost terrestrial photovoltaic devices. Indium gallium nitride alloy is a direct bandgap semiconductor with an energy gap in the range of $0.7\,eV$ to $3.4\,eV$ depending on the alloy composition. Here we explore a unique photovoltaic device design based on indium gallium nitride single-junction *pin* graded heterojunction cells arranged laterally and illuminated by a spectrally-split solar spectrum. Mathematical models for photon absorption, charge carrier generation, total charge carrier concentrations, and charge carrier flow are derived and suitable software tools are developed, implementing these equations as well as power density and efficiency calculations to simulate the photovoltaic device operation under maximum power point conditions. Efficiencies of the individual cells in the array differ significantly with the largest bandgap *pin* producing the highest fill factor and energy conversion efficiency. The small bandgap $n-doped$ layer contributes the largest amount of photogenerated electron-hole pairs, and increasing the width of this layer leads to significantly larger efficiencies. Overall, the photovoltaic device yields efficiencies competitive with existing technologies. Modifications to the design can be incorporated into the software to explore additional methods of increasing efficiencies.

Table of Contents

List of Tables vi
List of Figures vii
1. Introduction 1
1.1 Motivation 1
1.1.1 Demand for Alternative Energy Sources 1
1.1.2 Solar Energy As a Renewable 2
1.1.3 A Brief Historical Account of PV Techonology 3
1.1.4 PV Efficiencies 4
1.1.5 Group III Nitrides 5
1.1.6 Indium Gallium Nitride 5
1.2 System 7
1.3 Thesis Overview 13
2. Absorption and Generation 16
2.1 Introduction 16
2.2 Absorption 16
2.3 Generation 18
2.4 Conclusions 22
3. Electrostatics and Minority Carrier Profiles 23
3.1 Introduction 23
3.2 Electrostatics 23
3.2.1 Poisson's Equation and Charge Density 23
3.2.2 Electric Field 24
3.2.3 Electric Potential 25
3.2.4 Electrostatic Built-in Voltage 26
3.2.5 Depletion Region Widths 32
3.3 Excess Minority Carrier Profiles 32
3.3.1 Derivations 32
3.3.2 Results 38
3.4 Conclusions 41
4. Current Density 43
4.1 Introduction 43
4.2 Minority Carrier Diffusion Current Densities 45
4.3 Depleted and Intrinsic Region Photogeneration Current Density 46
4.4 Recombination Current Density 46
4.5 Results 48
4.5.1 Dark Current Density 48
4.5.2 Photocurrent Density 51
4.5.3 Effect of $n-In_{y_{\max}}Ga_{1-y_{\max}}N$ Layer Thickness on Photocurrent Density 54
4.6 Conclusions 57
5. Power Density and Performance Efficiency 59
5.1 Introduction 59
5.2 Power Density 59

5.3 Fill Factor 61
5.4 Energy Conversion Efficiency 62
5.5 Effect of $n-In_{y_{max}}Ga_{1-y_{max}}N$ Layer Thickness on Power Density and Performance Efficiency 64
5.5.1 Power Density 64
5.5.2 Fill Factor 66
5.5.3 Energy Conversion Efficiency 67
5.6 Conclusions 68
6. Future Work 70
6.1 Introduction 70
6.2 Parameter Adjustments 70
6.3 Parabolic Grading 71
6.4 Conclusion 72
Bibliography 73
A Photon Source 78
B Tridiagonal Matrix Algorithm 80
C Parasitic Resistance Effects 83
C.1 Overview 83
C.2 Equivalent Circuit Model and Parameters 84
C.2.1 Current Density 84
C.2.2 Slope 85
C.2.3 Open Circuit Voltage 85
C.2.4 Short Circuit Current Density 86
C.3 Results 86
C.3.1 Current Density 86
C.2.5 Power Density 88
C.2.6 Fill Factor 90
C.4 Conclusions 91
D Software Development 92
D.1 Overview 92
D.2 Source Code 92

List of Tables

Table 2.1 Total electron-hole pair generation of the *pin*, flux to generation ratios, and the total electron-hole pair generation of the individual layers. 21
Table 3.1 *InN* and *GaN* electron and hole effective masses and effective densities of states.. 27
Table 3.2 In_yN material dependent variables for compositions 0, 39.2, 62.4, and 100 %. 31
Table 3.3 Equilibrium depletion region widths.. 32
Table 3.4 Minority carrier concentrations under maximum power point operating conditions.. 38
Table 4.1 Open-circuit voltage and short-circuit current density for varying................. 56
Table 5.1 Maximum power point voltage, current, and power...................................... 61
Table 5.2 Overall and individual energy conversion efficiencies.................................. 63
Table 5.3 Maximum power point power, voltage, and current, for varying layer $n-In_{y_{max}}Ga_{1-y_{max}}N$ layer thickness (a) *Cell A* (b) *Cell B* (c) *Cell C* 66
Table 5.4 Fill factor for varying $n-In_{y_{max}}Ga_{1-y_{max}}N$ layer thickness............................... 67
Table 5.5 Energy conversion efficiency for varying $n-In_{y_{max}}Ga_{1-y_{max}}N$ layer thickness (a) *Cell A* (b) *Cell B* (c) *Cell C* and (d) overall.. 68

List of Figures

Figure 1.1 Global carbon emission from fossil fuels increases steadily with respect to time. (Carbon only accounts for 27% of the mass of carbon dioxide.) Figure originates from Carbon Dioxide Information Analysis Center. 2
Figure 1.2 Best research-cell efficiencies. Image originates from the National Renewable Energy Laboratory. 4
Figure 1.3 Indium gallium nitride alloys can absorb photons from the near infrared to deep ultraviolet........ 6
Figure 1.4 Structural design showing doping concentration and composition each as a function of position in the PV cell. 9
Figure 1.5 Laterally arranged three-cell solar cell arrays employing holographic diffracting and concentrating optics to spectrally split the light source and focus it on the cells with bandgaps optimized for the incident energy segment. 10
Figure 1.6 Each energy segment is focused on the cell of appropriate bandgap. 11
Figure 1.7 Energy-band diagram for the graded heterojunction solar cell under forward bias. 12
Figure 2.1 Absorption coefficient as a function of photon energy for alloys with indium compositions of 39.2, 62.4, 100%........ 18
Figure 2.2 Electron-hole pair generation rates for cell designs *A*, *B*, and *C*. 20
Figure 3.1 Energy-band diagrams of two isolated materials with straddling bandgap alignment; a wide bandgap *p-doped* material and a narrow bandgap *n-doped* material. The *p-doped* material has a smaller electron affinity, χ_p, than that of the *n-doped* material. In our system, the wide bandgap material is *GaN* and the narrow bandgap material is an $In_y Ga_{1-y}N$ alloy. 28
Figure 3.2 Dark excess minority carrier concentrations (a) electrons and (b) holes. 39
Figure 3.3 Excess minority carrier concentrations for the cells under illumination (a) electrons and (b) holes. 40
Figure 4.1 Carrier action in the *pin* PV cell. 43
Figure 4.2 Total dark current density. 48
Figure 4.3 Total dark current density and recombination current density (a) *Cell A* (b) *Cell B* and (c) *Cell C*. 50
Figure 4.4 Total photocurrent density. 52
Figure 4.5 Total photocurrent density and photocurrent density contributions for (a) *Cell A* (b) *Cell B* and (c) *Cell C*. 53
Figure 5.1 Power density as a function of applied cell voltage. 60
Figure 5.2 Example of maximum power point power, voltage and current density. 60
Figure 5.3 Fill factor is the ratio of the product of $J_m V_m$ to $J_{SC} V_{OC}$. 62
Figure 5.4 $n - In_{y_{max}} Ga_{1-y_{max}} N$ layer thickness effect on power density (a) *Cell A* (b) *Cell B* and (c) *Cell C*. 65
Figure 6.1 Parabolic grading of the $i\text{-}In_y Ga_{1-y} N$ layer shown with presently implemented linear grading scheme. 71

Figure A.1 The normalized 5200 K black body spectrum compared with the terrestrial AM1.5 solar spectrum.......... 78
Figure C.1 Circuit schematics for the ideal and non-ideal solar cell (a) A current source in parallel with a diode models the ideal solar cell. (b) The addition of parallel and series resistances to the circuit schematic models the non-ideal solar cell. J_p represents the current across the parallel resistance.......... 83
Figure C.2 Effects of parasitic resistances on total photocurrent density. (a) The smallest bandgap cell shows greatest sensitivity to series resistance. Relatively small value of series resistance will reduce the current density while leaving the short-circuit current density unchanged. (b) The cell with the highest resistance, or the GaN-rich cell, shows greatest sensitivity to junction leakage. Parallel resistance reduces the current density of the solar cell.......... 87
Figure C.3 Effects of parasitic resistances on power density. (a) Power-voltage characteristics, showing series resistance effects, for a *pin* design with a $p-GaN$ layer, graded intrinsic layer, and $n-InN$ layer. (b) Power-voltage characteristics, showing parallel resistance effects for a *pin* design with a $p-GaN$ layer, graded intrinsic layer, and $n-In_{0.624}Ga_{0.376}N$ layer.......... 89
Figure C.4 Effects of parasitic resistances on fill factor (a) Fill factor as a function of series resistance for a *pin* design with a $p-GaN$ layer, graded intrinsic layer, and $n-InN$ layer. (b) Fill factor as a function of parallel resistance for a *pin* design with a $p-GaN$, graded intrinsic layer, and $n-In_{0.624}Ga_{0.376}N$ layer.......... 90

1. Introduction

1.1 Motivation

1.1.1 Demand for Alternative Energy Sources

Solar energy has always been a principal energy source of mankind. We have used energy from the sun to facilitate basic survival and to enhance our lives. However, while the Earth's atmosphere, oceans, and land masses absorb 120,000 terawatts (TW) of solar energy,[1] we have been slow to evolve in our ingenuity of effectively capturing this abundant and clean resource. For most of history, only a small portion of the available energy has been actually captured and used effectively. Fossil fuels dominate our quests for electricity and have replaced preceding energy sources of wood and biomass while overshadowing solar energy and other renewables. The supply of fossil fuels has been sufficient to meet the needs of the human population, but the population today is expected to grow to over nine billion by 2050[2-5] with contributions almost completely from developing countries.[4,5] This leads to an energy demand expected to reach 30 TW that year which is more than twice the current energy demand of about 13 TW.[1] Fossil fuels will not be able to persevere indefinitely to meet demands. Further, rising energy consumption leads to rising carbon emissions, as Figure 1.1 indicates by showing metric tons of carbon in the atmosphere as a function of time.

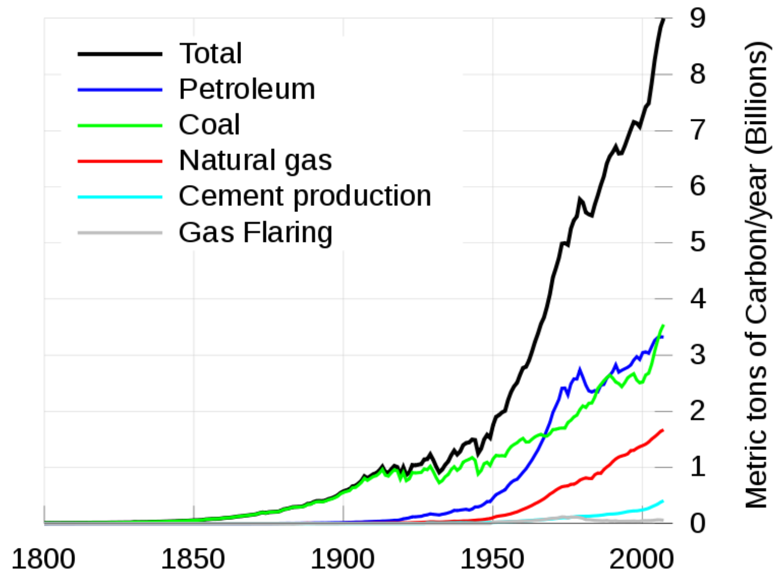

Figure 1.1 Global carbon emission from fossil fuels increases steadily with respect to time. (Carbon only accounts for 27% of the mass of carbon dioxide.) Figure originates from Carbon Dioxide Information Analysis Center (Ref. 6).

Natural processes can absorb only about 6.1 billion metric tons of the anthropogenic carbon dioxide produced annually. About 3.2 billion tons remain and completely contributes to atmospheric pollution.[7] The recent escalating environmental concern along with the rising world population greatly magnifies desires to bring to the foreground alternatives, primarily renewable energy sources such as solar energy.

1.1.2 Solar Energy As a Renewable

In 2005 solar energy only contributed about 10^{-6} of the total world electricity supply[1], but currently its market and production are quickly growing and solar capacity more than doubled from 2009 to 2010. In 2010, more than 100 countries acquired solar capacity and 17 GW was added globally; in 2009 only 7.3 GW was added.[8] Renewables make up 7 % of the total global energy consumption[9] and while new renewables such as solar energy (and others such as wind power, geothermal energy, and ocean energy) account for only 2.8 % of the total global energy consumption and biomass (at 10%) and hydropower (at 3.4%) account for the majority, solar technology is the world's fastest

growing power-generation technology.[8] Capturing sunlight effectively and converting it into electricity is especially desirable because it is an abundant, basically limitless, and naturally clean alternative to fossil fuels. Such is the abundance of solar energy that the amount provided to the Earth in one hour is more than the total energy used in an entire year![10,11]

1.1.3 A Brief Historical Account of PV Techonology

Photovoltaic (PV) devices, or solar cells, are engineered to take advantage of the photovoltaic effect which explains the absorption and conversion of photons into usable electrical energy. The PV effect was first observed in 1839 by A.E. Becquerel[12] and subsequently Charles Fritts created the first PV cell in 1883 producing an efficiency of only 1%.[13] Eventually, in 1954, Bell Laboratories developed the first modern PV cell using a diffused silicon *pn* junction.[14] Today, laboratory crystalline silicon single-junction cells are reaching efficiencies of 25%[15], approaching the Shockley and Queisser theoretical limit of 30%.[16] These efficiencies apply to small, expensive, and sophisticated designs appropriate for small scale laboratory production. Larger and less expensive commercial modules yield lower efficiencies between 15-20%.[15, 17]

Early development of high efficiency solar cells was aimed primarily at space applications because high production costs were basically irrelevant. Eventually, instigated by the late 1960's discovery of the role of 'reject' silicon in cost reduction by Elliot Berman of Solar Power Corporation, fabrication of PV devices began to drop in price. In 2010, large commercial arrays cost about $3.40 /Watt, down from $8/Watt in 2004.[18] While silicon dominates the industry, production costs are still more expensive than desirable. Other technologies, as shown in Figure 1.2, may have potential of yielding higher efficiencies and lowering costs.

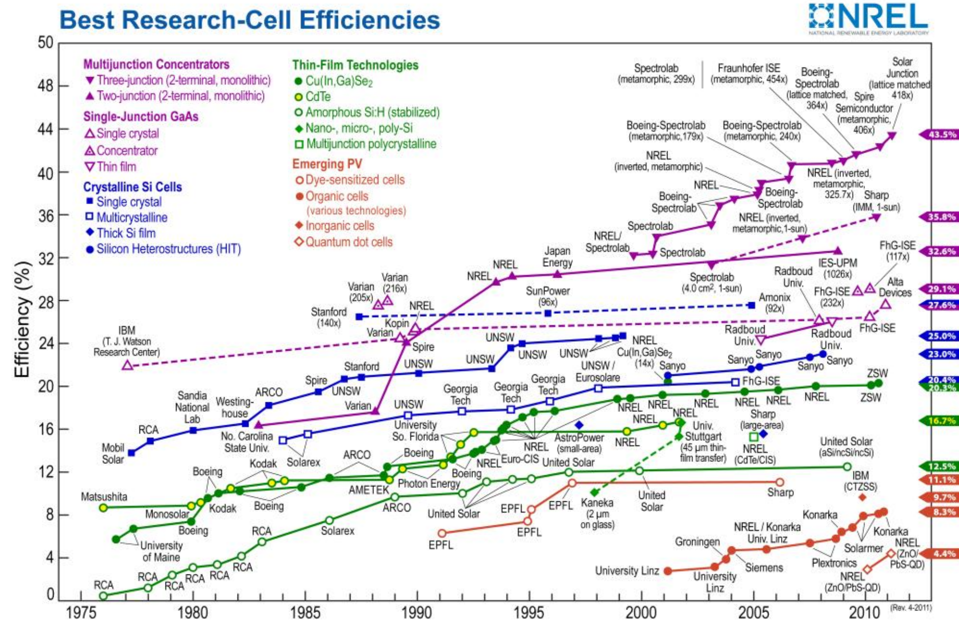

Figure 1.2 Best research-cell efficiencies. Image originates from the National Renewable Energy Laboratory.[19]

1.1.4 PV Efficiencies

Currently, the maximum solar energy conversion efficiency obtainable is about 43% and is achieved with the triple-junction of Ge, $GaAs$, and $GaInP$ [20], having bandgaps of 0.7, 1.4, and 1.9 eV, respectively.[21] To increase this efficiency by about 50% of its value, it would be necessary to have four or more junctions. Theoretically, an ideal four-junction solar cell can reach an efficiency of 62% with tandem junctions and bandgaps of 0.6, 1.11, 1.69, and 2.48 eV.[22] However, when increasing the number of junctions, it becomes difficult to find materials with the desired bandgaps. Fortunately, Group III nitride alloys introduce great optimization potential.

1.1.5 Group III Nitrides

Group III nitrides and their alloys have achieved much attention as they are currently among the most important material systems for optoelectronic and electronic applications.[21] They are direct bandgap semiconductors which means electron-hole pairs are created more efficiently than in indirect bandgap semiconductors such as silicon in which incoming photons require lattice vibrations to assist the electron from the valence band to the conduction band resulting in waste of the photon energy. Also, a PV fabricated from direct bandgap semiconductors can be made thinner than one made of indirect semiconductors because less material is necessary to ensure adequate absorption. As single-junction pn cells, the Group III nitrides alone are not greatly effective. The large bandgaps of 3.4 eV [20,23-26] and 6.2 eV [27,28], for gallium nitride and aluminum nitride, respectively, prevent most photon absorption. Indium nitride has the ability to absorb most of the photons from the solar spectrum, but most of the energy is wasted as heat. In addition, it remains very challenging to dope indium nitride $p-type$.[29,31] Thus, we turn to ternary alloys. When considering these alloys, employing aluminum is less desirable than gallium nitride because more of the solar spectrum is wasted on the former. In the optimistic vision of reaching large efficiencies of over 50%[32], indium gallium nitride ($InGaN$) alloys provide greatest potential of the Group III nitrides.

1.1.6 Indium Gallium Nitride

Interest in $InGaN$ PV devices has recently increased extensively due to the discovery that the bandgap of wurtzite InN is 0.7 eV [22,33-36] instead of about 1.9 eV [37-39] as previously concluded. As a result, $InGaN$ alloys introduce the ability to fabricate solar cells which can effectively utilize the entire solar spectrum, ranging from the near infrared to the deep ultraviolet as shown in Figure 1.3. That is, the bandgap of $InGaN$ can be graded to match most of the solar spectrum.

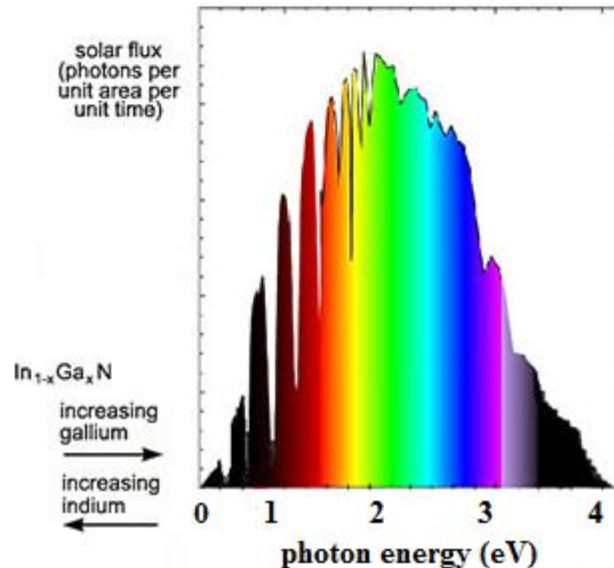

Figure 1.3 Indium gallium nitride alloys can absorb photons from the near infrared to deep ultraviolet.

Grading has been previously considered such as for alloys of *AlGaAs* and *CuInGaSe*.[40-42] Further, it has been shown that grading of materials such as *GaInAsP*, *AlGaAsSb*, and $a-SiGe$ leads to larger PV device efficiencies.[43] However, these material systems are limited in the range of the solar spectrum they can match. With *InGaN* grading can almost completely match the entire solar spectrum.

Due to the flexibility in the bandgap grading, efficiencies of *InGaN* PV devices have the potential of being very large. For example, in one theoretical study, it has been found that a six-junction *InGaN* design can yield an efficiency of 40.3%.[44] Although it has been shown[45] that the maximum theoretical efficiency of a double-junction solar cell with bandgaps of about 1.1 and 1.75 *eV* approaches 39%. Thus, fewer junctions may be sufficient to reach the same efficiency values. Double-junction *InGaN*/*Si* cells have been shown to have larger efficiencies than single-junction silicon cells, with efficiencies as high as 31%.[31] Adding the *InGaN* layer onto an otherwise single-junction silicon cell, can increase the efficiency by 50% of its value.[43] While incorporating discrete layers

of *InGaN* into multi-junction PV devices shows much promise, grading the *InGaN* may prove a better alternative as the number of junctions could be reduced and lattice matching would not be a factor. Studies regarding fabrication of epitaxial thin films of *InGaN* effectively graded across the entire composition range have also shown success with the films having good crystalline quality and electrical and optical properties while grown at low temperatures (450 deg C).[47] Such films have been fabricated with a process known as Energetic Neutral Atom Beam Lithography and Epitaxy (ENABLE). Incorporating graded layers of *InGaN* into devices allows the production of efficient indium rich cells.[31] To further increase efficiencies, it has been considered to split the solar spectrum into segments and focus each segment onto PV cells optimized for these energy segments.[30,48] The cells are single-junction and laid out laterally instead of stacked in tandem as multi-junction devices.

Indium gallium nitride alloys have other favorable characteristics beneficial for PV applications. They can be grown on substrates such as silicon[49,31] or sapphire[50],which although expensive is transparent. Also, they have tremendous heat capacity, extreme resistance to radiation,[20,23] and high mobilities.[30] Further, the cost could be very low[51] and *InGaN* solar cells have potential for higher efficiencies than single-junction silicon cells because *InGaN* is a direct bandgap semiconductor with the ability to almost completely cover the entire *solar* spectrum. Due to its great potential in PV technologies, we choose to investigate an *InGaN* PV system. In addition, we will apply a split-spectrum technique which will use the solar spectrum more efficiently than most existing designs.

1.2 System

We explore a potentially inexpensive laterally integrated PV system with solar cells optimized for spectral splitting through implementation of holographic concentration optics.[a] Split-spectrum PV devices have been considered in the past for space applications,[52] but little work has been done in considering these devices for

[a] A detailed discussion on holographic concentration optics is beyond the scope of this work.

terrestrial applications. The design considered in this system is a pin graded heterojunction with a gallium nitride (GaN) $p-doped$ layer, or the $p-GaN$ layer, an intrinsic linearly graded indium gallium nitride layer, or the $i-In_yGa_{1-y}N$ layer, and an $n-doped$ $In_{y_{max}}Ga_{1-y_{max}}N$ layer, or the $n-In_{y_{max}}Ga_{1-y_{max}}N$ layer. We may also refer to these regions in the more general sense with the terms $p-region$, $i-region$, and $n-region$. The variable y is the composition fraction of indium nitride (InN) and in the $i-In_yGa_{1-y}N$ layer depends on the position, x, by

$$y = \left(\frac{y_{max}}{(x_n - x_p)} \right)(x - x_p) \tag{1.1}$$

where x_p represents the position at the $p-GaN/i-In_yGa_{1-y}N$ junction and x_n represents that at the $i-In_yGa_{1-y}N/n-In_{y_{max}}Ga_{1-y_{max}}N$ junction. At x_n, the InN composition is equal to y_{max}. The system is simplified such that the cells are considered one-dimensional (1D) with dependence on x as shown in Figure 1.4. This figure also includes a depiction of the doping and indium nitride composition profiles.

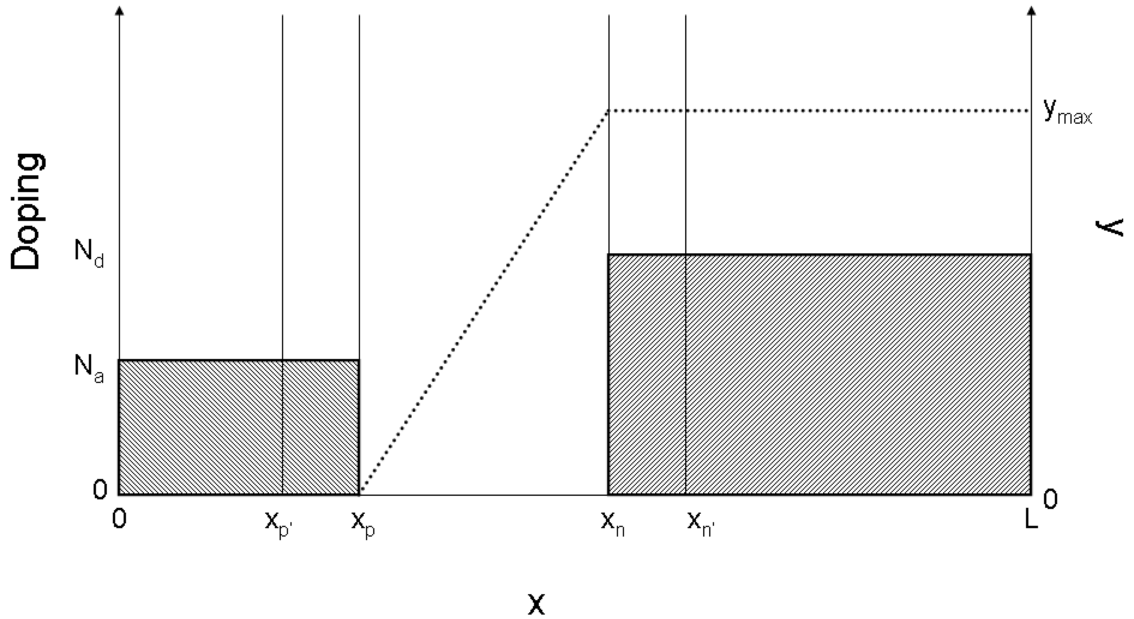

Figure 1.4 Structural design showing doping concentration and composition each as a function of position in the PV cell.

We have chosen the structural widths to be $x_p = 0.15\mu m$ for the $p-GaN$ layer, $x_i = (x_n - x_p) = 0.10\mu m$ for the $i-In_yGa_{1-y}N$ layer, $(L-x_n) = 0.82\mu m$ for the $n-In_{y_{max}}Ga_{1-y_{max}}N$ layer, and the total length of the diode is given by L. The $n-In_{y_{max}}Ga_{1-y_{max}}N$ layer is designed as the thickest since the bandgap is smallest thus, as we will see in Chapter 2, most of the electron-hole pair generation occurs there. The quasineutral regions are given by $x_{p'}$ and $L-x_{n'}$ and the depleted region widths are given by $\Delta x_p = x_p - x_{p'}$ and $\Delta x_n = x_{n'} - x_n$. The $p-GaN$ layer is doped with an acceptor concentration of $N_a = 10^{17} cm^{-3}$ and the $n-In_{y_{max}}Ga_{1-y_{max}}N$ layer is doped such that the donor concentration is $N_d = 4x10^{18} cm^{-3}$.

Unlike a tandem cell design, which can include multiple junctions, here single-junction cells are layed out laterally. This lateral arrangement is made of three cell arrays

in which the $n-In_{y_{max}}Ga_{1-y_{max}}N$ layer is unique in y_{max} for each cell. Figure 1.5 illustrates the lateral arrangement of the three-cell arrays along with the spectral-splitting of the solar spectrum.

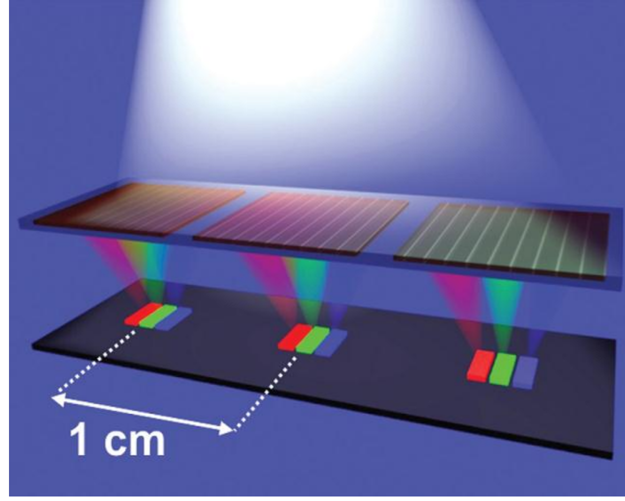

Figure 1.5 Laterally arranged three-cell solar cell arrays employing holographic diffracting and concentrating optics to spectrally split the light source and focus it on the cells with bandgaps optimized for the incident energy segment.

Based on efficiency calculations, when considering a source concentration of 100 suns, it is found that the array of $y_{max} = 1$, 0.624, and 0.392 for three cells generates the highest efficiencies.[52] These indium compositions correspond to bandgaps of 0.7, 1.38, and 2.0 eV where the bandgap depends on y by the standard equation

$$E_g(y) = E_{g_{GaN}} + y(E_{g_{InN}} - E_{g_{GaN}}) - by(1-y) \tag{1.2}$$

The parameters $E_{g_{GaN}}$ and $E_{g_{InN}}$ represent the bandgap for GaN and InN, respectively, and are set as 3.4 eV and 0.7 eV for this system. Throughout this thesis, we may also refer to $E_{g_{GaN}}$ as $E_g(GaN)$ and the bandgap of the $n-In_{y_{max}}Ga_{1-y_{max}}N$ layer as

$E_g(In_{y_{max}}Ga_{1-y_{max}}N)$. The parameter b is the bowing parameter and is set to a reasonable value of 1.43 eV.[21,53-55]

As mentioned, the solar cell arrays are situated under holographic optical films that work as diffractive and concentrating elements by splitting the light spectrum into segments and directing these appropriately onto the surface, that is, the $p-GaN$ layer, of the cells. This design is shown in more detail for one of the three-cell arrays in Figure 1.6.

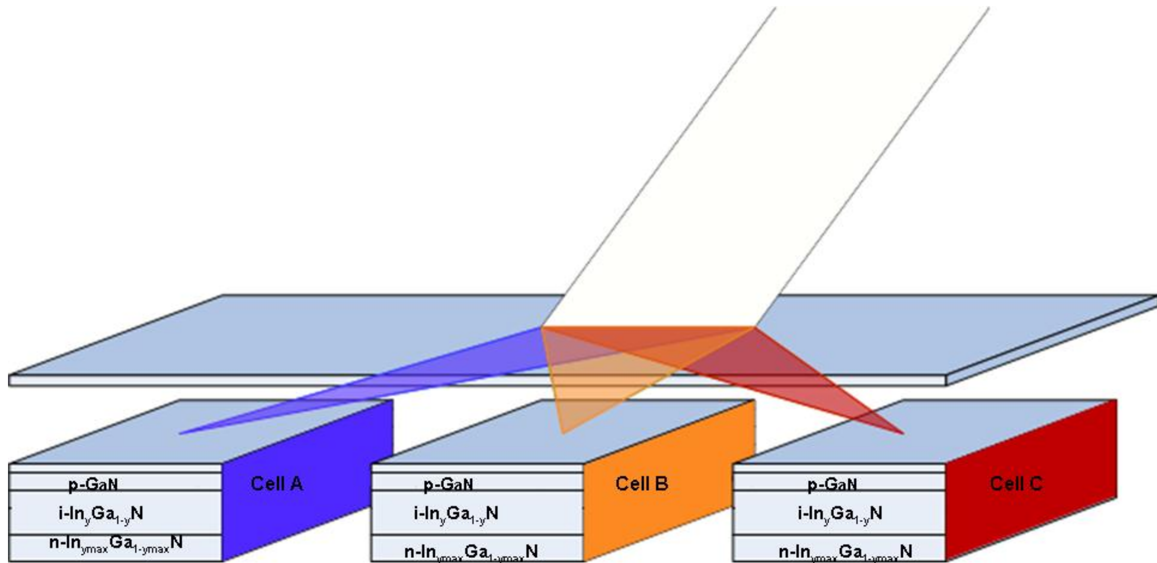

Figure 1.6 Each energy segment is focused on the cell of appropriate bandgap.

The cells are fabricated to have bandgaps allowing for optimal utilization of the partitioned range of photon energies. In this system, the photon energy interval limits are the bandgap energy of the specific cell and the bandgap of the cell with the next largest bandgap, or in the case of the highest bandgap cell, some reasonable maximum energy. In this thesis, we will commonly refer to the individual cells in the array therefore to simplify we let $Cell\ A$, $Cell\ B$, and $Cell\ C$ respectively represent the cells with $y_{max} = 1$, 0.624, and 0.392.

Solar cells perform most efficiently under maximum power point operating conditions thus, when generating current density and power density, we will operate the cells at this point. This is where the power delivered to the load reaches a maximum value, P_m, with corresponding current J_m and voltage V_m. The energy-band diagram for the *pin* graded heterojunction under a forward bias of V_A is shown in Figure 1.7.

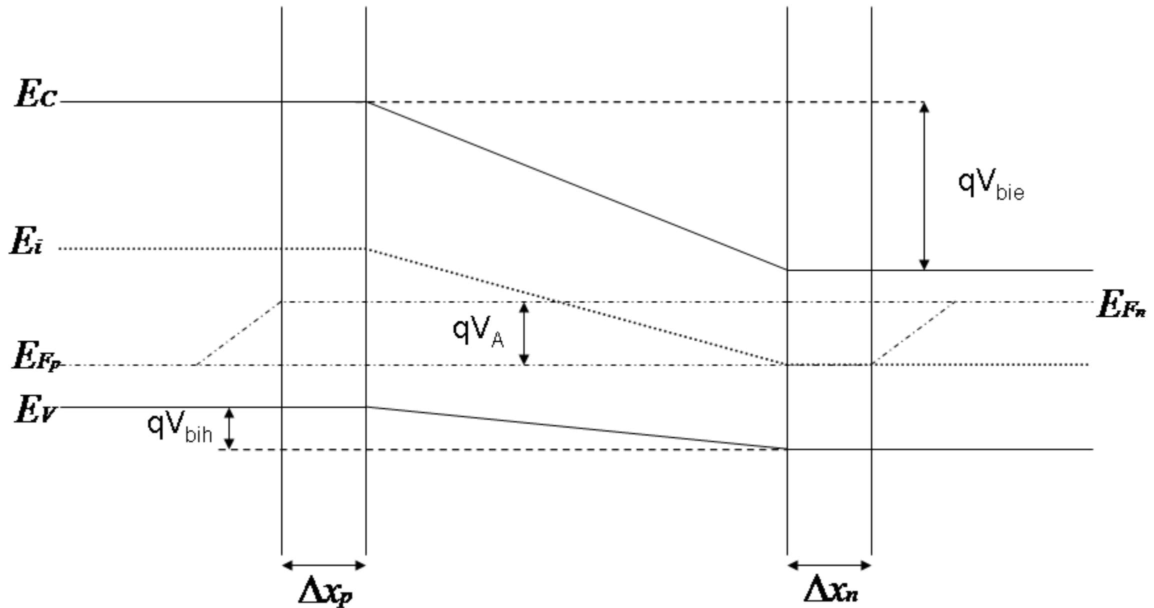

Figure 1.7 Energy-band diagram for the graded heterojunction solar cell under forward bias.

Built-in potential for the electrons and holes is V_{bie} and V_{bih}, respectively and E_C, E_i, E_V, E_{F_p}, and E_{F_n} represent the conduction band, intrinsic level, valence band, and the quasi Fermi levels for the holes and electrons, respectively. The depletion region widths are also shown. Since we will assume relatively low recombination of minority carriers throughout the intrinsic and depleted regions, the Fermi levels are shown to remain constant throughout these regions.

The photon source used to illuminate the cells emulates as closely as possible the AM1.5 solar spectrum. A normalized 5200 K black body spectrum models this

electromagnetic radiation. Appendix A addresses in more detail the photon source and the AM1.5 spectrum. Throughout this thesis, the photon source may also be referred to as the light source.

In addition to approximating the solar spectrum with a black body, we make other approximations and idealizing assumptions in order to simplify the model. Many of these are introduced throughout the body of the thesis. Additionally, we assume no surface reflection of photons occurs and the contacts to the cells are ohmic.

1.3 Thesis Overview

In Chapter 2, we discuss the absorption and generation of carriers in the cells. The absorption model is introduced and results are shown for $In_yGa_{1-y}N$ alloys having indium compositions of 39.2, 62.4, 100 % which are equivalent to the indium compositions in the $n-In_{y_{\max}}Ga_{1-y_{\max}}N$ layer of the three cells in this system. Subsequently, we derive the generation rate, which is dependent on the absorption coefficient and photon flux. Total electron-hole pair generation is found for the cells.

Electrostatics and minority carrier profiles are covered in Chapter 3. In the electrostatics section we derive the electric field, electric potential, electrostatic built-in potentials, and the depletion region widths by beginning with Poisson's equation and charge density. The electrostatics for a pin graded heterojunction differ from those of the pn homojunction covered in introductory semiconductor device textbooks. In deriving the electrostatic built-in potential, it is necessary to consider the effective masses of the electrons and holes and we show that it is reasonable to simplify the system by assuming the masses constant throughout the diode. In the second part of the chapter, we discuss the excess minority carrier profiles and begin by deriving the minority carrier diffusion equations from the equations describing the overall minority carrier action and the assumptions specific to our system. Boundary conditions are discussed and we acquire the excess minority carrier concentrations by implementing a tridiagonal matrix algorithm to solve the minority carrier diffusion equations. Finally, we obtain the excess

minority carrier electron and hole concentrations for the cells under dark and light conditions. Dark conditions imply the cells are not subject to the photon source whereas light conditions mean the cells are illuminated.

In Chapter 4 we examine the current densities, that is the minority carrier diffusion, carrier generation and the recombination-generation action in the depleted regions and intrinsic region. Minority carrier diffusion current density utilizes the excess minority carrier concentrations collected in Chapter 3, thus we use Fick's first law to model this carrier action. Carrier generation current in the depleted regions and intrinsic region is accounted for by finding the total carrier generation occurring in these regions and scaling by the electric charge. Recombination-generation in this region is modeled by the Shockley Read Hall equation. Results for the cells are shown graphically. First, the situation in which no photon source is present is considered. We compare the total dark current for all three cells, then the individual contributions for each of the cells independently. Current densities for all three cells under illumination are then compared. The total photocurrent densities are shown for each of the three cells, then the individual components are shown for each cell independently. Finally, we explore the influence of the $n-In_yGa_{1-y}N$ layer thickness on the total current density for the three cells under illumination.

Presented in Chapter 5, power density results and performance efficiencies provide insight as to the ability of the solar cell to effectively convert solar energy. The power density is determined when the cell is illuminated and is obtained by using the results obtained in Chapter 4. Power density is compared for the three cells and the maximum power point is determined for each cell. Operation at the voltage corresponding to the maximum power will yield the highest efficiencies. Two figures of merit, the fill factor and energy conversion efficiency, facilitate in the understanding of the solar cell performance.

Finally, Chapter 6 introduces further design considerations that can be addressed in future simulations and analysis. Currently, the PV cells in our system are fabricated such that the material in the intrinsic region is graded linearly. Considering other grading

profiles, such as a parabolic function, may lead to increased performance. Also, adjusting design parameters such as layer thicknesses, such as seen in Chapter 4 and Chapter 5, or doping concentrations may also raise efficiencies.

Three appendices are included at the end of the thesis. Appendix A discusses the model photon source in more detail and shows its fit to the AM1.5 solar spectrum. In Appendix B the tridiagonal matrix algorithm, which facilitates calculations performed in Chapter 3, is explained. Appendix C discusses the effects of parasitic resistances on the solar cell performance and is a brief summary of the work presented in the *E32010 (Energy, Economy, and Environment) the Upper Midwest's Premier Energy* conference. Finally, Appendix D outlines the software development and code utilized in implementation of the mathematical models and simulations.

2. Absorption and Generation

2.1 Introduction

Here, we discuss the absorption and generation of photons in the PV cells. We introduce the absorption coefficient model and show results for three *InGaN* alloy compositions. Subsequently, we derive the generation rate from the absorption and photon flux models. Finally, we graphically show the carrier generation results for the three cells.

2.2 Absorption

The absorption coefficient, α, quantifies how far into the material a photon of energy $\hbar\omega$ can travel before being absorbed. Absorption can occur only when $\hbar\omega$ exceeds the bandgap energy of the material. At photon energies near E_g, only electrons very close to the valence band edge can obtain enough energy to move to the conduction band therefore little absorption occurs. With increasing $\hbar\omega$, electrons deeper in the valence band can be excited into the conduction band, thus α increases.

In order to have an effective solar cell, it is desirable to have most of the absorption occur in the graded layer. Thus, knowledge of how the absorption coefficient varies with composition is important. We base our calculations on fits to experimental data of the absorption coefficient of $In_yGa_{1-y}N$ alloys with five different compositions ($0.5 \le y \le 1.0$)[50] and the absorption coefficient of GaN.[31] This experimental data is fit to the equation

$$\alpha = 10^5 \sqrt{a(\hbar\omega - E_g) + b(\hbar\omega - E_g)^2} \tag{2.1}$$

with a and b as indium nitride composition dependent fitting parameters and expressing the energies in eV and α in cm^{-1}. Assuming a linear relationship with y, we use linear interpolation to find that

$$a = \begin{cases} -6.0169y + 3.52417 & 0 \le y \le 0.5 \\ 1.32486y - 0.14571 & 0.5 < y \le 0.57 \\ -0.2365y + 0.744265 & 0.57 < y \le 0.69 \\ 0.620571y + 0.152886 & 0.69 < y \le 0.83 \\ 0.167412y + 0.529008 & 0.83 < y \le 1.0 \end{cases} \quad (2.2a)$$

$$b = \begin{cases} 2.2509y - 0.6571 & 0 \le y \le 0.5 \\ 2.19229y - 0.627785 & 0.5 < y \le 0.57 \\ 0.393333y + 0.39762 & 0.57 < y \le 0.69 \\ 0.141714y + 0.571237 & 0.69 < y \le 0.83 \\ -1.343y + 1.80355 & 0.83 < y \le 1.0 \end{cases} \quad (2.2b)$$

A plot of absorption as a function of photon energy for three $In_yGa_{1-y}N$ alloys is shown in Figure 2.1. For photons with $\hbar\omega < E_g$, absorption cannot occur, therefore $\alpha = 0$. In this model we assume at photon energies equivalent to the bandgap $\alpha = 0$. When photons of energy $\hbar\omega > E_g$ strike the material, absorption can occur, thus $\alpha > 0$. The absorption coefficient continues to increase with photon energy, however the cell can utilize only the energy equal to that of the bandgap and any excess energy may be lost as heat.

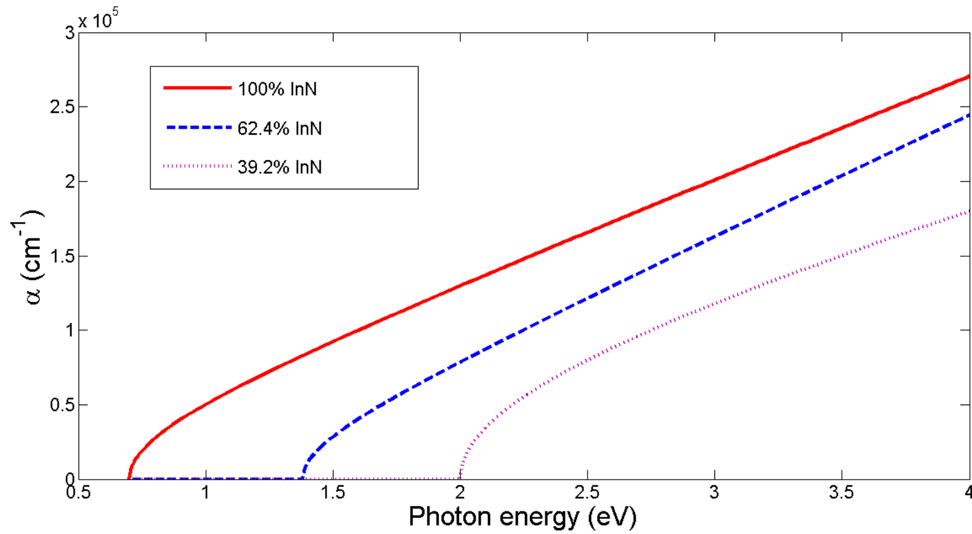

Figure 2.1 Absorption coefficient as a function of photon energy for alloys with indium compositions of 39.2, 62.4, 100%.

2.3 Generation

Assuming that each absorbed photon of energy greater than the bandgap energy creates one electron-hole pair, the product of the number of photons absorbed and the flux of the photons, ϕ, gives the general expression for the carrier generation rate, $G(x,\hbar\omega)$, or for a unit of volume, the rate of the number of electron-hole pairs generated per photon energy

$$G(x,\hbar\omega) = \alpha(x,\hbar\omega)\phi(x,\hbar\omega) \tag{2.3}$$

where $\alpha(x,\hbar\omega)$ and $\phi(x,\hbar\omega)$ emphasize the dependence of α and ϕ, respectively, on position and photon energy.

Integrating over the desired energy range gives the total generation rate per unit volume as a function of x

$$G(x) = \int_{\hbar\omega_{\min}}^{\hbar\omega_{\max}} d\hbar\omega \alpha(x,\hbar\omega)\phi\ (x,\hbar\omega) \tag{2.4}$$

In a homogeneous material, the flux decays exponentially with x as

$$\phi(x,\hbar\omega) = \phi(\hbar\omega)\exp\left(-\alpha(\hbar\omega)x\right) \tag{2.5}$$

Specifically, in the $p-region$ the flux is,

$$\phi_p(x,\hbar\omega) = \phi_0(\hbar\omega)\exp\left(-\alpha(\hbar\omega)x\right) \tag{2.6}$$

where $\phi_0(\hbar\omega)$ refers to the incident flux on the surface of the solar cell as a function of photon energy and $\alpha(\hbar\omega)$ indicates that absorption does not vary with position. In the graded region,

$$\phi_i(x,\hbar\omega) = \phi_p(x_p,\hbar\omega)\exp\left(-\int_{x_p}^{x} dx'\alpha\ (x',\hbar\omega)\right) \tag{2.7}$$

and finally, in the $n-region$,

$$\phi(x,\hbar\omega) = \phi_i(x_p + x_i,\hbar\omega)\exp\left(-\alpha(\hbar\omega)(x - x_p - x_i)\right) \tag{2.8}$$

Due to the segregation of photon energies incident on the individual cells, the integration for $G(x)$ will occur over a limited energy range, with the upper integration limit set such that the photon energy equals the bandgap energy of the subsequent solar cell in the lateral array. For example, for *Cell A* $\hbar\omega_{max} = 1.38\ eV$. Theoretically, *Cell C* has an upper bound approaching the highest energy photon, however actual implementation approximates the upper bound to $5.0\ eV$ without significant error.

Generation rates for the three cells are shown in Figure 2.2. Limiting the energy range of the incoming photons results in a completely transparent $p-GaN$ layer for *Cells A* and *B*. Part of the compositionally graded layer also acts as a window for the two indium rich cells until the bandgap reaches $1.38\ eV$ for *Cell A* and $2.0\ eV$ for *Cell B*.

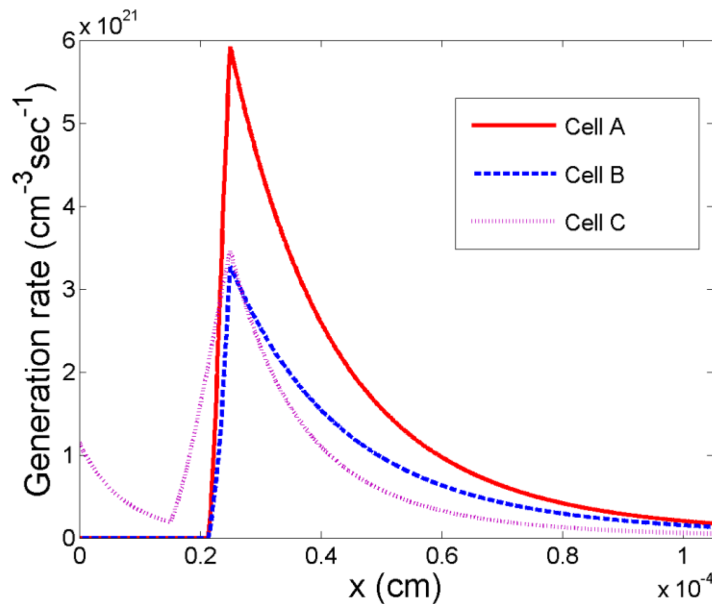

Figure 2.2 Electron-hole pair generation rates for cell designs *A*, *B*, and *C*.

While absorption occurs in the $p-GaN$ layer for *Cell C*, proceeding further into the bulk we see that the number of electron-hole pairs created quickly declines due to the

constant bandgap and the reduction in available photons. Where compositional grading commences, the bandgap begins to narrow and the number of photo-generated electron-hole pairs in *Cell C* starts to increase. Although flux declines moving into the bulk, the bandgap narrowing allows more photons to be utilized therefore the generation rate continues to increase until the bandgap regains a constant and minimum value at the $i-In_yGa_{1-y}N/n-In_{y_{\max}}Ga_{1-y_{\max}}N$ junction. Here the rate peaks, but declines as we move further into the $n-In_{y_{\max}}Ga_{1-y_{\max}}N$ layer because the semiconductor continues to absorb photons.

In addition to the graphical representation, Table 2.1 outlines several calculations providing insight as to the solar cell performance efficiency. The table shows total device generation, the ratio of the total generation to the total incident flux, the ratio of the total flux leaving the cell to the total incident flux, and the total generation occurring in each of the three layers of the cell.

Table 2.1 Total electron-hole pair generation of the *pin*, flux to generation ratios, and the total electron-hole pair generation of the individual layers.

Parameters	*Cell A*	*Cell B*	*Cell C*
$\int_0^L G(x)dx \quad (cm^{-2}\sec^{-1})$	1.734 x 10^{17}	9.087 x 10^{16}	7.307 x 10^{16}
$\int_0^L G(x)dx \Big/ \int_{\hbar\omega_{\min}}^{\hbar\omega_{\max}} \phi_0(\hbar\omega)\,d\hbar\omega$	0.944	0.925	0.971
$\int_{\hbar\omega_{\min}}^{\hbar\omega_{\max}} \phi_L(\hbar\omega)d\hbar\omega \Big/ \int_{\hbar\omega_{\min}}^{\hbar\omega_{\max}} \phi_0(\hbar\omega)\,d\hbar\omega$	0.056	0.075	0.028
$\int_0^{x_p} G_p(x)dx \quad (cm^{-2}\sec^{-1})$	0	0	5.736 x 10^{15}
$\int_{x_p}^{x_n} G_i(x)dx \quad (cm^{-2}\sec^{-1})$	1.375 x 10^{16}	5.744 x 10^{15}	1.577 x 10^{16}

$\int_{x_n}^{L} G_n(x)dx \quad (cm^{-2}\sec^{-1})$	1.597 x 10^{17}	8.512 x 10^{16}	5.157 x 10^{16}

As the table shows, *Cell A* experiences the largest total electron-hole pair generation while *Cell C* generates the least amount of electron-hole pairs. The ratio of the total generation to the total incident flux is high for all three cells, with the largest ratio occurring for *Cell C*. This suggests that the efficiency of *Cell C* may be highest of the three cells. Ideally, this ratio approaches unity, however, the absorption coefficient models the ability of the material to absorb the photons and not every photon of sufficient energy will be absorbed. The ratio of the total flux leaving the device through the $n-In_{y_{max}}Ga_{1-y_{max}}N$ layer to the total incident flux is low; ideally the ratio would approach zero. We see that *Cell C* absorbs a larger portion of the incident flux than the other two cells. For the three cells, most of the generation occurs in the $n-In_{y_{max}}Ga_{1-y_{max}}N$ layer and insignificant or no generation occurs in the $p-GaN$ layer.

2.4 Conclusions

The absorption coefficient model used to determine absorption in the PV cell was introduced. Using this model, we obtained absorption coefficient curves for the three $In_yGa_{1-y}N$ alloys of InN compositions 100, 62.4, and 39.2%. With the absorption coefficient known, the electron-hole pair generation rate could be determined and the results shown graphically for the three cells. For *Cells A* and *B*, the $p-GaN$ layer is completely transparent and for *Cell C* insignificant generation occurs. Figure 2.2 and Table 2.1 show that most of the generation occurs in the $n-In_{y_{max}}Ga_{1-y_{max}}N$ layer, therefore it is desirable to design this layer to be relatively thick.

3. Electrostatics and Minority Carrier Profiles

3.1 Introduction

Here we consider the electrostatics for the *pin* heterojunction under equilibrium conditions. The system is simplified by idealizing a doping profile as a step junction. Poisson's equation provides the starting point for the derivations of the electric field, electric potential, and depletion region widths. We derive the electrostatic and built-in potentials and provide specific results. In Section 3.3, we derive the minority carrier diffusion equations and subsequently apply a tridiagonal matrix algorithm to find the excess minority carrier concentrations. Results for the three cells under maximum power point forward bias with and without the photon source present are shown graphically.

3.2 Electrostatics

3.2.1 Poisson's Equation and Charge Density

Poisson's equation in 1D relates electric potential, $V(x)$, to electric charge, $\rho(x)$, and electric field, $E(x)$ by

$$\frac{d^2V(x)}{dx^2} = -\frac{\rho(x)}{\varepsilon_s} = -\frac{dE(x)}{dx} \tag{3.1}$$

where ε_s is the permittivity of the semiconductor. Charge density, or charge per unit volume, exists in the depletion regions due to the ionized $p-region$ acceptor concentration and $n-region$ donor concentration. By assuming total ionization of the dopants and then invoking the depletion approximation we find that,

$$\rho(x) = \begin{cases} -qN_a & x_{p'} \le x \le x_p \\ qN_d & x_n \le x \le x_{n'} \\ 0 & else \end{cases} \tag{3.2}$$

where q is the elementary charge .

3.2.2 Electric Field

Separation of positive and negative space charge densities creates the electric field across the depleted regions and graded region and we assume negligible electric field exists in the quasineutral regions. Considering Poisson's equation,

$$\frac{dE(x)}{dx} = \begin{cases} -qN_a / \varepsilon_s & x_{p'} \le x \le x_p \\ qN_d / \varepsilon_s & x_n \le x \le x_{n'} \\ 0 & else \end{cases} \tag{3.3}$$

and integrating once, yields

$$E(x) = \begin{cases} -qN_a\left(x - x_{p'}\right) / \varepsilon_s & x_{p'} \le x \le x_p \\ -qN_a\left(x_p - x_{p'}\right) / \varepsilon_s & x_p \le x \le x_n \\ -qN_d\left(x_{n'} - x\right) / \varepsilon_s & x_n \le x \le x_{n'} \end{cases} \tag{3.4}$$

where the electric field is continuous at the interfaces and constant in the graded layer.

3.2.3 Electric Potential

Due to the existence of an electric field, an electric potential can be derived by integrating $-E(x)$. This provides a quantitative description for the band-bending of the energy bands in the device. Analogous to a pn junction, $V(x)$ in the depleted regions has quadratic dependence on position. In the graded layer of the pin, the potential is linearly dependent on position. By letting $V(x_{p'})=0$, it follows that $V(x_2)=V_{bi}$. Solving for $V(x)$ in the GaN depleted layer, we find

$$V(x)=\int_{x_{p'}}^{x}\frac{qN_a}{\varepsilon_s}\left(x+\left(x_p-x_{p'}\right)\right)dx=\frac{qN_a}{2\varepsilon_s}\left(x+\left(x_p-x_{p'}\right)\right)^2+A \tag{3.5}$$

and since the potential is zero at the edge of the depleted region, $A=0$. In the graded layer,

$$V(x)=\int_{x_p}^{x}\frac{qN_a}{\varepsilon_s}\left(x_p-x_{p'}\right)dx=\frac{qN_a}{\varepsilon_s}\left(x_p-x_{p'}\right)x+B \tag{3.6}$$

and using the fact that $V(x)=\frac{qN_a}{2\varepsilon_s}\left(x+\left(x_p-x_{p'}\right)\right)^2$ at the boundary between the $p-GaN$ and graded layer, we find that $B=\frac{qN_a}{2\varepsilon_s}\left(x_p-x_{p'}\right)^2$. Finally, the potential in the $n-In_{y_{\max}}Ga_{1-y_{\max}}N$ is

$$V(x)=-\int_{x}^{x_{n'}}\frac{qN_D}{\varepsilon_s}\left(x_{n'}-x\right)dx=-\frac{qN_D}{2\varepsilon_s}\left(x_{n'}-x\right)^2+C \tag{3.7}$$

and obviously, $C=V_{bi}$. To summarize, the electric potential for the pin diode is given by

$$V(x) = \begin{cases} \frac{qN_a}{2\varepsilon_s}\left(x + \left(x_p - x_{p'}\right)\right)^2 & x_{p'} \le x \le x_p \\ \frac{qN_a}{\varepsilon_s}\left(x_p - x_{p'}\right)\left(x + \frac{1}{2}\left(x_p - x_{p'}\right)\right) & x_p \le x \le x_n \\ V_{bi} - \frac{qN_D}{2\varepsilon_s}\left(x_{n'} - x\right)^2 & x_n \le x \le x_{n'} \end{cases} \tag{3.8}$$

3.2.4 Electrostatic Built-in Voltage

In a homojunction, majority carrier electrons and holes observe a built-in voltage preventing most of the carriers from diffusing across the depleted regions when equilibrium conditions prevail. This barrier is given by[56]

$$V_{bi} = V_T \ln\left(\frac{N_a N_d}{n_i^2}\right) \tag{3.9}$$

with n_i, the intrinsic carrier concentration

$$n_i = \sqrt{N_C N_V}\exp\left(-\frac{E_g(x)}{2V_T}\right) \tag{3.10}$$

where V_T is the thermal voltage. Parameters N_C and N_V represent the effective density of conduction and valence band states, respectively.

To simplify the model, we let the effective mass of the electrons and holes, m_e and m_h, respectively, be constant throughout the diode. It follows that, N_C and N_V are also constant with chosen values of $N_C = 7.9035x10^{17} cm^{-3}$ and $N_V = 8.8364x10^{18} cm^{-3}$ where at room temperature, $N_{C,V}$ approximately equal[57]

$$N_{C,V} = \left(2.510x10^{19}\,cm^{-3}\right)\left(m_{e,h}/m_0\right)^{3/2} \tag{3.11}$$

Using the effective masses for InN and GaN we can calculate N_C and N_V and compare to our chosen values. These results are listed in Table 3.1.

Table 3.1 *InN* and *GaN* electron and hole effective masses and effective densities of states.

Parameter	*InN*	*GaN*
$\left(m_e/m_0\right)$	0.05[a]	0.2[b,c]
$\left(m_h/m_0\right)$	0.6[d]	1.25[e],0.8[c]
N_C $\left(cm^{-3}\right)$	2.806×10^{17}	2.245×10^{18}
N_V $\left(cm^{-3}\right)$	1.167×10^{19}	3.508×10^{18}, 1.796×10^{19}

[a] Reference 58, [b] Reference 59, [c] Reference 38, [d] Reference 31, [e] Reference 60

The results for N_C and N_V do not vary significantly from the chosen constant values. Further, they appear under the square root in Equation 3.10, while intrinsic carrier concentration depends exponentially on bandgap. Therefore, the dependence on effective mass is weak compared to the one on bandgap. It follows that we can neglect the effective mass dependence.

In the heterojunction, the electrostatic potential is not given by Equation 3.9. We begin the derivation for the heterojunction electrostatic potential by observing the energy-band diagram for the heterojunction before contact between the two materials. In this type of junction, the energy-band has a discontinuity at the junction interface. A straddling bandgap alignment, where the bandgap of the larger bandgap material

completely overlaps that of the narrower bandgap material, is assumed.[20] Figure 3.1 illustrates, for isolated $p-doped$ and $n-doped$ materials, the energy-band diagrams for this alignment. As discussed in Chapter 1, in our design the $p-doped$ material is GaN and the $n-doped$ material is $In_{y_{max}}Ga_{1-y_{max}}N$. The vacuum level and valence band edge provide points of reference for the derivations of the potential barrier.

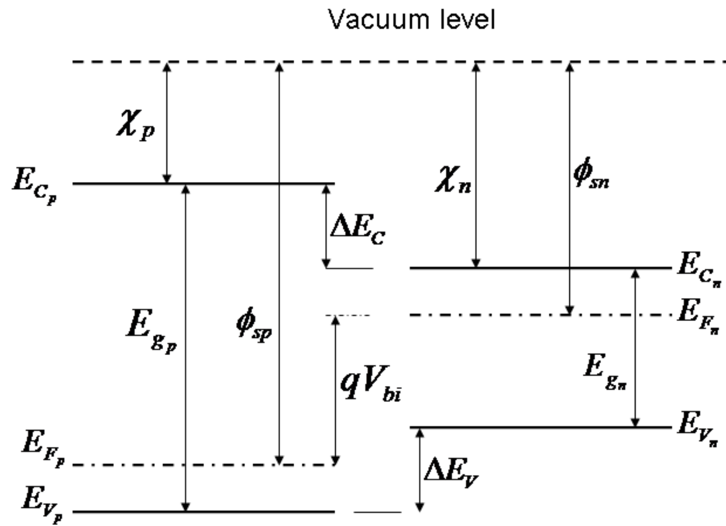

Figure 3.1 Energy-band diagrams of two isolated materials with straddling bandgap alignment; a wide bandgap *p-doped* material and a narrow bandgap *n-doped* material. The *p-doped* material has a smaller electron affinity, χ_p, than that of the *n-doped* material. In our system, the wide bandgap material is *GaN* and the narrow bandgap material is an $In_y Ga_{1-y}N$ alloy.

The above figure shows an ideal relationship between materials of differing bandgaps. This relationship, called the *electron affinity rule*, assumes an ideal abrupt heterojunction between charge neutral semiconductors. In this case, the vacuum level is parallel to the conduction and valence bands so it follows that the band offsets remain constant across the heterojunction interface. While some uncertainty exists regarding its validity, this rule is adequate for our model.

The heterojunction built-in potential barrier ideally equals the difference between the work functions, $\phi_{sp} - \phi_{sn}$, or

$$qV_{bi} = \chi_p + (E_{C_p} - E_{F_p}) - \left(\chi_n + (E_{C_n} - E_{F_n})\right) \tag{3.12}$$

To eliminate the quasi-fermi energy levels in the above equation, we employ the equations for the carrier concentrations and assuming that at room temperature all dopants are ionized

$$N_a \approx N_V \exp\left(\frac{E_{V_p} - E_{F_p}}{kT}\right) = N_V \exp\left(\frac{(E_{C_p} - E_{g_{GaN}}) - E_{F_p}}{kT}\right) \tag{3.13}$$

and

$$N_d \approx N_C \exp\left(\frac{E_{F_n} - E_{C_n}}{kT}\right) \tag{3.14}$$

where $kT = qV_T$. Solving for the quasi-fermi energies,

$$E_{F_p} = E_{C_p} - E_{g_{GaN}} - kT \ln\left(N_a / N_V \right) \tag{3.15}$$

and

$$E_{F_n} = E_{C_n} + kT \ln\left(N_d / N_C \right) \tag{3.16}$$

The conduction band and valence band offsets equal

$$\Delta E_C = \chi_n - \chi_p \tag{3.17}$$

and

$$\Delta E_V = \chi_p - \chi_n + E_g(GaN) - E_g(In_{y_{\max}} Ga_{1-y_{\max}} N) \tag{3.18}$$

respectively. Substituting Equations 3.15 and 3.16 into 3.12, using Equation 3.10 to obtain an expression for the product $N_C N_V$ in terms of the intrinsic carrier concentrations of both doped layers, and then manipulating and substituting Equations 3.17 and 3.18 to eliminate the electron affinities, yields the electrostatic potential as

$$V_{bi} = V_T \ln\left(\frac{N_a N_d}{n_{i_p} n_{i_n}}\right) + \frac{\Delta E_V}{2} - \frac{\Delta E_C}{2} \tag{3.19}$$

where the intrinsic carrier concentrations, n_{i_p} and n_{i_n} are given by Equation 3.10. The electrons and holes see different built-in voltages, as seen in Figure 1.7. For the electrons,

$$V_{bi_e} = V_{bi} + \Delta E_C = V_T \ln\left(\frac{N_a N_d}{n_{i_p} n_{i_n}}\right) + \frac{\Delta E_g}{2} \tag{3.20}$$

and for the holes,

$$V_{bi_h} = V_{bi} - \Delta E_V = V_T \ln\left(\frac{N_a N_d}{n_{i_p} n_{i_n}}\right) - \frac{\Delta E_g}{2} \tag{3.21}$$

Table 3.2 shows results for electron affinity, offsets, $n-region$ intrinsic carrier concentration, and potentials. To find the electron affinity as a function of indium nitride composition, we use an equation analogous to Equation 1.2

$$\chi(y) = \chi_{InN} y + \chi_{GaN}(1-y) - by(1-y) \tag{3.22}$$

with the bowing parameter, $b = 0.8\ eV$ [31] .

Table 3.2 In_yN material dependent variables for compositions 0, 39.2, 62.4, and 100 %.

Parameter	*Cell A*	*Cell B*	*Cell C*	*GaN*
$q\chi\ \ (eV)$	5.6[20,21]	4.81	4.44	4.0[20,21]
$\Delta E_C\ \ (eV)$	1.60	0.81	0.44	0.
$\Delta E_V\ \ (eV)$	1.10	1.21	0.96	0.
$\Delta E_G\ \ (eV)$	2.70	2.02	1.40	0.
$n_i\ \ (cm^{-3})$	3.486×10^{12}	6.771×10^{6}	41.968	7.303×10^{-11}
$V_{bi}\ \ (V)$	1.726	2.516	2.889	3.326
$V_{bie}\ \ (V)$	3.326	3.326	3.326	3.326
$V_{bih}\ \ (V)$	0.626	1.306	1.926	3.326

In the table, $q\chi$ and n_i refer to the electron affinity and the intrinsic carrier concentration corresponding to the indium nitride compositions of the $n-region$ of each of the three cells and to GaN. From the table we see that the conduction band offset increases as the cell becomes more InN-rich and obviously ΔE_G increases as well. However, the valence band offset varies non-monotonically due to the bowing. The intrinsic carrier concentration increases as the bandgap narrows because less energy is needed in order for carriers to be thermally created. Further, the built-in voltage and built-in voltage seen by the holes decreases as the bandgap narrows. The built-in voltage seen by the electrons does not change because because the gap dependence cancels out as can be seen from Eqs. 3.10 and 3.20.

3.2.5 Depletion Region Widths

Charge neutrality requires that $N_a \Delta x_p = N_d \Delta x_n$. Using the derived expressions for electric potential in Section 3.2.3, we can solve for either Δx_p or Δx_n and use this relationship to find the remaining depletion width. Choosing to solve for Δx_p, we find

$$\Delta x_p = \left(\frac{2\varepsilon_s}{q} \left(\frac{N_d}{N_a} \right) \left(\frac{1}{N_a + N_d} \right) V_{bi} + \left(\frac{N_d}{N_a + N_d} x_i \right)^2 \right)^{1/2} - \frac{N_d}{N_a + N_d} x_i \tag{3.23}$$

When a forward bias is applied, the potential barrier decreases and in the equation above, V_{bi} is replaced with $(V_{bi} - V_A)$. Table 3.3 provides the depletion region widths for each cell under equilibrium conditions.

Table 3.3 Equilibrium depletion region widths.

Parameter	*Cell A*	*Cell B*	*Cell C*
Δx_p (Å)	814	1080	1200
Δx_n (Å)	20.4	27.1	29.9

3.3 Excess Minority Carrier Profiles

3.3.1 Derivations

Any perturbation to the diode can lead to deviations of the minority carriers from their equilibrium values n_{p0} and p_{n0} for the electrons and holes, respectively. The excess minority carrier concentrations, $\Delta n(x) = n(x) - n_{p0}$ for the electrons and $\Delta p(x) = p(x) - p_{n0}$ for the holes, provide insight as to the effect of the perturbation on the device. When in equilibrium, $\Delta n(x) = \Delta p(x) = 0$, but for example under illumination photons have the potential to free electrons from their valence band, thus increasing the

number of minority carrier electrons, $n(x)$ and holes, $p(x)$ above their equilibrium value. Obviously, the perturbation in this system is illumination of the cells.

To find the minority carrier diffusion equations, subsequently allowing us to solve for the excess carrier concentrations, we begin with the equation of state that describes the overall minority carrier action. All carrier action occurrences lead to a time dependent total change in carrier concentrations to which individual changes contribute. That is, as the following equation summarizes, the total time dependent change in the minority carrier electron concentration or hole concentration can originate from on carrier drift, diffusion, thermal recombination, and possibly other processes such as photogeneration. The total time dependent change in electron concentration, dn/dt, is given as

$$\frac{dn}{dt} = \left(\frac{dn}{dt}\right)_{drift} + \left(\frac{dn)}{dt}\right)_{diffusion} + \left(\frac{dn}{dt}\right)_{\substack{thermal \\ R-G}} + \left(\frac{dn}{dt}\right)_{\substack{other \\ processes \\ (light, etc.)}} \tag{3.22}$$

Analogously, substituting dp/dt into the above equation gives the total time dependent change in hole concentration. From Equation 3.22, we can derive the minority carrier diffusion equations applicable to the areas outside the depleted regions. First we begin by recalling the system to be 1D, then we make the following assumptions:

(1) We consider only *minority carrier* action.
(2) Negligible electric field exists outside the depletion regions, thus we can neglect the terms due to drift.
(3) Equilibrium minority carrier concentrations do not depend on position. That is, $n_{p0} \neq n_{p0}(x)$.
(4) Majority carrier concentrations remain basically unperturbed such that *low-level injection* applies.
(5) $R-G$ center recombination acts as the dominant $R-G$ mechanism.

(6) The only "other process" occurring consists of photogeneration, hence $\left(dn/dt\right)\Big|_{\substack{other\\processes}} = G(x)$ and $\left(dp/dt\right)\Big|_{\substack{other\\processes}} = G(x)$.

(7) Steady-state conditions prevail, or $dn/dt = dp/dt = 0$.

The time dependent change in the minority carrier concentration due to diffusion is proportional to the gradient of the respective current density, discussed in Chapter 4, or

$$\left(\frac{dn}{dt}\right)_{diffusion} = D_e \frac{\mathrm{d}^2 \Delta n(x)}{dx^2} \tag{3.23}$$

where D_e represents the minority carrier electron diffusion coefficient. An analogous expression exists for the above equation in terms of holes and the minority carrier hole diffusion coefficient D_h.

With $R-G$ center recombination, energy levels exist in the bandgap and provide states for the electrons from the conduction band and holes from the valence band. These energy levels, or centers, promote increased recombination of carriers. Under steady-state conditions,

$$\left(\frac{dn}{dt}\right)_{\substack{thermal\\R-G}} = \frac{-\Delta n(x)}{\tau_e} \tag{3.24}$$

where τ_e symbolizes the minority carrier electron lifetime. Similarly, an expression for the minority carrier holes can be found by substituting into Equation 3.24 the terms relevant for holes. For the minority carrier holes, τ_h represents the minority carrier lifetime. (Equation 3.24 stems from Equation 4.3, in Chapter 4, for $R-G$.)

Applying to Equation 3.22 the assumptions and Equations 3.23 and 3.24, we obtain the minority carrier diffusion equation for the electrons,

$$D_e \frac{\mathrm{d}^2 \Delta n(x)}{dx^2} - \frac{\Delta n(x)}{\tau_e} + G(x) = 0 \tag{3.25}$$

Again, an analogous equation can be obtained for the holes by substituting in the appropriate terms.

To solve the second order differential equations above for the excess minority carrier concentrations, we first consider the derivative limit. Since an analogous process can be applied to the holes, we consider only the minority carrier electrons and discretize Equation 3.25 such that

$$D_e \frac{\Delta n(x+\Delta x) - 2\Delta n(x) + \Delta n(x-\Delta x)}{\Delta x^2} - \frac{\Delta n(x)}{\tau_e} = -G(x) \tag{3.26}$$

with interval Δx. We can set up a matrix system to allow us to efficiently solve for $\Delta n(x)$. Specifically, we use the matrix equation **AY** = **b** with matrix

$$\mathbf{A}=\begin{bmatrix} \left(D_e\frac{-2}{\Delta x^2}-\frac{1}{\tau_e}\right) & D_e\frac{1}{\Delta x^2} & 0 & \cdots & 0 \\ D_e\frac{1}{\Delta x^2} & \left(D_e\frac{-2}{\Delta x^2}-\frac{1}{\tau_e}\right) & D_e\frac{1}{\Delta x^2} & & \vdots \\ 0 & D_e\frac{1}{\Delta x^2} & \left(D_e\frac{-2}{\Delta x^2}-\frac{1}{\tau_e}\right) & \ddots & 0 \\ \vdots & & \ddots & \ddots & D_e\frac{1}{\Delta x^2} \\ 0 & \cdots & 0 & D_e\frac{1}{\Delta x^2} & \left(D_e\frac{-2}{\Delta x^2}-\frac{1}{\tau_e}\right) \end{bmatrix}$$

and vectors

$$\mathbf{Y}=\begin{bmatrix} \Delta n(\Delta x) \\ \Delta n(2\Delta x) \\ \Delta n(3\Delta x) \\ \vdots \\ \Delta n(x_{p'}-\Delta x) \end{bmatrix} \quad \mathbf{b}=\begin{bmatrix} -G(\Delta x)-\Delta n(x=0)D_e\frac{1}{\Delta x^2} \\ -G(2\Delta x) \\ -G(3\Delta x) \\ \vdots \\ -G(x_{p'}-\Delta x)-\Delta n(x_{p'})D_e\frac{1}{\Delta x^2} \end{bmatrix}.$$

The first and last elements of **b** depend on the boundary conditions $\Delta n(0)$ and $\Delta n(x_{p'})$. A tridiagonal matrix algorithm, or the Thomas Algorithm as discussed in Appendix B, provides an efficient method for solving **AY** = **b** for the excess minority carrier concentrations.

Before we can obtain $\Delta n(x)$ and $\Delta p(x)$, we must specify the boundary conditions. We chose as the boundary conditions for this system:

(1) $\Delta n(x=0)=0$

(2) $\Delta n(x=x_{p'})=\frac{n_{i_p}^{\ 2}}{N_a}\left(\exp\left(V_A/V_T\right)-1\right)=n_{p0}\left(\exp\left(V_A/V_T\right)-1\right)$

(3) $\Delta p(x'=0)=0$

(4) $\Delta p(x'=x_{n'})=\frac{n_{i_n}^{2}}{N_d}\left(\exp\left(V_A/V_T\right)-1\right)=p_{n0}\left(\exp\left(V_A/V_T\right)-1\right)$

Since we make ohmic contact to the doped regions and we will assume a surface recombination velocity approaching infinitely large magnitude, any non-equilibrium minority carriers recombine at the contacts. Therefore, under arbitrary conditions the minority carrier concentrations at the ohmic contacts equal the equilibrium concentrations and there is no excess concentration of carriers. This results in boundary conditions (1) and (3).

At the depletion region edges, the applied bias determines the minority carrier concentrations. Majority carriers occupy the band energy levels such that, in general, the lower levels contain most carriers and occupation decays in an exponential manner moving towards higher energy states. During equilibrium, very few of these carriers have enough energy to surmount the potential barrier between the doped regions and minority carrier drift balances the small level of diffusion. Application of a forward bias reduces the barrier, thus enabling more majority carriers to cross the depleted regions and further increasing the bias will continue to decrease the barrier in a linear manner. Since the majority carrier occupation decreases approximately exponentially as we move away from the band edges and the forward bias has a linear relationship with the potential barrier, increasing the forward bias will produce an exponentially increasing majority carrier concentration that can cross the depletion regions. The quantitative expressions for $\Delta n(x_{p'})$ and $\Delta p(x_{n'})$, or boundary conditions (2) and (4), stem from the carrier concentration expressions resulting from probability of band occupancy statistics and by applying an assumption that any majority carrier recombination between the doped regions has insignificant consequences on the minority carrier concentrations.

The boundary condition values for the illuminated system operating at maximum power point voltage are given in Table 3.4. The thermal equilibrium minority electron concentration in the $p-GaN$ layer is $n_{p0} = 5.33x10^{-38}\ cm^{-3}$.

Table 3.4 Minority carrier concentrations under maximum power point operating conditions.

Parameter	*Cell A*	*Cell B*	*Cell C*
$\Delta n(x_{p'})\quad (cm^{-3})$	1.538 x 10^{-32}	5.906 x 10^{-22}	7.106 x 10^{-12}
$p_{n0}\quad (cm^{-3})$	3.038 x 10^{6}	1.146 x 10^{-5}	4.403 x 10^{-16}
$\Delta p(x_{n'})\ (cm^{-3})$	8.765 x 10^{11}	1.270 x 10^{11}	5.870 x 10^{10}

3.3.2 Results

Considering operation at maximum power point voltage, V_m, since this produces the highest effificiences as we discuss further in Chapter 5, we find the excess minority carrier electron and hole concentrations with and without illumination. The boundary conditions are given in 3.3.1 and the specific values for our system operating at V_m are given in Table 3.4. The excess minority carrier electron concentration is smallest for *Cell A* because V_m is smallest and the concentration is largest for *Cell C* because V_m is largest. In the $n-region$, a larger concentration of minority carriers can exist than in the $p-region$ due to the smaller amount of energy necessary for the electrons to be promoted to the conduction band, that is, necessarily $E_g(In_{y_{max}}Ga_{1-y_{max}}N) \le E_g(GaN)$. As the bandgap increases, absorption decreases and therefore excess hole concentration is smaller so *Cell C* has the smallest excess minority carrier concentration.

Figure 3.2. shows (a) $\Delta n(x)$ and (b) $\Delta p(x)$ profiles for the cells under dark conditions. *Cell C* has the highest injection of electrons from the $n-In_{y_{max}}Ga_{1-y_{max}}N$ layer because the maximum power point voltage is largest for this cell. However, *Cell C*

has the lowest injection of holes from the $p-GaN$ layer because the injection barrier is largest for this cell. $Cell\ A$ has the smallest excess electron concentration because V_m is the smallest of all three cells, but it has the largest excess hole concentration because the $n-region$ bandgap is smallest.

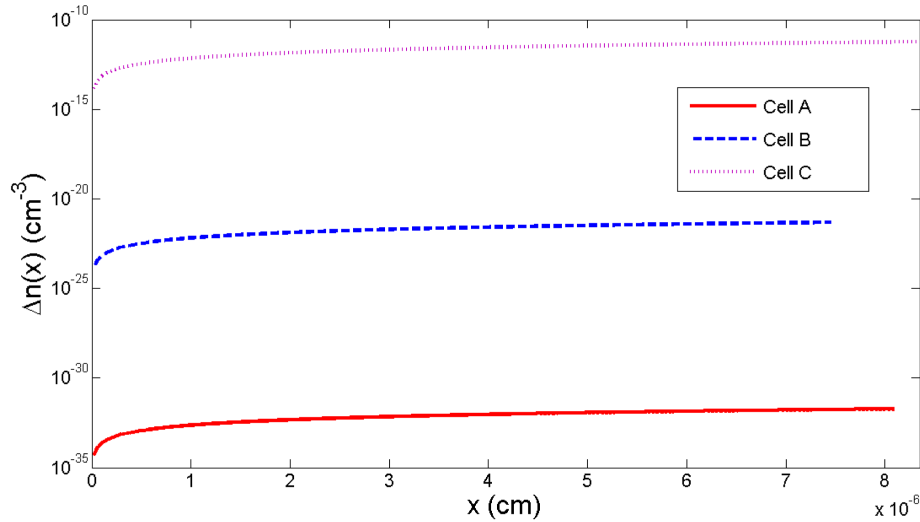

(a)

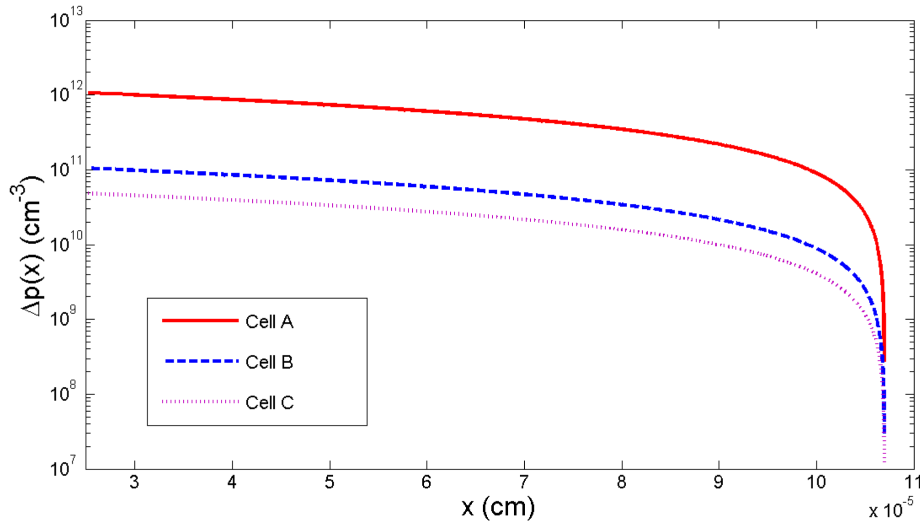

(b)

Figure 3.2 Dark excess minority carrier concentrations (a) electrons and (b) holes.

Photogeneration can dramatically increase the excess carrier concentrations as shown in Figure 3.3. Figure 3.3(a) shows the excess electron concentration in the $p-GaN$ layer for *Cell C*. The concentrations are not shown for the other two cells because the profiles do not differ from those seen in Figure 3.2. Compared with *Cell C*, the concentrations are insignificant and thus not shown. Figure 3.3(b) shows the excess minority carrier hole concentrations for all three cells.

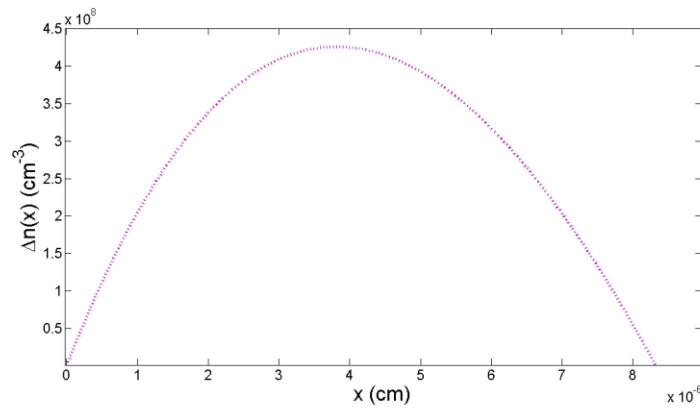

(a)

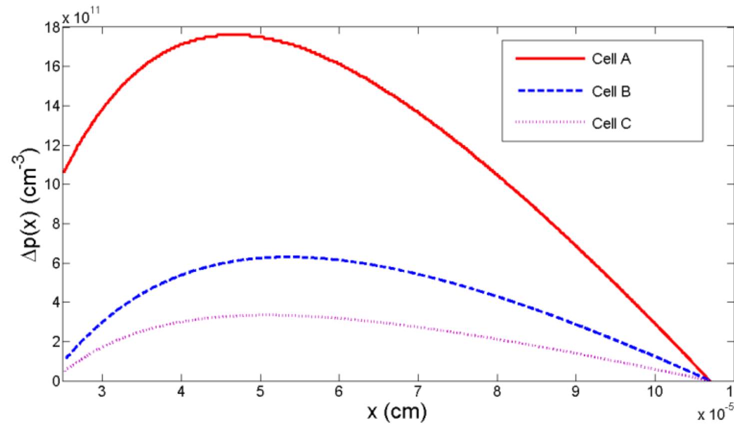

(b)

Figure 3.3 Excess minority carrier concentrations for the cells under illumination (a) electrons[a] and (b) holes.
[a]for *Cell C*

In the $p-GaN$ layer $Cell\ \ A$ and $Cell\ B$ do not experience any generation when exposed to the light source because incident photons do not have energy greater than $E_g(GaN)$. Therefore, $\Delta n(x)$ for these cells depends only on injection from the $n-region$. As opposed to $Cell\ A$ and $Cell\ B$, generation can occur in the $p-GaN$ layer for $Cell\ C$ when subject to light, since some incident photons for this cell have $\hbar\omega \geq 3.4\ eV$.

Unlike in the $p-GaN$ layer, the electron-hole pair generation occurs in the $n-In_{y_{\max}}Ga_{1-y_{\max}}N$ layer for all three cells. This is true because under illumination all available photons will have $\hbar\omega \geq E_g(In_{y_{\max}}Ga_{1-y_{\max}}N)$. $Cell\ A$ has the largest minority carrier hole concentration created because the bandgap is the smallest of the three cells. Conversely, $Cell\ \ C$ experiences the least amount of photon induced generation because the bandgap is widest for this cell.

3.4 Conclusions

We first discussed *pin* heterojunction electrostatics and, beginning with Poisson's equation for the 1D system, derived electric field, electric potential, electrostatic built-in voltage, and the depletion region widths. The electrostatic built-in voltage for the heterojunction differs from that for a homojunction device and is derived from the energy-band diagram assuming the *electron affinity rule*. The potential is given by the difference between the work functions. Due to the band offsets, the electrons and holes see different built-in potentials.

Assuming constant electron and hole effective masses is shown to be a reasonable approximation. The electron affinities, offsets, and potentials are calculated for the three cells and for GaN. Depletion region widths are derived and specific results are provided for the system in equilibrium. Depletion region widths in the $p-GaN$ layer are on the order of 10^2 Å and in $n-In_{y_{\max}}Ga_{1-y_{\max}}N$ layer, on the order of 10 Å.

We began the discussion on the excess minority carrier profiles by deriving the minority carrier diffusion equations from the equation of state and stated assumptions. Subsequently, we discretized the diffusion equations resulting in a system of equations solvable with a tridiagonal matrix algorithm. Boundary conditions were discussed and results provided for maximum power point operation. Finally, we showed excess minority carrier concentration results graphically for the cells under dark and light conditions. Under dark conditions, the largest electron injection into the $p-GaN$ layer occurs for $Cell\ C$ because the operating voltage is largest for this cell. However, the excess minority carrier hole concentration for $Cell\ C$ is lowest. $Cell\ A$ has the smallest excess minority carrier electron concentration because the operating voltage is smallest, but the excess minority carrier hole concentration is largest for this cell. Application of the photon source greatly increases the minority carrier concentrations in the $n-In_{y_{\max}}Ga_{1-y_{\max}}N$ layer for the three cells. Only $Cell\ C$ experiences increased minority carrier concentrations in the $p-GaN$ layer because for $Cell\ A$ and $Cell\ B$ this layer appears transparent.

4. *Current Density*

4.1 *Introduction*

As discussed in Chapter 3, application of a forward bias will cause minority carrier injection across the junction and exposure to a photon source with photons of sufficient energy will generate additional carriers. Figure 4.1 shows the majority carrier diffusion from regions of large concentration to regions of smaller concentration and the photogenerated carrier action. In equilibrium, the majority carrier diffusion is completely balanced by the drift of carriers in the region where the carrier density varies, i.e. the junction region. The photogenerated charge carries diffuse in the regions where the electric field vanishes and drift in the regions where it is non-zero.

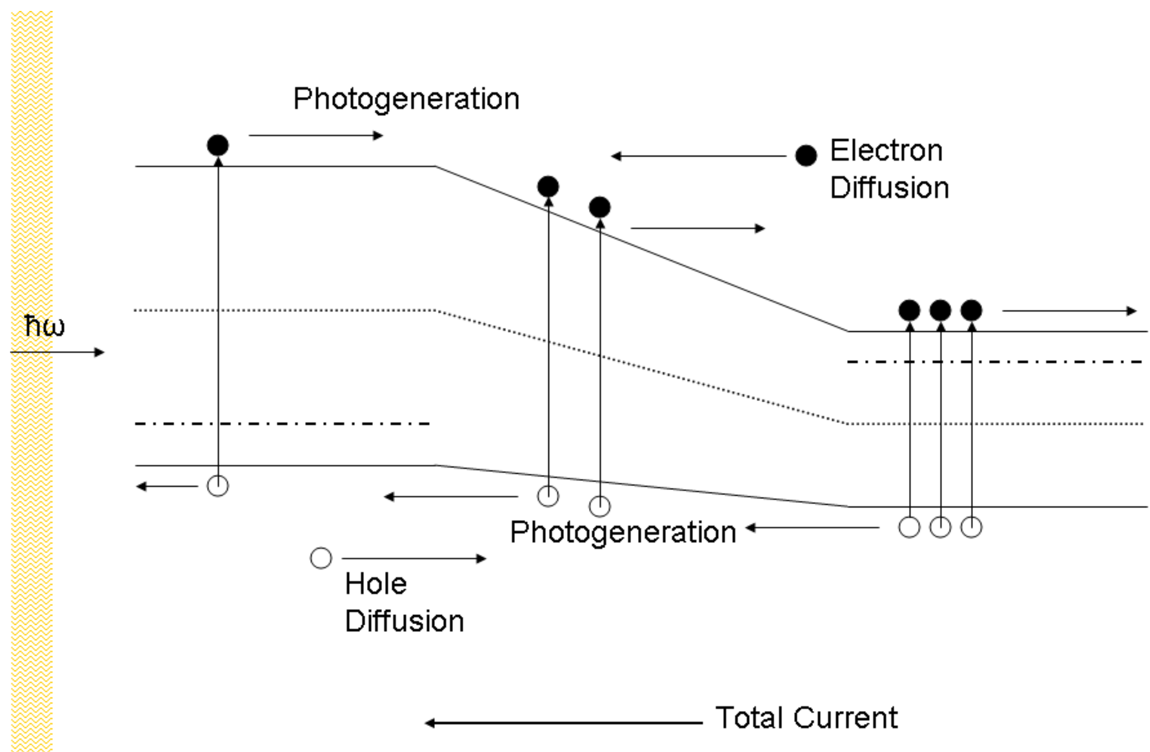

Figure 4.1 Carrier action in the *pin* PV cell.

With the minority carrier profiles found in Chapter 3, we can find the minority carrier diffusion current densities, J_n for the electrons in the $p-GaN$ layer and J_p for the holes in the $n-In_{y_{\max}}Ga_{1-y_{\max}}N$ layer. In the case of a pn diode, these current densities alone would provide a good estimate of the total carrier action present in the device. However, in the pin diode two other current density contributions also play an important role. These current densities arise in the depleted regions and intrinsic region. Further, they increase the overall device current density.

The intrinsic region carrier generation current density, J_i, accounts for the electron-hole pairs created in the $i-In_yGa_{1-y}N$ layer due to photon absorption. While this generation is occurring, recombination of carriers also takes place, although at a much smaller rate. We may assume this rate to be negligible if the electric field between $x_{p'} \le x \le x_{n'}$ is sufficiently large such that the transit time of the charge carriers is short compared to the recombination lifetime. However, some recombination may occur, leading to an $R-G$ current, J_{R-G}, in this region. In the system studied, we will consider this recombination current density.

In this chapter, we obtain expressions for the current densities, beginning with J_n and J_p , following with J_i, and finally J_{R-G}. The diffusion current densities are derived from Fick's first law, the intrinsic region carrier generation current is found by integration of the generation rate, and we find the recombination current density through the Shockley-Read Hall model. Graphical results of the total current densities for the three cells are compared and individual current density contributions are also shown for each of the cells. Results are presented for the cells under dark and light conditions. Finally, we end this chapter with a brief analysis showing the effect of the $n-In_{y_{\max}}Ga_{1-y_{\max}}N$ layer thickness on total current density for each of the cells under illumination.

4.2 Minority Carrier Diffusion Current Densities

Diffusion current densities arise from concentration gradients due to the doping of the $p-region$ and $n-region$. As Figure 4.1 illustrated, majority carrier electrons, provided by the $n-region$ donors, travel across the $i-region$ to the $p-region$ where they contribute to the minority carrier electron diffusion current density. Analogously, the majority carrier holes, provided by the $p-region$ acceptors, cross the $i-region$ and enter the $n-region$ where they contribute to J_p.

The diffusion current density is proportional to the number of carriers moving through a plane perpendicular to the carrier flow, or the flux of carriers, F. To obtain expressions for the diffusion currents, we use Fick's first law which says that F is proportional to the minority carrier electron and hole concentration gradients, ∇n and ∇p, such that $F_n = -D_e \nabla n$ for the minority carrier electrons and $F_p = -D_h \nabla p$ for the minority carrier holes. Current density has a proportional relationship to the flux as $J = \pm qF$. Applying Fick's first law to the electrons,

$$J_n = qD_e \frac{d\Delta n(x)}{dx} \tag{4.1}$$

which is the minority carrier electron diffusion current density. Analogously, we can find J_p by substituting in the appropriate terms for the holes. The $\Delta n(x)$ and $\Delta p(x)$ data collected in Chapter 3 is used in Equation 4.1 to produce the results for the minority carrier diffusion current densities. These results are shown in Section 4.5 along with the other current density contributions discussed in 4.3.

When solving for the diffusion currents, any $R-G$ has an assumed insignificant influence on the carrier concentrations between $x_{p'} \leq x \leq x_{n'}$. This implies the simplification that diffusion current densities remain unchanged throughout the region.

Consequently, the total current in the device results from summing the individual densities at the depletion region edges, or $J_{diff} = J_p(x_{p'}) + J_n(x_{n'})$.

4.3 Depleted and Intrinsic Region Photogeneration Current Density

The current density J_i accounts for carriers photogenerated between $x_{p'} \le x \le x_{n'}$. Obviously, J_i can exist only when the cell is illuminated. Since $G(x)$ gives the rate of electron-hole pair formation, summing $G(x)$ over the region will give the total number of carriers created and multiplying by q will provide the current density,

$$J_i(V) = q\int_{x_{p'}}^{x_{n'}} G(x)dx \tag{4.2}$$

While the generation rate does not depend on applied bias, the depletions widths do and thus so does J_i.

4.4 Recombination Current Density

As mentioned, we do not assume that the junction region is so thin as to make the recombination there negligible. Instead, under forward bias some carrier loss occurs at $R-G$ centers situated within the bandgap. We can model this process with the full Shockley Read Hall $R-G$ expression[56]

$$RG(x) = \frac{n(x)p(x) - n_i^2(x)}{\tau(n(x) + p(x) + 2n_i(x))} \tag{4.3}$$

assuming $\tau_p = \tau_n = \tau$.

The $i-region$ electron concentration is approximately given by,

$$n(x) = N_d \exp\left(\frac{F_e}{V_T}(x_{n'} - x)\right) \tag{4.4}$$

where F_e represents the electric field seen by the electrons; the ratio of the voltage over the region such that,

$$F_e = \frac{V - V_{bi_e}}{x_{n'} - x_{p'}} \tag{4.5}$$

Further, in the $i-region$ the hole concentration is approximately give by,

$$p(x) = N_a \exp\left(\frac{F_h}{V_T}\left(x - x_{p'}\right)\right) \tag{4.6}$$

where F_h represents the electric field seen by the holes and by replacing V_{bi_e} with V_{bi_h} has the expression given in Equation 4.5. Finally, the local intrinsic carrier concentration is

$$n_i(x) = n_{i_p} \exp\left(\frac{(E_{g_p} - E_{g_n})\left(x - x_p\right)}{2V_T\left(x_n - x_p\right)}\right) \tag{4.7}$$

Integrating over the depleted width the number of carriers recombining at the $R-G$ centers and multiplying by the charge, yields

$$J_{R-G} = q\int_{x_{p'}}^{x_{n'}} RG(x)dx \tag{4.8}$$

the current density associated with the carrier recombination.

4.5 Results

Here we provide graphical results for the current densities in the solar cell. We first look at the results for the system with no photon source present. The total dark current is compared for the three cells and the diffusion, recombination, and total current densities are compared for each cell. For the illuminated cells, we show the total current densities and compare the individual current components.

4.5.1 Dark Current Density

First consider the current density for the cells under dark conditions. The total dark current density is given by $J_{diff} + J_{R-G}$ and is shown on a semilog plot in Figure 4.2, as a function of applied cell voltage, for the three cells.

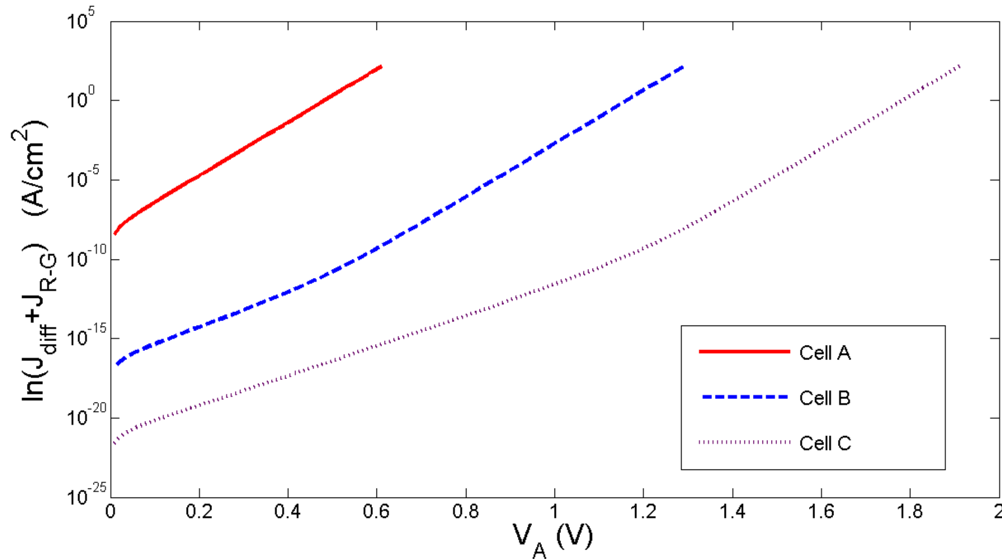

Figure 4.2 Total dark current density.

The total dark current is largest for the InN-rich *Cell A* because the bandgap is smallest, thus the device has the strongest hole injection. Conversely, *Cell C* is the least conductive because the bandgap is largest.

Figure 4.3 shows the total current density, diffusion current density, and recombination current density for (b) *Cell B* and (c) *Cell C*. The total current density and the recombination current density for *Cell A* is shown in Figure 4.3. (a).

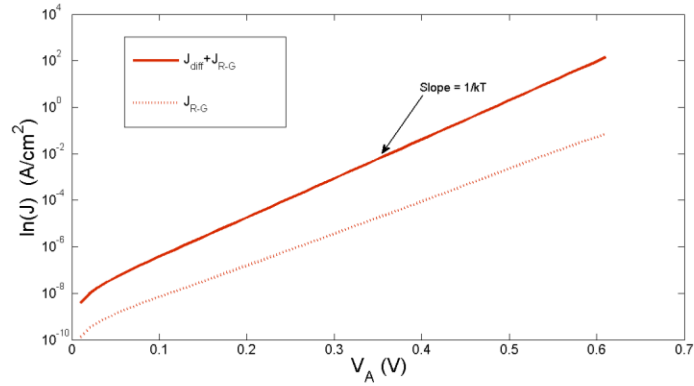

(a)

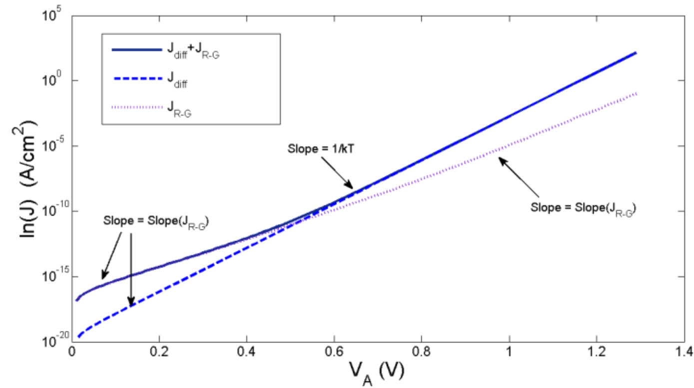

(b)

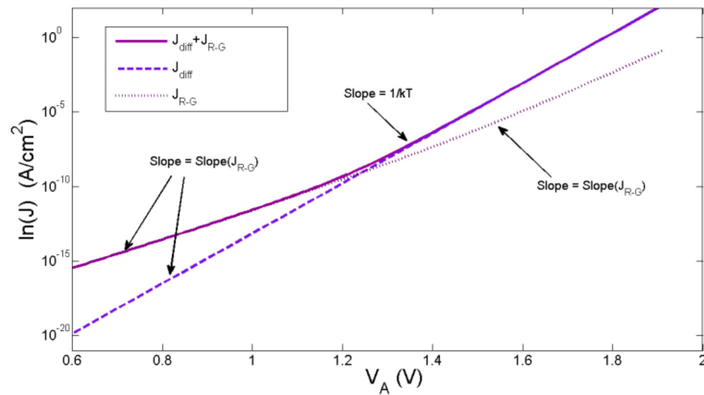

(c)

Figure 4.3 Total dark current density and recombination current density (a) *Cell A* (b) *Cell B* and (c) *Cell C*.

The current density for *Cell A* is shown in Figure 4.3(a). Only the total dark current density $J_{diff} + J_{R-G}$, and the recombination current density J_{R-G} are shown. The diffusion current density is not shown because it essentially overlaps $J_{diff} + J_{R-G}$. J_{R-G} makes only a very small contribution to the total current. Figure 4.3(b) shows the total current density and both contributions for *Cell B*. Until V_A is about $0.31\,V$, the slope of $J_{diff} + J_{R-G}$ equals $slope(J_{R-G})$ as theory specifies. At voltages lower than about $0.4\,V$, the total current is dominated by J_{R-G} and at voltages larger than about $0.4\,V$, the diffusion current dominates. In Figure 4.3(c), we show the results for *Cell C*. Here J_{R-G} dominates up to voltages of about $1.2\,V$. The slope of J_{R-G} for the three cells is less than $1/kT$ which is reasonable since J_{R-G} does not dominate at larger voltages.

These dark current density results, based on the excess minority carrier concentrations obtained using the tridiagonal matrix algorithm, have been compared with dark current density results obtained by directly solving the minority carrier diffusion equations with the boundary conditions. The results are almost an entirely perfect match which indicates that the generation rate calculations of Chapter 2 and the tridiagonal matrix algorithm method provide a good method to finding the dark current densities.

4.5.2 Photocurrent Density

As discussed in Chapter 3, when the cells are subjected to the photon source, the excess minority carrier concentrations may increase substantially. Recall that the excess minority hole concentration increases in the $n-In_{y_{\max}}Ga_{1-y_{\max}}N$ layer for the three cells. Further for *Cell A* and *Cell B* no electron-hole pair generation occurs in the $p-GaN$ layer therefore, excess minority electron concentrations remain unperturbed. As a result of the generation, the current density for the cells will be much larger than when no light source is present. Here we look at the current densities for the cells under illumination. Figure 4.4 shows the total photocurrent density for the three cells. The total photocurrent density is a summation of the current densities due to diffusion, recombination in the

depleted regions and intrinsic region, and generation in the depleted regions and intrinsic region, that is $J_{total} = J_p + J_n + J_i + J_{R-G}$.

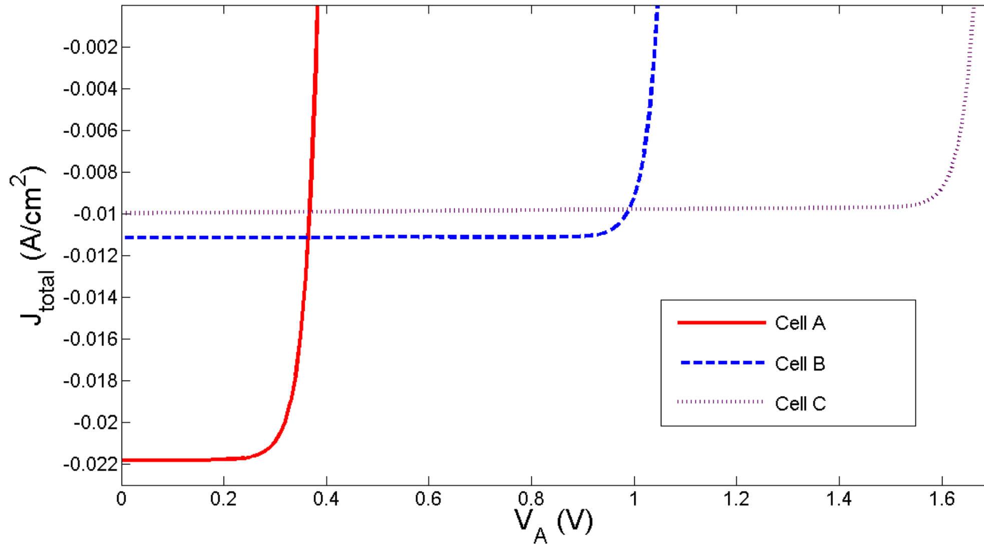

Figure 4.4 Total photocurrent density.

Cell A has the largest short-circuit current density at $-0.0218\ A/cm^2$, but the smallest open circuit voltage at $0.385\ V$. Cells B and C have short-circuit current densities of -0.0112 and $-0.0100\ A/cm^2$, respectively. *Cell C* has the largest open-circuit voltage at $1.665\ V$.

Figure 4.5 shows the current density components for each cell. That is, electron and hole diffusion currents, depleted region and intrinsic region generation and recombination currents. The total photocurrent density is also shown.

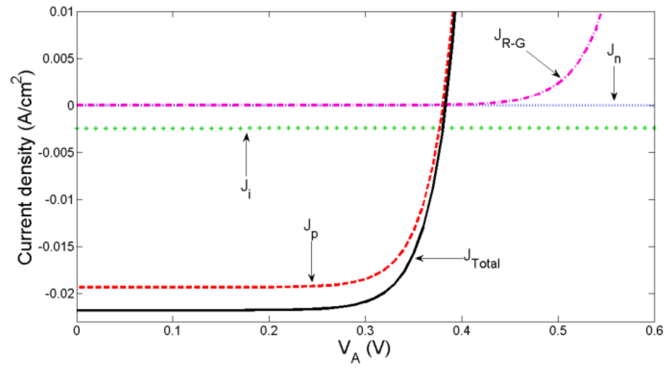

(a)

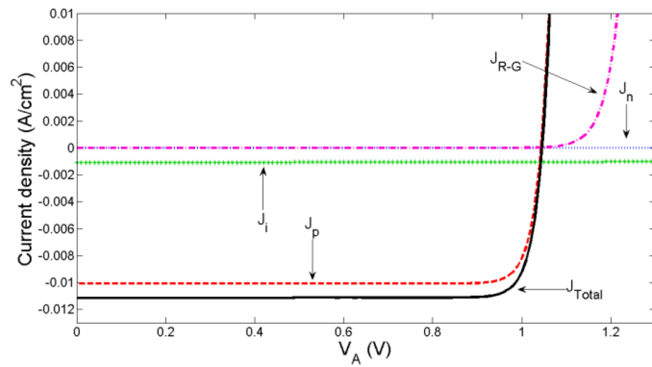

(b)

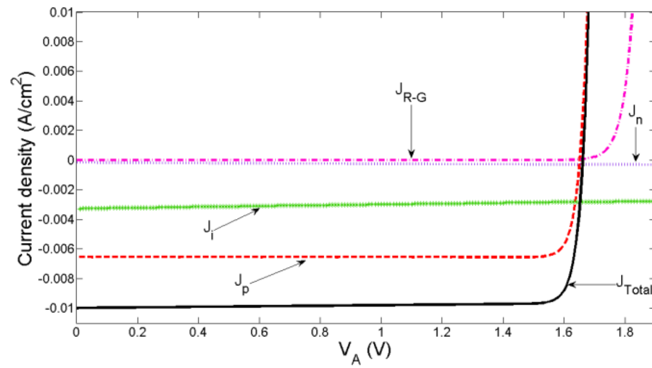

(c)

Figure 4.5 Total photocurrent density and photocurrent density contributions for (a) *Cell A* (b) *Cell B* and (c) *Cell C*.

The minority carrier hole diffusion current contributes most significantly to the total photocurrent density, with J_{total} almost equivalent to J_p. Since the $p-GaN$ layer is transparent for $Cell\ A$ and $Cell\ B$ and little carrier generation occurs in this region for $Cell\ C$, the minority carrier electron diffusion current is obviously very small. For $Cell\ A$ and $Cell\ B$, the minority carrier electron diffusion current density is due only to injection from the $n-In_{y_{max}}Ga_{1-y_{max}}N$ layer so J_n is the same as if no photon source is present. $Cell\ C$ has a slightly larger J_n than if no photon source is present. The generation current in the intrinsic and depleted regions affects the slope of the total photocurrent density at low voltages. This current is largest for $Cell\ C$ and smallest for $Cell\ B$. Finally, we see that J_{R-G} has insignificant influence on the total photocurrent density even though it is important for the dark current of cells B and C as seen in Figure 4.3.

4.5.3 Effect of $n-In_{y_{max}}Ga_{1-y_{max}}N$ Layer Thickness on Photocurrent Density

We next explore the effects of the $n-In_{y_{max}}Ga_{1-y_{max}}N$ layer thickness on the total photocurrent density for the illuminated cells. When considering the three layers of the cells, the thickness of the $n-In_{y_{max}}Ga_{1-y_{max}}N$ layer will have the most influence on the solar cell photocurrent density as we have discovered that most generation occurs in this layer and that the generation in the other two layers do not significantly contribute to the overall generation of the device. Here, we vary the thickness of the $n-In_{y_{max}}Ga_{1-y_{max}}N$ layer from $0.120\ \mu m$ to $0.920\ \mu m$ and observe the current density results. These results are shown in Figure 4.6 for each of the three cells.

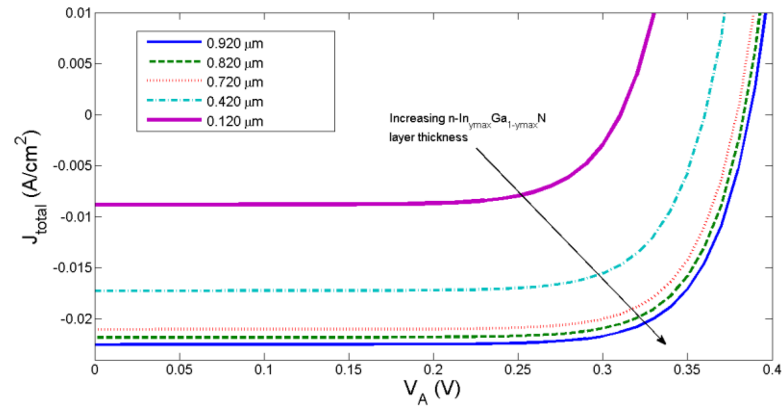

(a)

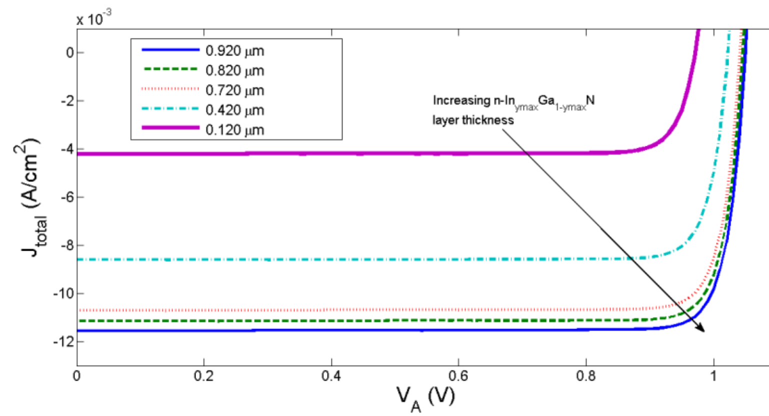

(b)

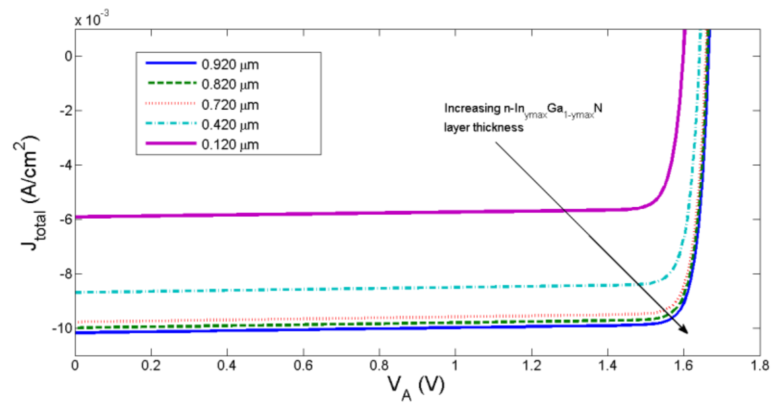

(c)

Figure 4. $n-In_{y_{\max}}Ga_{1-y_{\max}}N$ [a] layer thickness influence on total photocurrent density (a) *Cell A* (b) *Cell B* (c) *Cell C* .

[a]In the figure, the subscript $y\max$ is equivalent to $y_{\max}$.

From the figure, it is obvious that the current density increases as the $n-In_{y_{\max}}Ga_{1-y_{\max}}N$ layer thickness increases. However, once the layer thickness exceeds the diffusion length significantly, the increase in the photocurrent saturates. Table 4.1 gives the open-circuit voltages and the magnitude of the short-circuit current densities for the three illuminated cells as a function of $n-In_{y_{\max}}Ga_{1-y_{\max}}N$ layer thickness, including the thickness of the original design.

Table 4.1 Open-circuit voltage and short-circuit current density for varying $n-In_{y_{\max}}Ga_{1-y_{\max}}N$ layer thickness (a) *Cell A* (b) *Cell B* (c) *Cell C*

(a)

Width (μm)	0.920	0.820	0.720	0.420	0.120
V_{OC} (V)	0.385	0.385	0.375	0.365	0.315
$\lvert J_{SC}\rvert$ (A/cm^2)	0.0225	0.0218	0.0210	0.017	0.0088

(b)

Width (μm)	0.920	0.820	0.720	0.420	0.120
V_{OC} (V)	1.045	1.045	1.045	1.025	0.975
$\lvert J_{SC}\rvert$ (A/cm^2)	0.0115	0.0112	0.0107	0.00861	0.00421

(c)

Width (μm)	0.920	0.820	0.720	0.420	0.120
V_{OC} (V)	1.665	1.665	1.655	1.645	1.595
$\lvert J_{SC}\rvert$ (A/cm^2)	0.0101	0.0100	0.00978	0.00869	0.00591

The table shows that, in general, open-circuit voltage increases with increasing $n-In_{y_{\max}}Ga_{1-y_{\max}}N$ layer thickness. From 0.120 μm to 0.420 μm and 0.420 μm to 0.720 μm, the increase is obvious. However, further thickness increases do not show the increases in the open-circuit voltage at three significant figures. Short-circuit current density also obviously increases with increasing layer thickness.

4.6 Conclusions

In this chapter we explored the current density by discussing the individual contributions to the total current densities for the three PV cells under dark and light conditions. When the solar cell is not subject to light, the current density is the sum of the minority carrier diffusion current densities and the recombination current density. Under illumination, the photogeneration of carriers everywhere in the solar cell significantly increased the magnitude of the total current density.

The minority carrier diffusion current densities were derived beginning with Fick's first law. The total minority carrier diffusion in the solar cells is a sum of the individual diffusion current densities at the depletion region boundaries if recombination in the intrinsic and depleted regions is small. We obtained the intrinsic and depleted region current density by using the electron-hole pair generation data collected in Chapter 2. The recombination current in these regions was derived beginning with the Shockley Read Hall expression for carrier recombination-generation. This $R-G$ current density is important to consider for wide bandgap materials and for cases of wide junction regions.

Current density simulation results were shown graphically for the cells under dark and light conditions. Under dark and light conditions, *Cell A* experiences the largest total dark current density and *Cell C* experience the smallest total dark current density. *Cell A* has the largest dark current density because it involves the smallest bandgap $n-doped$ material. On the semilog plot, the slope of the total dark current density reaches $1/kT$ for all three cells at large bias. At low bias the current is dominated by the J_{R-G} component and the slope of $\log(J)$ versus V is smaller. For the illuminated cells,

the open-circuit voltage however is largest for *Cell C* and smallest for *Cell A*. The individual current density components were shown for each illuminated cell. The minority carrier diffusion current density is the largest contributor to the total photocurrent density as the $n-In_{y_{max}}Ga_{1-y_{max}}N$ layer experiences most of the generation. J_i influences J_{total} at lower voltages, but does not play a significant role at larger voltages. Further, J_n and J_{R-G} do not contribute significantly to the total photocurrent density.

Finally, we explored how the thickness of the $n-In_{y_{max}}Ga_{1-y_{max}}N$ layer affects the total current density of the illuminated cells. We observe that as the thickness of the layer increases, the total current density increases as does the open-circuit voltage and the short-circuit current density. With the results from Chapter 2, it is clear that this occurs because most of the carrier generation takes place in this layer.

5. Power Density and Performance Efficiency

5.1 Introduction

The photocurrent-voltage profiles obtained in Chapter 4 will be used to find the corresponding power-voltage curves and the maximum power point for each of the three cells. Operating a solar cell at the maximum power point voltage yields the highest efficiency. The figures of merit we consider for overall solar cell performance are the fill factor, FF, and energy conversion efficiency, η. Continuing with the analysis from Chapter 4, we will look at the effect of the $n-In_{y_{\max}}Ga_{1-y_{\max}}N$ layer thickness on the power density and performance efficiencies.

5.2 Power Density

We can obtain the power-voltage characteristics from $P = V * J$ and determine the maximum power point, P_m. This point is the maximum power deliverable to the PV load, thus it is most efficient to operate the solar cell at the corresponding voltage, V_m. The resulting current density is J_m. Figure 5.1 shows the power density curves as a function of applied cell voltage for the three cells under illumination. From the figure, it is obvious that *Cell C* provides the most power to the load while *Cell A* provides the least.

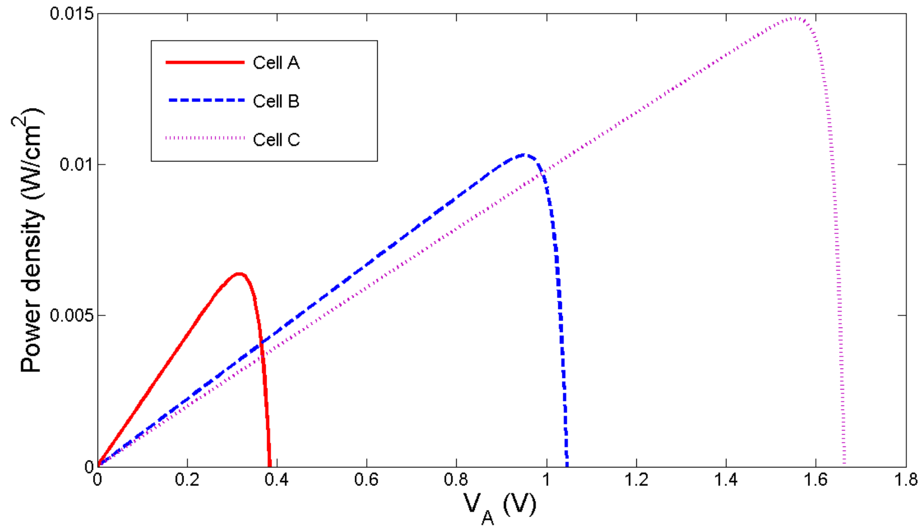

Figure 5.1 Power density as a function of applied cell voltage.

To illustrate the maximum power point power, current, and voltage, the maximum power point for *Cell A*, is shown in Figure 5.2 for the power-voltage and current-voltage profiles. A vertical line connects the apex of the power-voltage curve to the corresponding current density on the current-voltage curve. Since power density is a product of the current density and corresponding voltage, the maximum power point is the product of V_m and J_m.

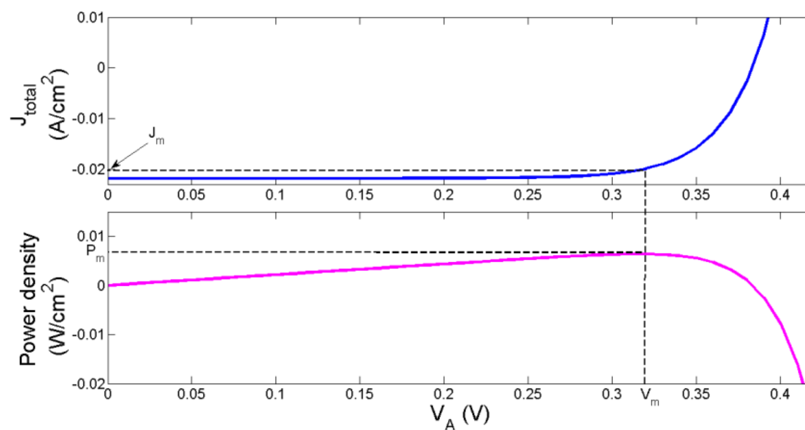

Figure 5.2 Example of maximum power point power, voltage and current density.

Table 5.1 shows the values of the maximum power point power, voltage, and current density for the three cells. Maximum P_m occurs for the GaN-rich cell and the InN-rich cell provides the smallest P_m.

Table 5.1 Maximum power point voltage, current, and power.

Parameter	$Cell\ A$	$Cell\ B$	$Cell\ C$
$V_m\quad(V)$	0.325	0.955	1.555
$J_m\quad(A\cdot cm^{-2})$	0.0202	0.0109	0.00960
$P_m\quad(W\cdot cm^{-2})$	0.00657	0.0104	0.0150

If we were to design the system without spectral splitting, the maximum operating voltages would be slightly larger for $Cell\ A$ and $Cell\ B$.

5.3 Fill Factor

The Fill factor expresses the solar cell conversion efficiency by relating the actual obtainable maximum output power (P_m) to the product $V_{OC}J_{SC}$:

$$FF = \frac{P_m}{V_{oc}J_{sc}} \tag{5.1}$$

and is depicted in Figure 5.3 below.

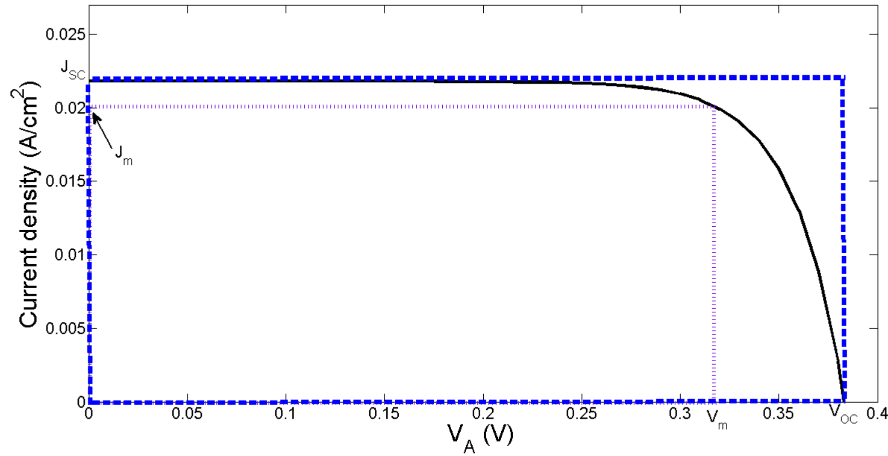

Figure 5.3 Fill factor is the ratio of the product of $J_m V_m$ to $J_{SC} V_{OC}$.

In the figure, FF is the ratio of the large rectangle to the smaller rectangle. The figure shows how FF can approach unity as the current-voltage curve becomes more square shaped. However, necessarily $FF < 1$ for all realistic diodes. For cells A, B, and C, we calculate FF = 0.782, 0.892, and 0.897, respectively. These values are within the typical range for commercial grade PV technologies which have fill factors greater than 0.7. (Less expensive, or Grade B, PV technologies generally have fill factor values between 0.4 and 0.7.)

5.4 Energy Conversion Efficiency

The energy conversion efficiency, η, gives the ratio of the output power to the input power, P_{in}, or

$$\eta = \frac{P_m}{P_{in}} \tag{5.2}$$

where we let the output power equal P_m because we want to operate the PV cell at the maximum power since this is the most efficient operating mode. We calculate the overall efficiency of the three cell array and the efficiencies of the individual cells. The overall

efficiency is the sum of P_m for the three cells divided by the input power provided by the photon source, or,

$$\eta = \frac{P_{m_A} + P_{m_B} + P_{m_C}}{\int_{\hbar\omega_{\min}}^{\hbar\omega_{\max}} d\hbar\omega \phi(\hbar\omega)\hbar\omega} \tag{5.3}$$

where the subscript of P_m indicates $Cell\ A$, B, or C. In calculating the overall efficiency, in this system, $\hbar\omega_{\min} = 0.7\ eV$ and $\hbar\omega_{\max} = 5.0\ eV$.

The individual efficiencies are the ratio of the cell maximum power to the cell incident power provided by the photon source. In Equation 5.3, the numerator is reduced to the maximum power of the specific cell and the denominator has the integration limits of the appropriate segment of the solar spectrum for the specific cell; e.g for $Cell\ A$, the $\hbar\omega_{\min}$ = 0.7 eV and the $\hbar\omega_{\max}$ = 1.38 eV. These results are also shown in Table 5.2.

Table 5.2 Overall and individual energy conversion efficiencies.

Calculation	Overall	$Cell\ A$	$Cell\ B$	$Cell\ C$
$P_{in}\ (W/cm^2)$	0.0886	0.0300	0.0261	0.0316
η (%)	36.12	21.2	39.5	46.9

The overall efficiency, 36.12 %, is competitive with existing technologies. As mentioned in Chapter 1, existing silicon PV devices can only reach efficiencies approaching 30%. Multi-junction devices yield higher efficiencies and currently the largest efficiencies achieved are approximately 43%. Further optimization of our PV design, could lead to higher efficiencies and thus approach (and potentially exceed) current maximum obtainable values. For example, earlier simulations, based on an analogous system design to that explored in this thesis, resulted in inadequate η values.

To increase η, the system was modified such that the donor doping concentration and the $n-In_{y_{\max}}Ga_{1-y_{\max}}N$ layer width was increased in each cell. Increasing these parameters increased η because, as we know, most of the electron-hole pair generation occurs in this layer. Next, we will show how increasing the $n-In_{y_{\max}}Ga_{1-y_{\max}}N$ layer width leads to higher efficiencies.

5.5 Effect of $n-In_{y_{\max}}Ga_{1-y_{\max}}N$ Layer Thickness on Power Density and Performance Efficiency

5.5.1 Power Density

Using the total current density data collected in Chapter 4, we can find the power density of the cells for differing $n-In_{y_{\max}}Ga_{1-y_{\max}}N$ layer thicknesses. The results are presented in Figure 5.4.

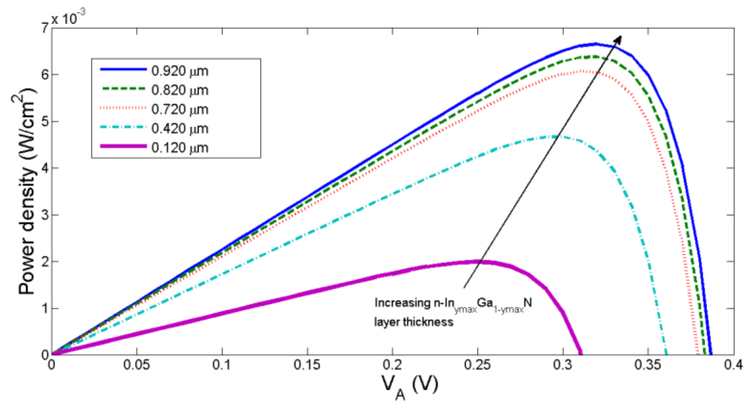

(a)

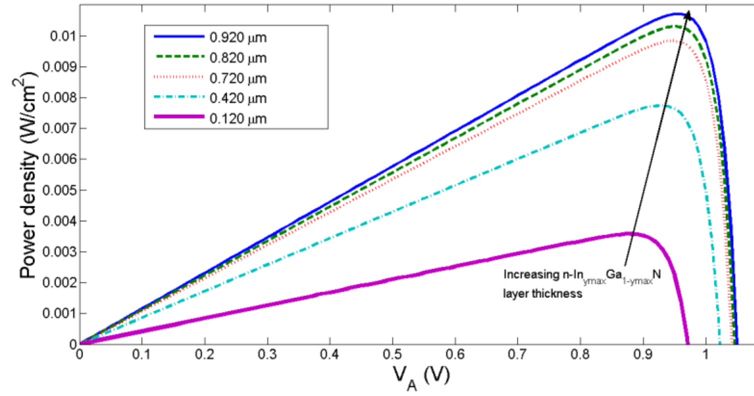

(b)

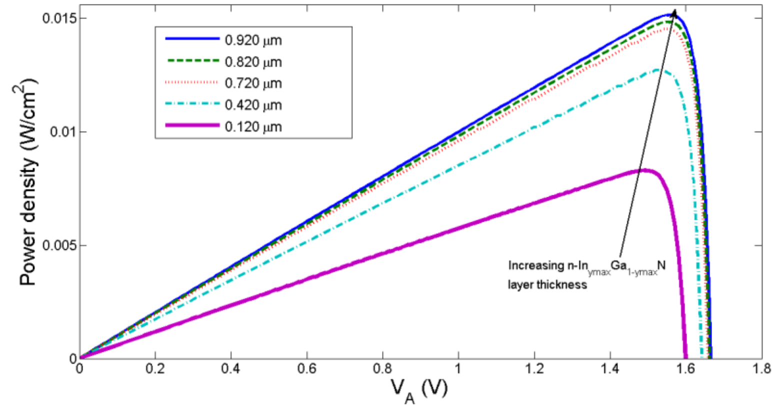

(c)

Figure 5.4 $n-In_{y_{max}}Ga_{1-y_{max}}N$ [a] layer thickness effect on power density (a) *Cell A* (b) *Cell B* and (c) *Cell C*

[a] in the figure, the subscript $y\max$ is equivalent to y_{max}

Increasing the $n-In_{y_{max}}Ga_{1-y_{max}}N$ layer thickness leads to increased power output of the solar cell. Table 5.3 shows the maximum power point power, voltage, and current as a function of thickness for each of the three cells, including the thickness of the original design.

Table 5.3 Maximum power point power, voltage, and current, for varying layer $n-In_{y_{\max}}Ga_{1-y_{\max}}N$ layer thickness (a) *Cell A* (b) *Cell B* (c) *Cell C*.

(a)

width (μm)	0.920	0.820	0.720	0.420	0.120
V_m (V)	0.325	0.325	0.315	0.305	0.255
J_m (A/cm^2)	0.021	0.0202	0.0198	0.0158	0.00807
P_m (W/cm^2)	0.00684	0.00657	0.00623	0.00482	0.00206

(b)

width (μm)	0.920	0.820	0.720	0.420	0.120
V_m (V)	0.965	0.955	0.955	0.935	0.885
J_m (A/cm^2)	0.0112	0.0109	0.0104	0.00837	0.00408
P_m (W/cm^2)	0.0108	0.0104	0.00994	0.00782	0.00361

(c)

width (μm)	0.920	0.820	0.720	0.420	0.120
V_m (V)	1.565	1.555	1.555	1.535	1.495
J_m (A/cm^2)	0.00973	0.00960	0.00936	0.00831	0.00558
P_m (W/cm^2)	0.0152	0.0150	0.0146	0.0128	0.00834

5.5.2 Fill Factor

Table 5.4 lists the fill factors for each of the three cells as a function of the $n-In_{y_{\max}}Ga_{1-y_{\max}}N$ layer thickness. In general, the fill factor increases as the

$n-In_{y_{max}}Ga_{1-y_{max}}N$ layer is made thicker. The oscillation for the fill factor of *Cell A* at 0.820 μm is due to rounding error.

Table 5.4 Fill factor for varying $n-In_{y_{max}}Ga_{1-y_{max}}N$ layer thickness

width (μm)	0.920	0.820	0.720	0.420	0.120
Cell A FF	0.789	0.782	0.790	0.767	0.713
Cell B FF	0.896	0.892	0.888	0.886	0.879
Cell C FF	0.899	0.897	0.896	0.892	0.884

5.5.3 Energy Conversion Efficiency

Table 5.5 shows the results for the energy conversion efficiency as a function of $n-In_{y_{max}}Ga_{1-y_{max}}N$ layer thickness for all three cells. The input power for *Cell A*, *B*, and *C* is 0.0300, 0.0261, and 0.0316 W/cm^2, respectively. Increasing the $n-In_{y_{max}}Ga_{1-y_{max}}N$ layer thickness leads to larger η values.

Table 5.5 Energy conversion efficiency for varying $n - In_{y_{max}}Ga_{1-y_{max}}N$ layer thickness (a) *Cell A* (b) *Cell B* (c) *Cell C* and (d) overall

(a)

width (μm)	1.20	0.920	0.820	0.720	0.420	0.120
η (%)	24.02	22.0	21.20	20.77	16.07	6.87

(b)

width (μm)	1.20	0.920	0.820	0.720	0.420	0.120
η (%)	44.15	41.38	39.50	38.08	29.96	13.83

(c)

width (μm)	1.20	0.920	0.820	0.720	0.420	0.120
η (%)	49.84	48.10	46.90	46.20	40.51	26.39

(d)

width (μm)	1.20	0.920	0.820	0.720	0.420	0.120
η (%)	39.42	37.09	36.12	34.75	28.73	15.82

5.6 Conclusions

In this chapter we explored power density and performance efficiency. Using the total photocurrent density results obtained in Chapter 4, we generated the data necessary to create plots of the power density. We discussed maximum power point and found the maximum power point power, voltage, and current density for each of the three cells under illumination. The largest maximum power point is provided by *Cell C* while *Cell A* provides the smallest.

Following the power density discussion, we introduced two figures of merit. Individually, the cells provided fill factors and energy conversion efficiencies within a competitive range, based on existing technologies. Overall, the widegap cell performed the most efficiently as a PV. As the three cell array, the energy conversion efficiency obtained also lies within a competitive range.

Finally, we concluded our analysis of the $n-In_{y_{max}}Ga_{1-y_{max}}N$ layer thickness effects on the solar cell performance. Specifically, we observed that a positive relationship exists between the thickness of this region and the power density, fill factor, and energy conversion efficiencies or the solar cell. That is, as the cell is designed with larger $n-In_{y_{max}}Ga_{1-y_{max}}N$ layer thickness, the solar cell performance improves. However, there are clear limitations that prevent an indefinite increase in the thickness, but these are beyond the scope of this thesis.

6. Future Work

6.1 Introduction

Here we briefly explore possibilities for future work on the system based on the desire to further increase efficiencies. No systematic optimization of the design parameters was attempted in this research. However, several modifications appear to merit further invesitigation. We discuss possible parameters to be adjusted that may further better design performance. Then we explore another $i-In_yGa_{1-y}N$ layer grading scheme.

6.2 Parameter Adjustments

In Chapter 4 we briefly explored the effects of the $n-In_{y_{\max}}Ga_{1-y_{\max}}N$ layer thickness on the current density for the cells under illumination. Chapter 5 continued this analysis by extending the discussion to power density and performance efficiency. Based on such results, we could potentially choose a better design. For example, as we saw, increasing the $n-In_{y_{\max}}Ga_{1-y_{\max}}N$ layer thickness leads to more efficient operation.

Varying the thickness of the $n-In_{y_{\max}}Ga_{1-y_{\max}}N$ layer is one example of a design parameter adjustment reasonable to consider. There are other parameters we could adjust as well. In consideration of the layer thicknesses, varying the $p-GaN$ layer does not appear to be promising because this layer basically is transparent, but examining the influence of the $i-In_yGa_{1-y}N$ layer thickness may be rewarding. Other parameters to consider would be the doping concentrations. For example, as mentioned in Chapter 5, by increasing the doping concentration of N_D, we were able to increase the energy conversion efficiency. This would also vary material parameters such as mobility and lifetime. For this material system, such parameters are difficult to control and determine experimentally so by varying them through simulation we can determine their relative importance on the results. Another parameter that could be varied is the composition of

the $n-In_{y_{\max}}Ga_{1-y_{\max}}N$ layer. While, as mentioned in Chapter 1, an earlier analysis has shown that the compositions used in this work yield the highest efficiencies, further study is definitely warranted.

6.3 Parabolic Grading

Currently, the design implements linear grading of the $i-In_yGa_{1-y}N$ layer. This grading scheme is not necessarily the best and thus analyzing various alternatives is of interest for future work. Suppose the $i-In_yGa_{1-y}N$ layer is fabricated such that the grading is parabolic as shown in Figure 6.1.

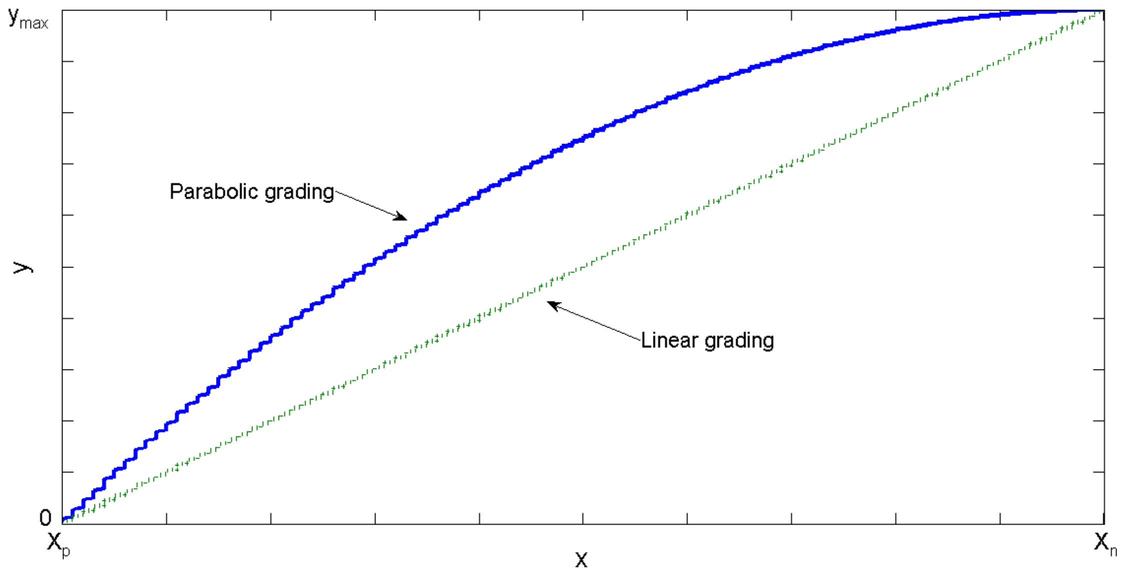

Figure 6.1 Parabolic grading of the $i\text{-}In_yGa_{1\text{-}y}N$ layer shown with presently implemented linear grading scheme.

Then, we let the composition depend on the position as

$$y(x) = y_{\max} - \frac{y_{\max}}{(x_n - x_p)^2}(x_n - x)^2 \tag{6.1}$$

Now the bandgap is dependent on Equation 6.1 instead of Equation 1.2 and the analysis performed in this thesis can be redone with this grading scheme. Comparing these results with those of the linear grading scheme can provide insight which may lead to a more efficient solar cell. The grading is not necessarily limited to parabolic grading, but the latter provides a good starting point.

6.4 Conclusion

Here we introduced possible design modifications for future work considerations. Adjusting the parameters also may lead to more efficient devices, such as we saw with the $n-In_{y_{\max}}Ga_{1-y_{\max}}N$ layer thickness discussions of Chapters 4 and 5. Therefore, we mentioned a few possible parameters to further explore. Finally, while our design implements linear grading of the intrinsic region, other grading schemes may further increase PV performance, thus parabolic grading was introduced.

Bibliography

1) Basic Research Needs for Solar Energy Utilization: Report of the Basic Energy Sciences Workshop on Solar Energy Utilization April 18 – 21 2005, http://chem.ps.uci.edu/~lawm/DOE%20Solar%20Pathways%20Report.pdf. (Retrieved August 15, 2011).

2) Worldometers, http://www.worldometers.info/population/. (Retreived August 9, 2011).

3) U. S. Census Bureau, http://www.census.gov/population/international/data/idb/worldpopgraph.php. (Retrieved August 9, 2011).

4) Department of Economic and Social Affairs : Population Division, *World Population Prospects: The 2008 Revision*, http://www.un.org/esa/population/publications/popnews/Newsltr_87.pdf. (Retrieved August 9, 2011).

5) Department of Economic and Social Affairs: United Nation Population Division, *World Population Prospects, the 2000 Revision, Vol. III,* p. 171, http://www.un.org/esa/population/publications/wpp2000/chapter5.pdf. (Retrieved August 9, 2011).

6) Carbon Dioxide Information Analysis Center, http://cdiac.ornl.gov/. (Retrieved August 15, 2011.)

7) U. S. Energy Information Administration, http://www.eia.gov/. (Retrieved August 16, 2011).

8) Renewables 2011 Global Status Report, www.ren21.net. (Retrieved August 14, 2011).

9) U.S. Department of Energy, The History of Solar. http://www1.eere.energy.gov. (Retrieved July 22, 2011).

10) Oliver Morton, *Nature*, **443**, 19-22 (2006).

11) Environmental Defense Fund, http://www.edf.org. (Retrieved August 8, 2011).

12) Richard Williams, *J. Chem. Phys.*, **32**, 1505 (1960).

13) Perlin, From Space to Earth (The Story of Solar Electricity). Harvard University Press (1999).

14) Acetal-Lucent, http://www.alcatel-lucent.com/wps/portal/belllabs. (Retrieved August 8, 2011).

15) A. Shah, et al., *Science*, **285**, 692 (1999).

16) William Shockley and Hans J. Queisser, *J. Appl. Phys.*, **32**, 510 (1961).

17) Renewable Energy Focus, www.renewableenergyfocus.com. (Retrieved August 12, 2011).

18) U.S. Department of Energy, 1$/W Photovoltaic Systems, http://www1.eere.energy.gov. (Retrieved August 16, 2011).

19) National Renewable Energy Laboratory. http://rredc.nrel.gov/solar/spectra/am1.5/. (Retrieved May 2, 2011).

20) Junqiao Wu, *J. Appl. Phys.*, **106**, 011101 (2009).

21) J. Wu and W. Walukiewicz, *Superlattices and Microstructures*, **34**, 63-75 (2003).

22) A. Devos, *Endoreversible Thermodynamics of Solar Energy Conversion*, Oxford University Press, New York (1992).

23) J. Wu, W. Walukiewicz, K. M. Yu, W. Shan, J. W. Ager III, E. E. Haller, Hai Lu, William J. Schaff, W. K. Metzger, and Sarah Kurtz, *J. Appl. Phys.*, **94**, 6477 (2003).

24) Robert F. Davis, *Journal of Crystal Growth*, **137**, 161-169 (1994).

25) H. Z. Xu, A. Bell, Z. G. Wang, Y. Okada, M. Kawabe, I. Harrison, C. T. Foxon, *Journal of Crystal Growth*, **222**, 96-103 (2001).

26) H. P. Maruska and J. J. Tietjen, *Appl. Phys. Lett.* **15**, 327 (1969).

27) W. M. Yim, E. J. Stofko, P. J. Zanzucchi, J. I. Pankove, M. Ettenberg, and S. L. Gilbert, *J. Appl. Phys.*, **44**, 292 (1973).

28) I. Vurgaftman, J. R. Meyer, and L. R. Ram-Mohan, *J. Appl. Phys.*, **89**, 5815 (2001).

29) A. Barnett, et al, Milestones Toward 50% Efficient Solar Cell Modules, *22nd European Photovoltaic Solar Energy Conference* (Milan, Italy 3 September 2007).

30) Elaissa Trybus, Gon Namkoong, Walter Henderson, Shawn Burnham, W. Alan Dooltile, Maurice Cheung, Alexander Cartwrite, *Journal of Crystal Growth*, **288**, 218-224 (2006).

31) G. F. Brown, et al., Sol. Energy Mater. Sol. Cells (2009), doi :10.1016/j.solmat.2009.11.010.

32) Antonio Luque, *J. Appl. Phys.*, **110**, 031301 (2011).

33) Ashraful Ghani Bhuiyan, Kenichi Sugita, Ken Kasashima, Akihiro Hashimoto, Akio Yamamoto, and Valery Yu. Davydov, *Appl. Phys. Lett.* **83**, 4788 (2003).

34) Takashi Matsuoka, Hiroshi Okamoto, Masashi Nakao, Hiroshi Harima, and Eiji Kurimoto, *Appl. Phys. Lett.* **81**, 1246 (2002).

35) W. Walukiewicz, S. X. Li, J. Wu, K. M. Yu, J. W. Ager III, E. E. Haller, Hai Lu, William J. Schaff, *Journal of Crystal Growth* **269**, 119-127 (2004).

36) J. Wu, W. Walukiewicz, W. Shan, K. M. Yu, J. W. Ager III, S. X. Li, E. E. Haller, Hai Lu, and William J. Schaff, *J. Appl. Phys.* **94**, 4457 (2003).

37) T. L. Tansley and C. P. Foley, *J. Appl. Phys.* **59**, 3241 (1986).

38) H. Morkoç, Nitride Semiconductors and Devices 2nd edition, (Spring, Heidelberg).

39) J. Wu, W. Walukiewicz, K. M. Yu, J. W. Ager III, E. E. Haller, Hai Lu, and William J. Schaff, *phys. stat. sol (b)*, **240**, No. 2, 412-416 (2003).

40) M. Gloeckler and J. R. Sites, *J. Phys. Chem. Solids*, **66**, 1891 – 1894 (2005).

41) G. Sassi, *J. Appl. Phys.*, **54**, 5421 (1983).

42) G. F. Virshup, C. W. Ford, and J. G. Werthen, *Appl. Phys. Lett.*, **47**, 1319 (1985).

43) Nadia H. Rafat and S. E. –D. Habib, *Solar Energy Materials and Solar Cells*, **55**, 341 (1998).

44) Hasna Hamzaoui, Ahmed S. Bouazzi, Bahri Rezig, *Solar Energy Materials and Solar Cells*, **87**, 595 (2005).

45) Sarah R. Kurtz, P. Faine, and J. M. Olson, *J. Appl. Phys.*, **68**, 1890 (1990).

46) L. Hsu and W. Walukiewicz, *J. Appl. Phys.*, **104**, 024507 (2008).

47) N. Miller, R. E. Jones, K. M. Yu, J. W. Ager, Z. Liliental-Weber, E. E. Haller, W. Walukiewicz, T. L. Williamson, and M. A. Hoffbauer, *phys. stat. sol (c)*, **5**, No. 6, 1866 - 1869 (2008).

48) A. Barnett et al, *33rd IEEE Photovoltaic Specialists Conference* (San Diego, May 12-16 2008).

49) L. A. Reichertz, et al., *AIP Conference Proceedings*, **1068**, 159 – 164 (2008).

50) J. Wu, W. Walukiewicz, K. M. Yu, J. W. Ager III, E. E. Haller, Hai Lu, William J. Schaff, *Applied Physics Letters* **80**, 4741-4743 (2002).

51) Science @ Berkeley, http://enews.lbl.gov/. (Retrieved August 18, 2011).

52) E. R. Torrey, P.P. Ruden, and P. I. Cohen, *J. Appl. Physics.* **109**, 074909 (2011).

53) C. Caetano, L. K. Teles, M. Marques, A. Dal Pni, Jr., and L. G. Ferreira, *Phys. Rev. B*, **74**, 045215 (2006).

54) I. Vurgaftman and J. R. Meyer, *J. Appl. Phys.*, **94**, 3675 (2003).

55) Wei Li, Peder Bergman, Ivan Ivanov, Wei-Xin Ni, H. Amano, and I. Akasa, *Appl. Phys. Lett.* **69**, 3390 (1996).

56) Donald A. Neaman, Semiconductor Physics and Devices, Third Edition, Tate McGraw-Hill, (2007).

57) Robert F. Pierret, Semiconductor Device Fundamentals, Addison-Wesley Publishing Company, Inc. (1996).

58) S. P. Fu and Y. F. Chen, *Applied Physics Letters* **85**, 1523-1525 (2004).

59) M.E. Levinshtein, S.L. Rumyantsev, M.S. Shur, Properties of Advanced Semiconductor Materials: GaN, AlN, InN, BN, SiC, SiGe, John Wiley & Sons, New York (2001).

60) B. Santic, *Semicond. Sci. Technol*. **18** 219–224 (2003).

61) National Renewable Energy Laboratory, http://rredc.nrel.gov/solar/spectra/am1.5/. (Retrieved August 9, 2011).

A Photon Source

In our system, a normalized $5200\,K$ black body spectrum emulates the direct-plus-circumsolar AM1.5 ASTM standard G173-03 solar spectrum.[61] As shown below in Figure A.1, this black body spectrum provides an acceptable approximation to this solar spectrum.

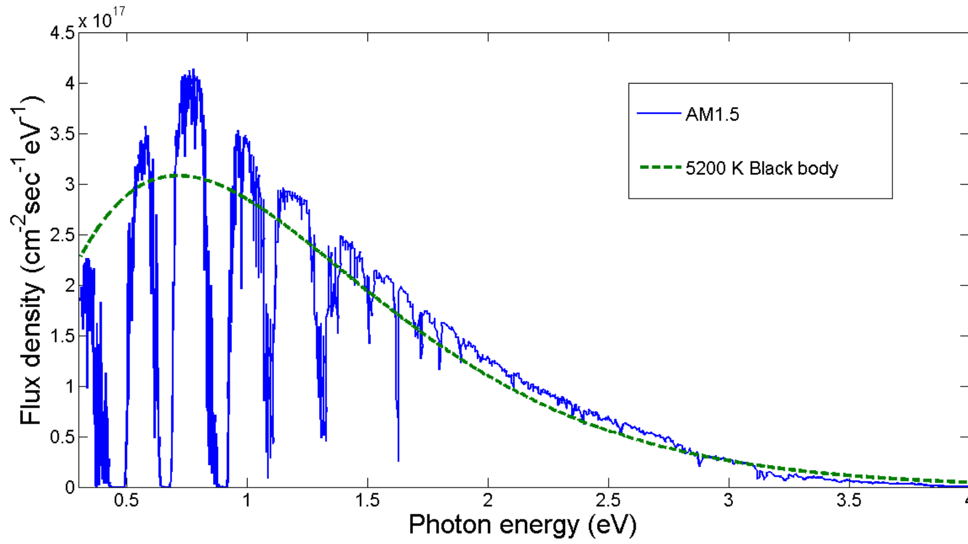

Figure A.1 The normalized $5200\,K$ black body spectrum compared with the terrestrial AM1.5 solar spectrum.

Total flux density of the AM1.5 solar spectrum is 3.99 x 10^{17} $cm^{-2}\sec^{-1}eV^{-1}$ and the total power per area is 900 W/m^2. For the black body spectrum the total flux density is 4.71 x 10^{17} $cm^{-2}\sec^{-1}eV^{-1}$ and the total power per area is 970 W/m^2.

The photon flux as a function of photon energy, provided by the black body spectrum, is given by the equation

$$\phi(\hbar\omega) = \frac{N(\hbar\omega)^2}{\left(\exp\left(\hbar\omega/kT\right)-1\right)} \tag{A.1}$$

where N is the normalizing factor, k is Boltzmann's constant, $\hbar$ is Planck's constant, and T is the temperature of the black body. We use the normalizing factor and the temperature to fit the black body spectrum to the solar spectrum.

B Tridiagonal Matrix Algorithm

In numerical linear algebra, the tridiagonal matrix algorithm, also called the Thomas Algorithm, enables one to efficiently solve a tridiagonal system of equations for N unknowns, σ_i, using Gaussian elimination techniques. Commonly encountered actual systems benefiting from this method include one-dimensional diffusion problems, for example those in Chapter 3 with $\Delta n(x)$ and $\Delta p(x)$ as unknowns. The following equation satisfies the characterization of a tridiagonal system:

$$a_i\sigma_{i-1} + b_i\sigma_i + c_i\sigma_{i+1} = d_i \tag{B.1}$$

with $a_1 = c_N = 0$. Recalling Equation 3.26, we can see that our system also satisfies that of a tridiagonal one with N unknowns, Δn_i, and

$$a_i = c_i = D_e \frac{1}{(\Delta x)^2} \quad ; \quad a_i \neq a_1 \; c_i \neq c_N \tag{B.2}$$

$$b_i = \left(D_e \frac{-2}{(\Delta x)^2} - \frac{1}{\tau_e} \right) \tag{B.3}$$

$$d_i = -G_i,\ d_1 = -G_1 - \Delta n_0 D_e \frac{1}{(\Delta x)^2}, \text{ and } d_N = -G_N - \Delta n_{N+1} D_e \frac{1}{(\Delta x)^2} \tag{B.4}$$

Putting Equation B.1 into matrix form,

$$\begin{bmatrix} b_1 & c_1 & 0 & \cdots & 0 \\ a_2 & b_2 & c_2 & & \vdots \\ 0 & a_3 & b_3 & \ddots & 0 \\ \vdots & & \ddots & \ddots & c_{N-1} \\ 0 & \cdots & 0 & a_N & b_N \end{bmatrix} \begin{bmatrix} \sigma_1 \\ \sigma_2 \\ \sigma_3 \\ \vdots \\ \sigma_N \end{bmatrix} = \begin{bmatrix} d_1 \\ d_2 \\ d_3 \\ \vdots \\ d_N \end{bmatrix} \tag{B.5}$$

basically illustrates the method to solving this system. For example, we see that $\sigma_N = {d_N}/{a_N + b_N}$ and by substituting this into the $N-1$ equation will eliminate σ_N. Proceeding in this manner until $N=1$ will yield an expression dependent only on σ_1, which in turn supplies an expression for σ_2 and so forth until one finds σ_N. Indirectly, the Thomas Algorithm performs this process through implementation of the following three steps: *(1) Decomposition*, *(2) Forward Substitution,* and *(3) Back Substitution*.

(1) Decomposition

Modify the matrix elements such that for $2 \le i \le N$, $a_i' = a_i / b_{i-1}'$ where $b_i' = b_i - a_i' c_{i-1}$ and $b_1' = b_1$. Software implementation includes the simple DO loop:

$b_1' = b_1$

DO $i = 2, N$

$a_i' = a_i / b_{i-1}'$

$b_i' = b_i - a_i' c_{i-1}$

END DO

(2) Forward Substitution

Modify the $d_i's$ such that $d_i' = d_i - a_i' d_{i-1}'$ for $2 \le i \le N$. Similarly to the above, a DO loop contains the calculations:

DO $i = 2, N$

$$d_i' = d_i - a_i' d_{i-1}'$$

END DO

(3) Back Substitution

Finally, this step finds the solutions for the $x_i's$ in the following loop:

$\sigma_N = d_N' / b_N'$

DO $i = N-1, 1, -1$

$$\sigma_i = \frac{d_i' - c_i \sigma_{i-1}}{b_i}$$

END DO

C Parasitic Resistance Effects*

C.1 Overview

Ideally, the solar cell equivalent circuit model consists of a photocurrent source in parallel with a diode as shown in Figure C.1(a). The solar cell is forward biased with a voltage, *V*. A more realistic approach includes the addition of inevitable parasitic factors, specifically, series resistance, R_S, and parallel resistance, R_P, as shown in Figure C.1(b). Series resistance models the resistance of the cell material and contacts, while the parallel resistance accounts for current leakage through the diode junction due to defects. The ideal diode model assumes $R_S \rightarrow 0$ and $R_P \rightarrow \infty$, and large values of R_S and small values of R_P will degrade the solar cell performance.

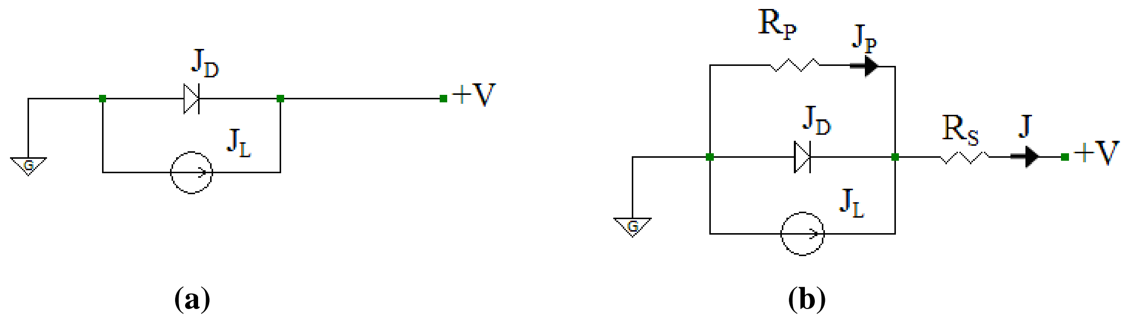

Figure C.1 Circuit schematics for the ideal and non-ideal solar cell (a) A current source in parallel with a diode models the ideal solar cell. (b) The addition of parallel and series resistances to the circuit schematic models the non-ideal solar cell. J_p represents the current across the parallel resistance.

*The work presented in this appendix summarizes presented material at *E32010 (Energy, Economics, and Environment) Upper Midwest's premier renewable energy conference.*

Here we explore the effects of the parasitic resistances on the *pin* graded heterojunction solar cell with the same structure as discussed in Chapter 1, but with different design parameters. To model the current density, we use the Shockley ideal diode equation for the diffusion current density and for the photocurrent density, we make the assumption that every photon of sufficient energy incident on the surface of the solar cell creates one electron-hole pair. Thus, the photocurrent density is the product of the electric charge and integral of the photon flux incident on the solar cell surface. We adjust the ideal current density equation to account for the parasitic resistances. The equation is obtained by simple circuit analysis and can be verified by referencing Figure C.2. Using the Equation C.1 and C.2, the slope of the non-ideal current densities when considering either series resistance or parallel resistance can be compared with the slope of the ideal current density. Finally, we show the influences of the resistances on solar cell current density, power density, and fill factor.

C.2 Equivalent Circuit Model and Parameters

C.2.1 Current Density

The sum of the Shockley ideal diode current, J_D, and the photocurrent, J_L,

$$J = J_L + J_s\left(e^{qV/kT} - 1\right) \tag{C.1}$$

provides the current-voltage characteristic of an ideal solar cell with $J_L < 0$ and $J_S > 0$. With the addition of the parasitic resistances, Equation C.1 becomes

$$J = J_L + J_s\left(e^{(V - JR_s)/V_T} - 1\right) + \frac{V - JR_S}{R_P} \tag{C.2}$$

where V_T refers to the thermal voltage and we assume a unity valued ideality factor.

C.2.2 Slope

The ideal diode has the forward bias slope,

$$\frac{dJ}{dV} = \frac{J_s e^{V/V_T}}{V_T} \tag{C.3}$$

which is proportional to the normalized conductance J_S / V_T. Considering series resistance only, the slope reduces such that

$$\frac{dJ}{dV} = \frac{J_s}{V_T} e^{(V - JR_s)/V_T} \tag{C.4}$$

and considering only parallel resistance, under forward bias,

$$\frac{dJ}{dV} \cong \frac{J_s e^{V/V_T}}{V_T} + \frac{1}{R_P} \tag{C.5}$$

For reverse bias the parallel resistance produces a slope proportional to $1/R_P$

$$\frac{dJ}{dV} = \frac{1}{R_P} \tag{C.6}$$

C.2.3 Open Circuit Voltage

Series resistance has no influence on V_{OC}, but the parallel resistance does. For the ideal case (C.1), we find

$$V_{OC} \cong V_T \ln\left(\frac{-J_L}{J_S}\right) \tag{C.7}$$

Now considering R_P we obtain the following implicit relationship:

$$V_{OC} \cong V_T \ln\left(\frac{-\left(J_L R_P + V_{OC}\right)}{J_S R_P}\right) \tag{C.8}$$

C.2.4 Short Circuit Current Density

The short circuit current density results mostly from the creation and collection of photon created carriers. That is, ideally, $J_{SC} = J_L$. To find the short-circuit current density in the parasitic model, we employ Equation C.2, set $J = J_{SC}$ and $V = 0$, and solve, yielding the transcendental equation,

$$J_{SC} = \frac{J_L + J_S(e^{-J_{SC}R_s/V_T} - 1)}{1 + \frac{R_S}{R_P}} \tag{C.9}$$

which simplifies to $J_{SC} = J_L$ for the ideal diode. Observably, both parasitic resistance terms act to reduce the short-circuit current density.

C.3 Results

C.3.1 Current Density

Smaller gap devices have higher conductivity and consequently exhibit increased current sensitivity to series resistance. Junction leakage greatly affects the current density for highly resistive, large gap devices. Figure C.2 shows the effects of the parasitic resistances on the cells most sensitive to each resistance. Figure C.2(a) shows

the influence of series resistance on current density of a cell with an $n-InN$ layer and Figure C.2(b) shows the influence of parallel resistance on current density of a cell with an $n-In_{0.624}Ga_{0.376}N$ layer.

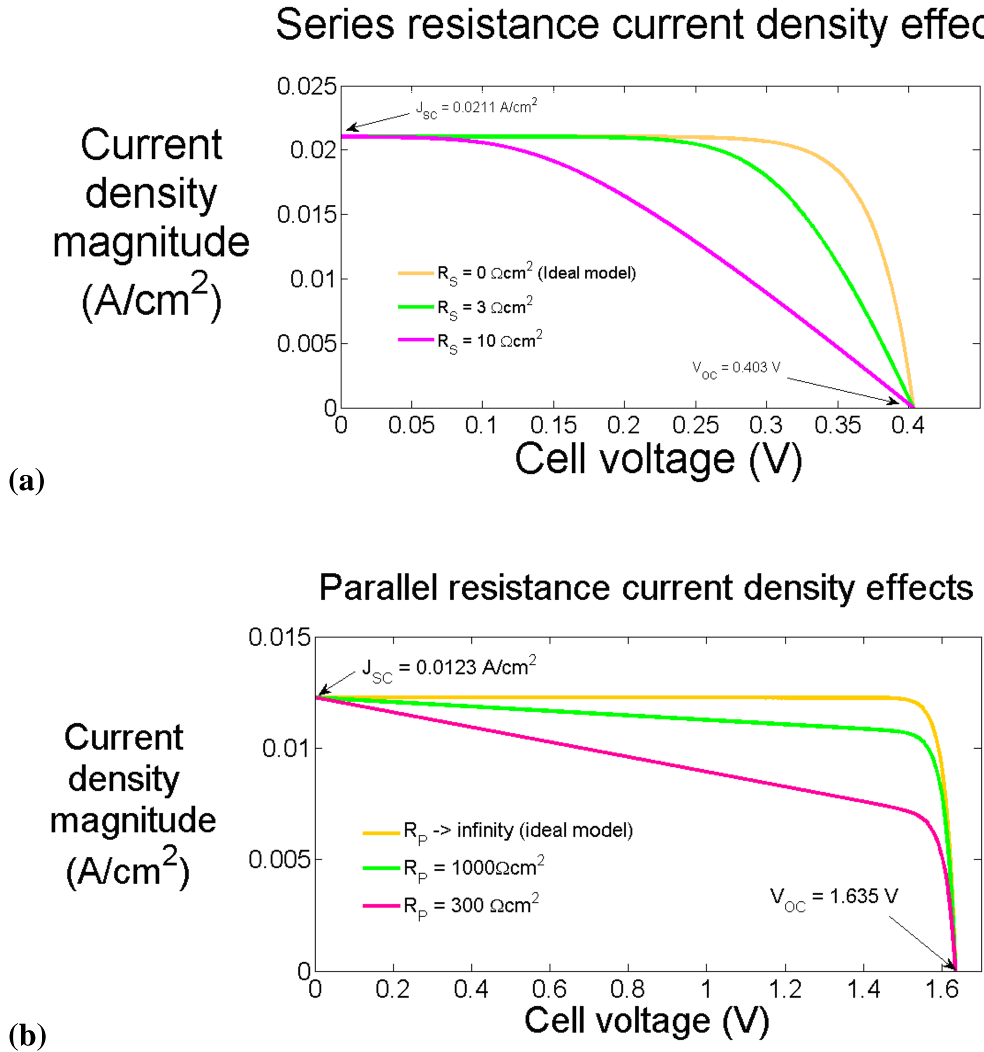

Figure C.2 Effects of parasitic resistances on total photocurrent density. (a) The smallest bandgap cell shows greatest sensitivity to series resistance. Relatively small value of series resistance will reduce the current density while leaving the short-circuit current density unchanged. (b) The cell with the highest resistance, or the GaN-rich cell, shows greatest sensitivity to junction leakage. Parallel resistance reduces the current density of the solar cell.

Series resistance reduces the current density while the open-circuit voltage remains unchanged. For relatively small values of series resistance, the short circuit current density also remains unchanged. However, sufficiently large values of R_S will reduce J_{SC}. Conversely, parallel resistance increases the current density. Parallel resistance tends to reduce the open-circuit voltage.

C.2.5 Power Density

As shown in Figure C.3, the parasitic resistances both reduce the power density of the solar cell. Series resistance reduces the maximum power point, as a function of the maximum power point current and voltage. In contrast, the parallel resistance does not reduce the maximum power point voltage. This can be seen in Figure C.3 (b).

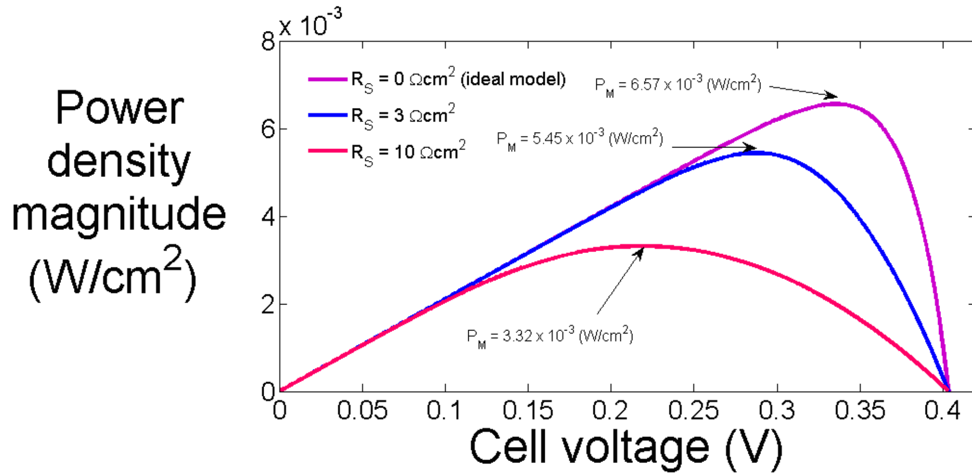

(a)

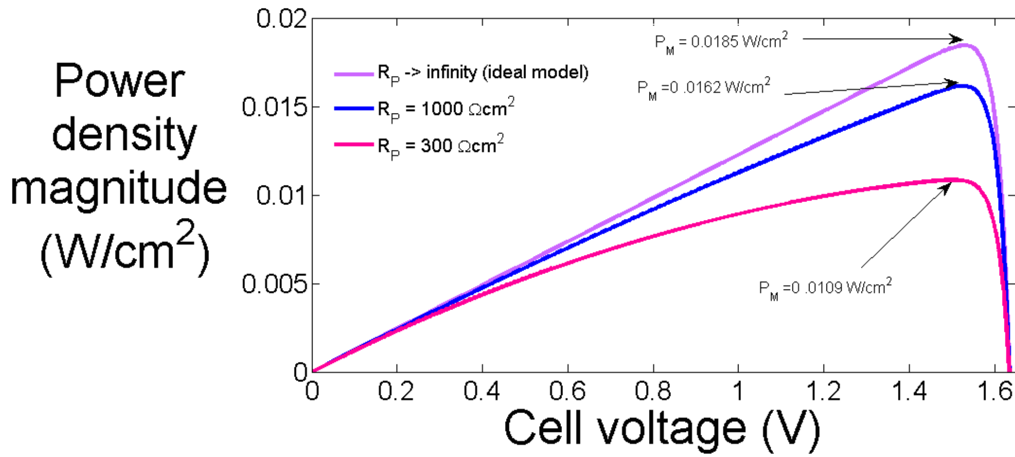

(b)

Figure C.3 Effects of parasitic resistances on power density. (a) Power-voltage characteristics, showing series resistance effects, for a *pin* design with a $p-GaN$ layer, graded intrinsic layer, and $n-InN$ layer. (b) Power-voltage characteristics, showing parallel resistance effects for a *pin* design with a $p-GaN$ layer, graded intrinsic layer, and $n-In_{0.624}Ga_{0.376}N$ layer.

C.2.6 Fill Factor

The fill factor decreases as parasitic resistances become significant. As shown in Figure C.4, the fill factor is reduced most quickly for the $n-InN$ cell when series resistance is considered. When parallel resistance is considered, the GaN-rich cell has the highest fill factor in the ideal case, but decreases quickest when parallel resistance decreases.

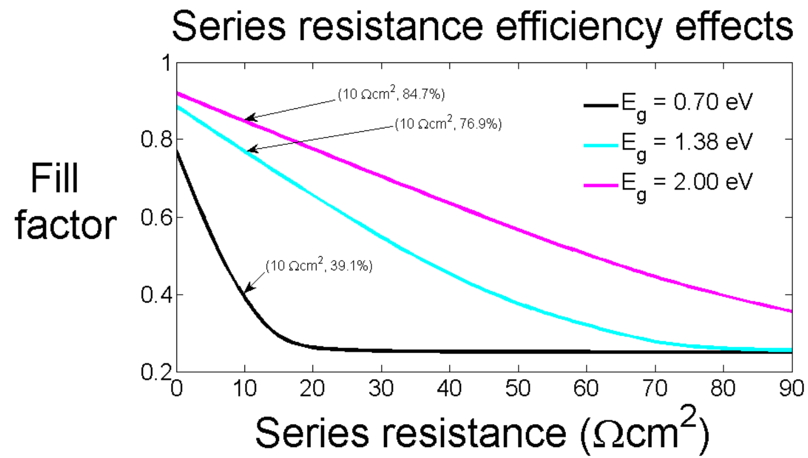

(a)

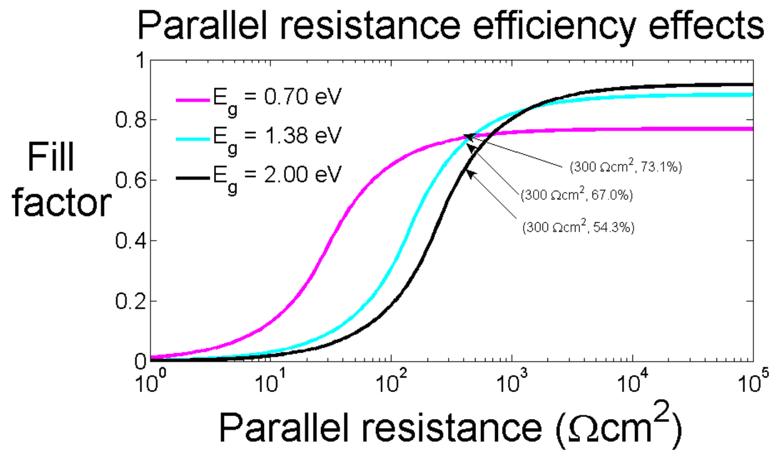

(b)

Figure C.4 Effects of parasitic resistances on fill factor (a) Fill factor as a function of series resistance for a *pin* design with a $p-GaN$ layer, graded intrinsic layer, and $n-InN$ layer. (b) Fill factor as a function of parallel resistance for a *pin* design with a $p-GaN$, graded intrinsic layer, and $n-In_{0.624}Ga_{0.376}N$ layer.

C.4 Conclusions

Highly conductive, small bandgap devices show great sensitivity to series resistance. From the equivalent circuit model, this is apparent because the current flows through the series resistance and the diode; it does not have any alternative paths. Also, for small-gap devices, the device voltage is low, hence the voltage drop across the series resistance will be significant when this resistance increases.

Conversely, highly resistive large bandgap devices exhibit significant performance degradation due to parallel resistance, that is, junction leakage. The circuit model shows the alternative path across the parallel resistance where current can flow. An ideal model has infinite parallel resistance, but the realistic model has a finite resistance. Reduction in parallel resistance leads to increased current through this resistance leading to voltage and current decrease across the diode.

D Software Development

D.1 Overview

A software tool is developed to implement the mathematical models of our *pin* heterojunction PV device. We are able to simulate realistic operation of the individual PV cells in the three cell lateral array and analyze the results as presented in the thesis. The source code is written in Fortran (Fortran 77/90) as it is a standard programming language especially suitable for scientific computing. We use Force 2.0.9p for the Fortran compiler and editor. Modified for presentation in this thesis, the source code is provided below.

D.2 Source Code

```
!August 18, 2011
!Jennifer J. Krohn, Grad. RA University of Minnesota, M.S.E.E.
!This software tool is used to simulate a pin heterojunction solar
!     cell for both dark and illuminated conditions.  Under
!     illumination, a portion of the black body spectrum (used to
!     emulate the solar spectrum) is incident on the p-GaN layer
!     of the solar cell. To simulate a specific cell under
!     dark(light) conditions, set the 'dark' variable to 0(1) and
!     set the desired values for the n-region bandgap Egn. For
!     spectral splitting, set the appropriate EgBound.
!This version has been modified from version 2011June1 for
!     inclusion in Appendix D of thesis.  For simulation purposes
!     use version 2011June1.

Program Study1
Implicit none

Double precision V,dV,Vinitial,Vcheck,RangeV,V_array(5000)
Double precision Vbi,Vbie,Vbih,Vs,Vt
Double precision x1,xi,x2,xpprime(5000),xnprime(5000),delxn(5000)
Double precision delxp,dx,x(5000),points,y,yp,yn
```

```
Double precision chin,chip,osEc,osEv,slope
Double precision Egn,Egp,Egy,dEg,Egx(5000),EgGaN,EgInN,bowing
Double precision Ks,Ln,Lp,Na,Nc,Nd,nin,nip,npo,Nv,pno,q,Tn,Tp,e0
Double precision Fe,Fh,Dn,Dp
Double precision nix(5000),n(5000),p(5000),textn(5000)
Double precision textp(5000),RG(5000),RGpeak,Jdark_recomb(5000)
Double precision Jdark_recomb_no_Jrg(5000),Jdark_no(5000)
Double precision Jndark(5000),Jpdark(5000),Jrg(5000)
Double precision JndarkNoRg,JpdarkNoRg,JrgTemp
Double precision alpha(1501),EgBound,dhbarw
Double precision BcnX1(5000),BcpX2(5000),Bcn0,Bcp0
Double precision temp,temptemp,temptemp2,temptemp3,ytemp
Real kt,ue,uh
Integer i,ii,jj,xRGright,xRGleft_of_peak,xRGright_of_peak
Integer xRGleft,xRGpeak,iterations,PointsV,Check,endI(5000),dark
Integer endP(5000),endN(5000)

Common /c_Egp/ Egp
Common /c_Egn/ Egn
Common /c_EgInN/ EgInN
Common /c_EgGaN/ EgGaN
Common /c_bowing/ bowing
Common /c_x1/ x1
Common /c_x2/ x2
Common /c_xi/ xi
Common /c_yp/ yp
Common /c_yn/ yn
Common /c_EgBound/ EgBound
Common /c_Dn/ Dn
Common /c_Dp/ Dp
Common /c_Tn/ Tn
Common /c_Tp/ Tp
Common /c_npo/ npo
Common /c_pno/ pno
Common /c_Vt/ Vt
Common /c_q/ q
Common /c_Ln/ Ln
Common /c_dV/ dV
Common /c_Vinitial/ Vinitial
```

```
Common /c_RangeV/ RangeV
Common /c_PointsV/ PointsV
Common /c_Jndark/ Jndark
Common /c_Jpdark/ Jpdark
Common /c_Jrg/ Jrg
Common /c_BcnX1/ BcnX1
Common /c_BcpX2/ BcpX2
Common /c_Vbih/ Vbih
Common /c_Vcheck/ Vcheck
Common /c_Check/ Check
Common /c_n/ n
Common /c_Nd/ Nd
Common /c_dx/ dx
Common /c_Na/ Na
Common /c_points/ points
Common /c_dark/ dark
Common /c_dhbarw/ dhbarw
Common /c_Bcn0/ Bcn0
Common /c_Bcp0/ Bcp0
Common /c_endP/ endP
Common /c_endN/ endN
Common /c_xpprime/ xpprime
Common /c_xnprime/ xnprime
Common /c_delxn/ delxn
Common /c_endI/ endI

!Set-----------------------------------------------------------------
!FLAG:
!Set to 'dark' 1 (dark conditions) or 0 (illumination conditions):
dark = 0

points = 5000 !set total number of x increments for cell.
!    This is number of x loop iterations and length of x arrays.
Bcn0 = 0. !boundary condition: minority carrier electrons at
!    p-region surface (x=0)
Bcp0 = 0. !boundary condition: minority carrier holes at n-region
!    surface (x=x1+xi+x2)
dhbarw = 0.01 !set photon energy incremental value (eV)
dV = 0.01 !set voltage incremental value (volts)
```

```
Vinitial = 0. !set intitial voltage value at which to begin
!    calculations dependent on voltage (volts)
Vcheck = 0.325 ! set: Vcheck must be some multiple of dV; set
!    desired value to analyze x,V functions for this one V value
       If(Vcheck==Vinitial)then
                  Check = 1
       Else
                  Check = (Vcheck-Vinitial)/dV  + 1
       End if

EgGaN = 3.4 !bandgap of GaN (eV)
EgInN = .7  !bandgap of InN (eV)
bowing = 1.43 !bowing parameter for InGaN
!Set either yn or Egn and yp or Egp and calculate the other;
!     comment out appropriately:
!------------------Set block-----------------------------------:
!yp =  !InN composition in the p-region (if setting Egp and Egn,
!   comment out this line and next line).
!yn =  !InN composition in the n-region.
Egp = 3.4 !p-region bandgap (eV).
Egn =   2. !n-region bandgap (eV).
EgBound = 5. !set upper limit of incident photon flux.
!-----------------------------------------------------------------
!Egp = EgGaN+ EgInN*yp - EgGaN*yp - bowing*yp*(1-yp)  !(if Egp and
!    Egn are set, comment out this line and next line).
!Egn = EgGaN+ EgInN*yn - EgGaN*yn - bowing*yn*(1-yn)
!calculate the InN composition, yp, in the p-region based on Egp:
yp =(-(EgInN-EgGaN-bowing)-DSQRT((EgInN-EgGaN-bowing)*
&       (EgInN-EgGaN-bowing)-4.*bowing*(EgGaN-Egp)))/(2.*bowing)
!calculate the InN composition, yn, in the n-region based on Egn:
yn =(-(EgInN-EgGaN-bowing)-DSQRT((EgInN-EgGaN-bowing)*
&         (EgInN-EgGaN-bowing)-4.*bowing*(EgGaN-Egn)))/(2.*bowing)
!----------------------------------------------------------------
Nd = 4.D18 !n-region electron doping concentration (cm^-3).
Na = 1.D17 !p-region hole doping concentration (cm^-3).
x1 = .15D-4 !p-region structural width (cm).
xi = .1D-4 !i-region structural width (cm).
x2 = .12D-4 !n-region structural width (cm).
ue = 400. !minority carrier electron mobility in the GaN p-region
```

```
!  (cm^2/Vsec).
!ue = 55.+(1000.-55.)/(1.+(Na/(2.D17))) !Brown paper electron
!   mobility calculation. Currently not used.
uh = 50. !hole mobility  (cm^2/Vsec).
Vs = 1.D9 !surface recombination velocity (cm/sec).
Ks = 12.10 !dielect.const.(unitless)Note:relativ. arbitrary here.
Tn = 8.D-8 !minority carrier electron lifetime (sec).
Tp = Tn !minority carrier hole lifetime (sec).
kt = 0.0258522! thermal voltage(volts).
Vt = kt !(redundant) thermal voltage (volts).
q = 1.602176487D-19! elementary charge(C).
e0 = 8.854188D-14 !permittivity of free space (F/cm).
Nc = 7.9035D17 !effective DOS in the conduction band (cm^-3).
Nv = 8.8364D18 !effective DOS in the valence band (cm^-3).
!------------------------------------------------------------------

dEg = Egp - Egn
dx = (x1+xi+x2)/points !x interval value (cm).
nip = DSQRT(Nc*Nv)*DEXP(-Egp/(2.*0.0258522))!p-region intrinsic
!   hole concentration (cm^-3).
nin = DSQRT(Nc*Nv)*DEXP(-Egn/(2.*0.0258522))!n-region intrinsic
!   electron concentration (cm^-3).
Dn = ue*0.0258522 !electron diffusion coefficient (cm^2/sec).
Dp = uh*0.0258522 !hole diffusion coefficient (cm^2/sec).
Vbie = (0.0258522)*DLOG((Na*Nd)/(nip*nin))  + dEg/2. !built-in
!    voltage seen by the n-region electrons (volts).
Vbih = (0.0258522)*DLOG((Na*Nd)/(nip*nin)) - dEg/2. !built-in
!    voltage seen by the p-region holes (volts).
RangeV = Vbih-Vinitial !stay within this voltage range.
PointsV = RangeV/dV !incremental voltage width.
chip = 5.6*yp+4.*(1-yp)-0.8*yp*(1-yp) !n-region e- affinity (eV).
chin = 5.6*yn+4.*(1-yn)-0.8*yn*(1-yn) !p-region e- affinity (eV).
osEc = chin-chip !conduction band offset (eV).
osEv = chip-chin+Egp-Egn !valence band offset (eV).
Vbi = kt*DLOG((Na*Nd)/(nin*nip))+osEv/2.-osEc/2. !built-in voltage
!   (volts).
npo = (nip*nip)/Na !p-region thermal equilibrium minority carrier
!   electron concentration (cm^-3).
pno = (nin*nin)/Nd !n-region thermal equilibrium minority carrier
```

```
!   hole concentration (cm^-3).
Ln = DSQRT((Dn*Tn)) !minority carrier e- diffusion length (cm)
Lp = DSQRT((Dp*Tp)) !minority carrier hole diffusion length (cm)

Call open_Jdark  !open files

i = 1 !voltage loop index
V = Vinitial
  Do i = 1,PointsV

      !calculate the depletion region widths as function of V:
      delxp = DSQRT(((2*Ks*e0)/q)*(Nd/Na)*(1./(Na+Nd))*(Vbi-V) +
&          ((Nd*xi)/(Na+Nd))*((Nd*xi)/(Na+Nd))) - (Nd*xi)/(Na+Nd)
      delxn(i) = (Na/Nd)*delxp
      Write(4,*)V,',',delxp
      Write(58,*)V,',',delxn(i)

      endI(i) = (delxp+xi+delxn(i))/dx +1
      xpprime(i) = x1-delxp
      xnprime(i) =  x2-delxn(i)
      endP(i) = xpprime(i)/dx + 1
      endN(i) = xnprime(i)/dx +1
      Write(59,*)V,',',xpprime(i)
      Write(60,*)V,',',xnprime(i)
      Write(61,*)V,',',endP(i)
      Write(62,*)V,',',endN(i)

      !Calculations for NO recombination-------------------------:
      temp = ((Dn/(Vs*Ln))-1.)/((Dn/(Vs*Ln))+1.)
      !minority carrier electron dark diffusion current density:
      JndarkNoRg = ((q*Dn*npo)/Ln)*(DEXP(V/kt)-1.)*(-temp*DEXP(
&               -xpprime(i)/Ln)+DEXP(xpprime(i)/Ln))/(temp*DEXP(
&               -xpprime(i)/Ln)+DEXP(xpprime(i)/Ln))
      Write(1,*)V,',',JndarkNoRg
      !minority carrier hole dark diffusion current density:
      JpdarkNoRg = ((q*Dp*pno*(DEXP(V/kt)-1.))
&              /(Lp*((DEXP(xnprime(i)/Lp))+((((Dp/(Vs*Lp))-1.)
&              /((Dp/(Vs*Lp))+1.))*DEXP(-xnprime(i)/Lp)))))
&              *((-((Dp/(Vs*Lp))-1.)/((Dp/(Vs*Lp))+1.))
```

```
&              *DEXP(-xnprime(i)/Lp)+DEXP(xnprime(i)/Lp))
       Write(2,*)V,',',JpdarkNoRg
       !calculate total dark diffusion current density:
       Jdark_no(i) = JpdarkNoRg + JndarkNoRg
       !------------------------------------------------------------

       !Calculations for NO recombination AND letting Vs approach
       !             infinity-------------------------------------:
       JndarkNoRg = ((q*Dn*npo)/Ln)*(DEXP(V/kt)-1.)*(DEXP(
&               -xpprime(i)/Ln)+DEXP(xpprime(i)/Ln))/(-DEXP(
&               -xpprime(i)/Ln)+DEXP(xpprime(i)/Ln))
       JpdarkNoRg = ((q*Dp*pno*(DEXP(V/kt)-1.))
&              /(Lp*((DEXP(xnprime(i)/Lp))+(((-1.)
&              /(+1.))*DEXP(-xnprime(i)/Lp)))))
&              *((-(-1.)/(+1.))
&              *DEXP(-xnprime(i)/Lp)+DEXP(xnprime(i)/Lp))
       Jdark_no(i) = JpdarkNoRg + JndarkNoRg
       Write(8,*)V,',',Jdark_no(i)
       Write(5,*)V,',',DLOG(Jdark_no(i))
       !------------------------------------------------------------

       !Recombination calculations--------------------------------:
       Fe = (V-Vbie)/(delxp+xi+delxn(i)) !electric field seen by
       !  electrons  (volts/cm).
       Fh = (V-Vbih)/(delxp+xi+delxn(i)) !"" holes (volts/cm)
       Write(45,*)V,',',Fe
       Write(46,*)V,',',Fh

       RGpeak = 0. !initialize RG peak value.
       xRGpeak = 1. !intinitalize position x at value of RG peak.
       ii = 1 !(index for following loop.)
       x(ii) = 0.
       Do ii = 1, endI(i)
           If(x(ii)<=delxp)then
              Egx(ii) = Egp !constant bandgap outside i-region and
              !       depleted p-region.
           Else if(x(ii)>=delxn(i))then
              Egx(ii) = Egn !constant bandgap outside i-region and
              !       depleted n-region.
```

```
          Else
             Egx(ii) =x(ii)*((Egn-Egp)/xi) + Egp !i-region bandgap
             !       is linearly dependent on position.
          End if

          !calculate InN composition as a function of x:
          ytemp =(-(EgInN-EgGaN-bowing)-DSQRT((EgInN-EgGaN-bowing)
&              *(EgInN-EgGaN-bowing)-4.*bowing*
&              (EgGaN-Egx(ii))))/(2.*bowing)

          nix(ii) = nip*DEXP(((Egp-Egn)*x(ii))/(2.*kt* !i-region
          !       intrinsic carrier concentration (cm^-3).
&            (xi+delxp+delxn(i))))
          !intrinsic region electron concentration
          ! (btw, will not be intrinsic value because RG occurs):
          textn(ii) = Nd*DEXP((Fe/kt)*(xi+delxn(i)+delxp-x(ii)))
          !intrinsic region hole concentration (""):
          textp(ii) = Na*DEXP((Fh/kt)*(x(ii)))

          If(i==Check)then
             Write(25,*)V,',',x(ii)
             Write(79,*)V,',',x(ii),',',ytemp,',',Egx(ii)
             Write(34,*)V,',',x(ii),',',nix(ii)
             Write(37,*)V,',',x(ii),',',textn(ii)
             Write(38,*)V,',',x(ii),',',textp(ii)
          Else
          End if
          temptemp = textn(ii)*textp(ii)!for simplification of RG.
          temptemp2 = nix(ii)*nix(ii) !""
          temptemp3 = temptemp-temptemp2 !""
          RG(ii) = (temptemp3)/(tp* !SRH recombination.
&                (textn(ii)+nix(ii))+tn*(textp(ii)+nix(ii)))
          IF(RG(ii)>RGpeak)Then !then haven't found peak RG yet.
           RGpeak = RG(ii)! and set to next highest value.
           xRGpeak = ii !and set corresponding x integer.
          Else
          End if
          x(ii+1) = x(ii) + dx
      End do  !end x loop (indexed by ii).
```

```
!determine xRGleft which corresponds to 0.1RGpeak:
xRGleft = 1.
xRGright = endI(i)
IF(RG(1)>.1*RGpeak)Then
    xRGleft = 1.
Else
    Do ii = 1,xRGpeak
        IF(RG(ii)<.1*RGpeak)Then
          xRGleft = ii
        Else
        End if
    End do
 End if

 xRGleft_of_peak = nint((xRGleft+xRGpeak)/2.)!find midpoint;
                 ! is integer.

 !determine xRGright which corresponds to 0.1RGpeak:
 IF(RG(points)>.1*RGpeak)Then
 xRGright = endI(i)
 Else
     Do ii = xRGpeak, endI(i)
        If(RG(ii)>.1*RGpeak)Then
            xRGright = ii
        Else
       End if
     End do
 End if

 xRGright_of_peak=nint((xRGright+xRGpeak)/2.)!find midpoint;
           ! is integer.

 Do ii = 1, xRGleft
 !hole concentration between 1 and xRGleft (cm^-3):
 p(ii) = textp(ii)
 !electron concentration "":
 n(ii) = textn(ii) - RG(xRGright_of_peak)*(x(xRGpeak)-
&           x(xRGright))/(ue*Fh)-RG(xRGleft_of_peak)*(x(xRGleft)-
```

```
&           x(xRGpeak))/(ue*Fh)
        End do

        !calculate concentrations between given interval:
        Do ii = xRGleft, xRGpeak
        p(ii) = textp(ii) - RG(xRGleft_of_peak)*(x(xRGleft)-
&          x(ii))/(uh*Fe)
        n(ii) = textn(ii) - RG(xRGright_of_peak)*(x(xRGpeak)-
&          x(xRGright))/(ue*Fh)-RG(xRGleft_of_peak)*(x(ii)-
&           x(xRGpeak))/(ue*Fh)
        End do
        !calculate concentrations between given interval:
        Do ii = xRGpeak,xRGright
        p(ii) = textp(ii) - RG(xRGleft_of_peak)*(x(xRGleft)-
&          x(xRGpeak))/(uh*Fe) - RG(xRGright_of_peak)*(x(xRGpeak)
&          -x(ii))/(uh*Fe)
        n(ii) = textn(ii) - RG(xRGright_of_peak)*(x(ii)-
&          x(xRGright))/(ue*Fh)
        End do
        !calculate concentrations between given interval:
        Do ii = xRGright, endI(i)
        p(ii) = textp(ii) - RG(xRGleft_of_peak)*(x(xRGleft)-
&          x(xRGpeak))/(uh*Fe) - RG(xRGright_of_peak)*(x(xRGpeak)
&          -x(xRGright))/(uh*Fe)
        n(ii) = textn(ii)
        End do

        Do ii = 1, endI(i)
           If(n(ii)<((nix(1)*nix(1))/Na))Then
               n(ii)=((nix(1)*nix(1))/Na)
           End if
           If(p(ii)<((nix(endI(i))*nix(endI(i)))/Nd))Then
               p(ii)=(nix(endI(i))*nix(endI(i)))/Nd
           End if

           !We are simplifying the model so that now n(ii) and
           !   p(ii) are independent of the RG:--------------------
           n(ii) = textn(ii)
           p(ii) = textp(ii)
```

```
   !--------------------------------------------------------

   If(i==Check)then
     Write(13,*)ii,',',V,',',x(ii),',',n(ii)
     Write(9,*)ii,',',V,',',x(ii),',',p(ii)
     Write(11,*)ii,',',V,',',DLOG(n(ii))
     Write(12,*)ii,',',V,',',DLOG(p(ii))
     Write(92,*)ii,',',x(ii),',',V,',',RG(ii)
     Write(44,*)ii,',',x(ii),',',V,',',DLOG(RG(ii))
     Else
   End if

x(ii+1) = x(ii)+dx
End do !end x loop (indexed by ii).

!integrate q*RG(ii) over i-region and depleted region
! to get the total current density in this region:
JrgTemp = 0.  !initialize
Do ii = 1, endI(i)
   JrgTemp = JrgTemp + q*RG(ii)*dx  !integrate.
End do
Jrg(i) = JrgTemp !as function of voltage.
Write(7,*)V,',',Jrg(i)
Write(3,*)V,',',DLOG(Jrg(i))

!Boundary condition: change in e- carrier concentration at
!         x = x1-delxp as a function of voltage:
BcnX1(i) = npo*(DEXP(V/Vt)-1.)
!Boundary condition: change in h+ carrier concentration at
!         x = x1+xi+delxn as a function of voltage:
BcpX2(i) = pno*(DEXP(V/Vt)-1.)
Write(20,*)V,',',BcnX1(i)
Write(21,*)V,',',BcpX2(i)

temp = ((Dn/(Vs*Ln))-1.)/((Dn/(Vs*Ln))+1.)!simplify Jndark.
!minority carrier electron diffusion dark current density
!         at x = x1 considering recombination:
Jndark(i) = ((q*Dn)/Ln)*(n(1)-npo)*(-temp*DEXP(
&                -xpprime(i)/Ln)+DEXP(xpprime(i)/Ln))/(temp*DEXP(
```

```
&                  -xpprime(i)/Ln)+DEXP(xpprime(i)/Ln))
        write(14,*)V,',',Jndark(i)
        !minority carrier hole diffusion dark current density at
        !         x'=x2 considering recombination:
        Jpdark(i) = ((q*Dp*(p(endI(i))-pno))
&                /(Lp*((DEXP(xnprime(i)/Lp))+((((Dp/(Vs*Lp))-1.)
&                /((Dp/(Vs*Lp))+1.))*DEXP(-xnprime(i)/Lp)))))
&                *((-((Dp/(Vs*Lp))-1.)/((Dp/(Vs*Lp))+1.))
&                *DEXP(-xnprime(i)/Lp)+DEXP(xnprime(i)/Lp))
        write(15,*)V,',',Jpdark(i)
        !total dark current density considering recombination:
        Jdark_recomb(i) = Jndark (i)+ Jpdark(i)+Jrg(i)
        Write(16,*)V,',',Jdark_recomb(i)
        Write(10,*)V,',',DLOG(Jdark_recomb(i)) !for semilog plot.
        Jdark_recomb_no_Jrg(i) = Jndark(i) + Jpdark(i)
        Write(19,*)V,',',Jdark_recomb_no_Jrg(i)

        V_array(i) = V !put V in array for slope calculation.
        V = V + dV
 End do !end voltage loop (indexed by i).

 iterations = i-1
 Do i = 2,iterations
    slope = (DLog(Jdark_no(i))-DLog(Jdark_no(i-1)))/dV
    write(17,*)V_array(i),',',slope
    slope = (DLog(Jdark_recomb(i)) - DLog(Jdark_recomb(i-1)))/dV
    write(18,*)V_array(i),',',slope
    slope = (DLog(Jrg(i))-DLog(Jrg(i-1)))/dV
    write(84,*)V_array(i),',',slope
 End Do

 Call generation

 End program
 !_________________________________________________________________
 Subroutine open_Jdark

 !Main Program files:
 Open(1, file = 'Jndark_No_Recombination(V).xls')
```

```
Open(2, file = 'Jpdark_No_Recombination(V).xls')
Open(3, file = 'DLOG(Jrg(V)).xls')
Open(4, file = 'delxp(V).xls')
Open(5, file = 'DLOG(JDarkNoRecomb(V)).xls')
Open(7, file = 'Jrg(V)_iRegion.xls')
Open(8, file = 'JdarkTotal_No_Recombination(V).xls')
Open(9, file = 'p(ii).xls')
Open(10,file = 'DLOG(JDarkRecomb(V)).xls')
Open(11,file = 'DLOG(n(ii)).xls')
Open(12,file = 'DLOG(p(ii)).xls')
Open(13, file = 'n(ii).xls')
Open(14, file = 'Jndark_Recombination(V,x1).xls')
Open(15, file = 'Jpdark_Recombination(V,x2).xls')
Open(16, file = 'JdarkTotal_Recombination(V).xls')
Open(17, file = 'slope(DLOG(JDarkNoRecomb.(V)).xls')
Open(18, file = 'slope(DLOG(JDarkRecomb.(V)).xls')
Open(19, file = 'Jdark_Recomb_Jn+JpOnly.xls')
Open(20, file = 'BcnX1(V).xls')
Open(21, file = 'BcpX2(V).xls')
Open(25, file = 'x(ii).xls')
Open(34, file = 'nix(ii).xls')
Open(37, file = 'textn(ii).xls')
Open(38, file = 'textp(ii).xls')
Open(44, file = 'DLOG(RG(ii)).xls')
Open(45, file = 'Fe(V).xls')
Open(46, file = 'Fh(V).xls')
Open(58, file = 'delxn(V).xls')
Open(59, file = 'xpprime(V).xls')
Open(60, file = 'xnprime(V).xls')
Open(61, file = 'endP(V).xls')
Open(62, file = 'endN(V).xls')
Open(79, file = 'Egx(ii).xls')
Open(84, file = 'slope(DLOG(Jrg(V)).xls')
Open(92, file = 'RG(ii).xls')
!Subroutine generation Files:
!---G(x) calculations:
Open(22, file = 'PhotonFlux(hw).xls')
Open(23, file = 'AbsorptionCoefficient(hw)_pRegion.xls')
Open(24, file = 'SumTemp(hw,some x).xls')
```

```
Open(26, file = 'alphatemp(hw).xls')
Open(27, file = 'AbsorptionCoefficient(hw)_nRegion.xls')
Open(29, file = 'Gtemp(hw,some x)_pin.xls')
Open(30, file = 'Egi(x).xls')
Open(31, file = 'yi(x).xls')
Open(32, file = 'Balpha(x).xls')
Open(33, file = 'Aalpha(x).xls')
Open(35, file = 'alpha(x1+xi,hw)_iRegion.xls')
Open(36, file = 'alpha(x1,hw)_iRegion.xls')
Open(40, file = 'photonflux(x=0,hw)_pRegion.xls')
Open(41, file = 'photonflux(x1,hw)_pRegion.xls')
Open(42, file = 'alpha(some x, hw)_iRegion.xls')
Open(43, file = 'PhotonFluxEnd(hw).xls')
Open(47, file = 'DeltaN(Vcheck,x)pRegionApril25.xls')
Open(48, file = 'DeltaP(Vcheck,x)_indexedBackwards.xls')
Open(51, file = 'G(x)_pin.xls')
Open(57, file = 'G(x)_iRegion.xls')
Open(63, file = 'Ji(V)May4.xls')
Open(52, file = 'GMod(Vcheck,x)_pRegion.xls')
Open(53, file = 'TempArray(Vcheck,x)_nRegion.xls')
Open(54, file = 'TermMod(Vcheck,x)_pRegion.xls')
Open(55, file = 'TempArray(Vcheck,x)_pRegion.xls'
Open(56, file = 'GMod(Vcheck,x)_nRegion.xls')
Open(65, file = 'G(x)_pRegion.xls')
Open(66, file = 'G(x)_nRegion.xls')
Open(70, file = 'DeltaN(Vcheck,x)_pRegion.xls')
Open(71, file = '-G(xBackwards)_nRegion.xls')
Open(72, file = 'DeltaP(Vcheck,x)_nRegion.xls')
Open(80, file = 'JminoritydiffeMay4(V,x1).xls')
Open(81, file = 'JminoritydiffhMay4(V,x1+xi).xls')
Open(82, file = 'slope(DLOG(JnGen(V,x1))).xls')
Open(83, file = 'slope(DLOG(JpGen(V,x1+xi))).xls')
Open(85, file = 'hwPhi(hw).xls')
Open(87, file = 'JTotal(V)May4.xls')
Open(90, file = 'slope(DLOG(JTotalDarknoRG(V))May10.xls')
Open(91, file = 'slope(DLOG(JTotalDark(V))May10.xls')
Open(93, file = 'slope(DLOG(Jrg(V)).xls')
Open(94, file = 'dPower(V).xls')
Open(95, file = 'Power(V).xls')
```

```
End subroutine
!_________________________________________________________________

Subroutine generation

Double precision Egi,Egn,Egp,EgGaN,EgInN,EgBound,bowing,y,yi,yn,yp
Double precision hbarw,dhbarw,c,k,N,pie,T,hbar,PhotonFlux
Double precision PhotonFluxIntegrated,PhotonFluxEnd,PFEIntegrated
Double precision Aalpha,Balpha,Aalpha_i,Balpha_iBalpha_p,Aalpha_p
Double precision Aalpha_n,Balpha_n
Double precision x,x1,x2,xi,dx,xpprime(5000),xnprime(5000)
Double precision delxn(5000),Vt
Double precision Dn,Dp,Tn,Tp,npo,pno,q,Ln,Nd,Na
Double precision alpha_i(5000,10000),alpha_n,alpha_p
Double precision alphaT(5000),alphaTemp,SumTemp
Double precision Gtemp,GtempIntegrated,GpTemp,GiTemp,GnTemp
Double precision GiTempPrime,GTIPrime,Ji_V(5000)
Double precision GTIp,GTIi,GTIn,G_x(5000),G_x_pRegion(5000)
Double precision G_x_nRegion(5000),G(5000),GMod(5000)
Double precision Term,PlusTerm,MinusTerm,TermMod(5000)
Double precision MinusTermMod,TempArray(5000),DeltaN(5000)
Double precision DeltaNintegral, nTotal(5000)
Double precision DeltaNx1V(2,450),DeltaN0(2,450)
Double precision DeltaP(5000),pTotal(5000)
Double precision DeltaPintegral,DeltaPx2V(2,450),DeltaP0(2,450)
Double precision JpGen0,JpGenTemp,JnGenTemp,JnGen0,Ji,Jrg(5000)
Double precision JTotalTotal(5000),JTotalDark(5000)
Double precision JTotalPhoto(5000)
Double precision Bcn0,Bcp0,BcnX1(5000),BcpX2(5000)
Double precision V,dV,Vbih,Vinitial,Vcheck
Double precision JnGen(450),JpGen(450),Jndark(5000),Jpdark(5000)
Double precision temptemp,slope
Double precision Power(5000),dPower(5000)
Double precision MaxPower,MaxPowerVoltage,MaxPowerCurrent,Voc
Double precision FillFactor,Jsc,hwPhi,hwPhiIntegrated
Integer i,ii,j,jj,kk,EgBoundInt,dark,Check,PointsV
Integer endPI,endPIN,endP(5000),endN(5000),endI(5000)
```

```
Common /c_Egp/ Egp
Common /c_Egn/ Egn
Common /c_EgInN/ EgInN
Common /c_EgGaN/ EgGaN
Common /c_bowing/ bowing
Common /c_y /y
Common /c_Aalpha/ Aalpha
Common /c_Balpha/ Balpha
Common /c_x1/ x1
Common /c_x2/ x2
Common /c_xi/ xi
Common /c_yp/ yp
Common /c_yn/ yn
Common /c_EgBound/ EgBound
Common /c_Dn/ Dn
Common /c_Dp/ Dp
Common /c_Tn/ Tn
Common /c_Tp/ Tp
Common /c_npo/ npo
Common /c_pno/ pno
Common /c_Vt/ Vt
Common /c_q/ q
Common /c_Ln/ Ln
Common /c_dV/ dV
Common /c_Vbih/ Vbih
Common /c_Vinitial/ Vinitial
Common /c_PointsV/ PointsV
Common /c_Jndark/ Jndark
Common /c_Jpdark/ Jpdark
Common /c_Jrg/ Jrg
Common /c_BcnX1/ BcnX1
Common /c_BcpX2/ BcpX2
Common /c_Vcheck/ Vcheck
Common /c_Check/ Check
Common /c_Nd/ Nd
Common /c_dx/ dx
Common /c_Na/ Na
Common /c_dark/ dark
Common /c_dhbarw/ dhbarw
```

```
Common /c_Bcn0/ Bcn0
Common /c_Bcp0/ Bcp0
Common /c_endP/ endP
Common /c_endN/ endN
Common /c_xpprime/ xpprime
Common /c_xnprime/ xnprime
Common /c_delxn/ delxn
Common /c_endI/ endI

!photon flux parameters:
T = 5200.!temperature of black body (K).
hbar = 6.5822D-16 !Plank's constant  (eVsec).
pie = 3.14159265 !pi.
c = 2.9979D10 !speed of light  (cm/sec).
k = 8.6174D-5 !Boltzmann's constant (eV/K).
N = 2.4D-5 !normalizing factor.

V = Vinitial
hbarw = Egn + dhbarw !photon energy (eV).
EgBoundInt = (EgBound - hbarw)/dhbarw  !photon energy max limit
           !integer (unitless).

endPIN = (x1+xi+x2)/dx  !incremental width of entire solar cell.

y = yp !set coefficients subroutine variable to yp.
Call coefficients !calculate coefficients for absorption
!    coefficient for p-region InN composition.
Aalpha_p = Aalpha !p-reg. var. set to coefficient subroutine var.
Balpha_p = Balpha !""

y = yn !set coefficients subroutine variable to yn.
Call coefficients !calculate coefficients for absorption
!    coefficient for n-region InN composition.
Aalpha_n = Aalpha !n-reg. var. set to coefficient subroutine var.
Balpha_n = Balpha !""

x = 0. !start calculations a p-region surface where x = 0.
Do ii=1,endPIN !x loop
  Egi = 100. !intialize to a relatively large value when we are
```

```
!   not in i-region because then alpha_i(ii) will be zero. Egi
!   will be 100 before and after the i-region.
If(x1<x .AND. x<=(x1+xi))then ! i-region calculations
   yi = ((yn-yp)/xi)*x+yp-((yn-yp)/xi)*x1 !calculate InN
   !  composition as a function of position in i-region.
   Egi=EgGaN+EgInN*yi-EgGaN*yi-bowing*yi*(1-yi)!calculate
   !  bandgap as a function of yi.
   !calculate coeff. for absorption coeff. as a function of yi:
   Call coefficients
   Aalpha_i = Aalpha !i-reg. var. set to coeff. subroutine var.
   Balpha_i = Balpha !""
   Write(31,*)x,',',yi
   Write(30,*)x,',',Egi
   Write(33,*)x,',',Aalpha
   Write(32,*)x,',',Balpha
Else
End if

hbarw = Egn+dhbarw !start a little above Egp because anything
!     less won't be absorbed.
!NOTE: ---------------------------------------------------------
!hw loop to calculate absorption coefficient as a function
!of hbarw for each x. Then we get an array alpha(x,hbarw)
!and we integrate over intervals of x. E.g. x = x3, then
!we integ. alpha(x3,hbarw1) where hbarw1 is one hbarw val.
!and then we integrate alpha over x1 to x3 for this
!one hbarw value. Then we increment hbarw and repeat
!for this interval until the hbarw range is complete.
!We are calculating G(hbarw) at this same time.
!Then we increment x and repeat this process.
!---------------------------------------------------------------
Do i=1,EgBoundInt !hbarw loop
 !calculate the absorption coefficient in the i-region.
    !(It will be zero (and Egi is set to 100. until in i-region)
    ! until we are in the i-region):
 If(hbarw<=Egi)Then  !no photons are absorbed if hwbarw < Egi
      alpha_i(ii,i) = 0.
 Else !calculate i-region absorption coefficient
      alpha_i(ii,i) = 1.D5*DSQRT(Aalpha_i*(hbarw -
```

```
&              Egi)+Balpha_i*(hbarw-Egi)*(hbarw-Egi))
    End if

    If(x>=x1.AND.x<=(x1+dx))then !if at p-/i- junction
        write(36,*)Egi,',',hbarw,',',alpha_i(ii,i)
    Else if (x==(x1+xi))then  !if at i-/n-region junction
        Write(35,*)hbarw,',',alpha_i(ii,i)
    Else
    End if

    !write for several iterations:
    If((x1+100.*dx)<x.AND.x<=(x1+xi))then
            Write(42,*)x,',',Egi,',',hbarw,',',alpha_i(ii,i)
    Else
    End if

   hbarw = hbarw + dhbarw !increment hbarw
   End do  !end hw loop (indexed by i)

   x = x+dx !increment x
 End do !end x loop (indexed by ii)

 hbarw = Egn + dhbarw
 Do i = 1,EgBoundInt
    alphaTemp = 0. !initialize integration variable to zero
    Do ii = 1,endPIN
      !integrate absorption coefficient in i-region:
      alphatemp = alphaTemp + dx*alpha_i(ii,i)
    End do
    alphaT(i) = alphaTemp !store integrated value in array.
    Write(26,*)hbarw,',',alphaTemp
    hbarw = hbarw + dhbarw !increment hbarw for next iteration
 End do !end hbarw loop indexed by i

 jj = 0 !p-region array index
 kk = 0 !n-region array index
 x = 0. !begin at surface of p-region
 GtempIntegrated = 0. !initiatlize gen. rate integrat. var. to zero
 !   final integ. val. will give total area under the G(x) curve;
```

```
!   that is, the total generation in the device.
GTIp = 0. !init. p-reg. gen. rate integrat. var.;
!    final value of GTIp is total G(x) in p-region.
GTIi = 0. !init. i-reg. gen. rate integrat. var.;
!    final value of GTIi is total G(x) in i-region.
GTIn = 0. !init. n-reg. gen. rate integrat. var.;
!    final value of GTIn is total G(x) in n-region
GTIPrime = 0.!
PhotonFluxIntegrated = 0. !init. incident p. flux integrat. var;
!    final value is total incident p. flux for entire hbarw range.
hwPhiIntegrated = 0. !
PFEIntegrated = 0. !init. final p. flux integrat. var.;
!    final value is total p. flux leaving n-region.
!x loop:
Do ii=1,endPIN
  Gtemp = 0. !initialize. Final value after hw loop gives G(x).
  GpTemp = 0. !"" in p-region.
  GiTemp = 0. !"" in i-region.
  GnTemp = 0. !"" in n-region.
  GiTempPrime = 0. !
  hbarw = Egn+dhbarw
  !hw loop:
  Do i=1,EgBoundInt
     !calculate photon flux incident on p-region surface:
     PhotonFlux =(N*hbarw*hbarw)/(4.*pie*pie*hbar*hbar*hbar*c*c*
&        (DEXP(hbarw/(k*T))-1.))
     hwPhi = hbarw*PhotonFlux
     If(ii==1)then  !(p. flux indep. of x)
       Write(22,*)hbarw,',',PhotonFlux
       Write(85,*)hbarw,',',hwPhi
       !integrate over hbarw:
       PhotonFluxIntegrated=PhotonFluxIntegrated+dhbarw*PhotonFlux
       !integrate over hbarw:
       hwPhiIntegrated=hwPhiIntegrated+dhbarw*hwPhi
     Else
     End if
     !calculate p-region absorption coefficient:
     If(hbarw<=Egp)Then !then no photons are absorbed
        alpha_p = 0.
```

```
      Else !photons have sufficient energy
         alpha_p =1.D5*DSQRT(Aalpha_p*(hbarw -
&         Egp)+Balpha_p*(hbarw-Egp)*(hbarw-Egp))
      End if
      If(ii==1)then !(alpha_p is independent of x)
         Write(23,*)hbarw,',',alpha_p
      Else
      End if

      If(ii==1)then !x = 0 and p. flux = PhotonFlux
        Write(40,*)hbarw,',',PhotonFlux*DEXP(-alpha_p*x)
      Else
      End if
      If(ii==endP(i))then !x = x1
      Write(41,*)hbarw,',',x,',',x1,',',PhotonFlux*DEXP(-alpha_p*x)
      Else
      End if

      !integrate alpha_i(x,hbarw) for this one hw over the current
      !         x interval:
      SumTemp = 0. !initialize integration variable
      Do iii = 1,ii !integrate over x (indexed by ii):
          SumTemp =  SumTemp + dx*alpha_i(iii,i) !integrate
       End do
       If((x1+xi)<=x.AND.x<=(x1+xi+dx))Then
          !write for one iteration of x for observation of data:
          Write(24,*)x,',',hbarw,',',SumTemp
       Else
       End if

       !calculate n-region absorption coefficient (function of
       !          hbarw only):
       alpha_n = 1.D5*DSQRT(Aalpha_n*(hbarw -
&           Egn)+Balpha_n*(hbarw-Egn)*(hbarw-Egn))
       If(ii==1)then !(alpha_n indep. of x)
          Write(27,*)hbarw,',',alpha_n
       Else
       End if
```

```
      !p-region gen. rate integration:
      !   (final value will be Gp(x) for all hbarw)
      If(0.<=x .AND. x<=x1)Then
         Gtemp = Gtemp+ dhbarw*alpha_p*PhotonFlux*DEXP(-alpha_p*x)
         GpTemp=GpTemp+ dhbarw*alpha_p*PhotonFlux*DEXP(-alpha_p*x)
         y = yp
      !i-region gen. rate integration:
      !  (final value will be Gi(x) for all hbarw)
      Else if(x1<x .AND. x<=(x1+xi))then
         Gtemp = dhbarw*alpha_i(ii,i)*PhotonFlux*DEXP(-alpha_p*x1)
&                  *DEXP(-SumTemp) + Gtemp
         GiTemp =dhbarw*alpha_i(ii,i)*PhotonFlux*DEXP(-alpha_p*x1)
&                  *DEXP(-SumTemp) + GiTemp
         y = ((yn-yp)/xi)*x+yp-((yn-yp)/xi)*x1
      !n-region gen. rate integration:
      !   (final value will be Gn(x) for all hbarw)
      Else if((x1+xi)<x .AND. x<=(x1+xi+x2))Then
         Gtemp = dhbarw*alpha_n*PhotonFlux*DEXP(-alpha_p*x1)*
&          DEXP(- alphaT(i))*DEXP(-alpha_n*(x-x1-xi))+Gtemp
         GnTemp =dhbarw*alpha_n*PhotonFlux*DEXP(-alpha_p*x1)*
&          DEXP(- alphaT(i))*DEXP(-alpha_n*(x-x1-xi))+GnTemp
         y = yn
      Else
      End if
      If(ii==endPIN)Then !calculate p. flux leaving n-region
         PhotonFluxEnd = PhotonFlux*DEXP(-alpha_p*x1)*
&                        DEXP(-alphaT(i))*DEXP(-alpha_n*x2)
         Write(43,*)x,',',hbarw,',',PhotonFluxEnd
         !integrate p. flux leaving n-region:
         PFEIntegrated = PFEIntegrated+dhbarw*PhotonFluxEnd
      Else
      End if
      If(dark==1)then !if solar cell is not illuminated
         Gtemp=0. !no photon induced generation occurs
      Else
      End if
      If(ii==1)then !for one x write Gtemp to observe data
         Write(29,*)hbarw,',',Gtemp
      Else
```

```
     End if

     hbarw = hbarw + dhbarw !increment photon energy
End do !end hbarw loop indexed by i (we are still in x loop)

!Assign p-Region gen. rate to an array and write to a file:
If(0.<=x .AND. x<=x1)Then
  jj = jj+1 !start array index at 1
   If(dark==1)then !if solar cell is not illuminated
       GpTemp = 0. !no photon induced generation occurs
   Else
   End if
   G_x_pRegion(jj) = GpTemp  !put GpTemp in array
   Write(65,*)x,',',jj,',',G_x_pRegion(jj)
Else
End if

!Write i-Region gen. rate to file:
 If(x1<x .AND. x<=(x1+xi))Then
      If(dark==1)then !if solar cell is not illuminated
         GiTemp = 0. !no photon induced generation occurs
      Else
      End if
      Write(57,*)x,',',ii,',',GiTemp
 Else
 End if

 !Assign n-Region G(x) to an array and write to file:
 If((x1+xi)<x .AND. x<=(x1+xi+x2))then
  kk = kk+1 !begin index at 1
   If(dark==1)then
     GnTemp = 0.
   Else
   End if
   G_x_nRegion(kk) = GnTemp  !array to hold GnTemp
   Write(66,*)x,',',kk,',',G_x_nRegion(kk)
 Else
 End if
```

```
  G_x(ii) = Gtemp ! final Gtemp is gen. rate for entire cell
  Write(51,*)x,',',y,',',G_x(ii)

  !integrate gen. rate over entire cell:
  GtempIntegrated = GtempIntegrated + dx*Gtemp
  !integrate gen. rate in p-region only:
  GTIp = GTIp + dx*GpTemp
  !integrate gen. rate in i-region only:
  GTIi = GTIi + dx*GiTemp
  !integrate gen. rate in n-region only:
  GTIn = GTIn + dx*GnTemp

x = x+dx  !increment x
End do !end x loop (indexed by ii)

If(dark==1)Then !if solar cell is not illuminated
   Ji = 0. !no photon induced i- or deplet. reg. current exists

Else !solar cell is illuminated
    Do i = 1,PointsV !dep. reg. are dependent on voltage
       GTIprime = 0. !intialize
       x = 0. !start at p-region surface
       Do ii = 1,endPIN
          If(xpprime(i)<x .AND. x<=(x1+xi+delxn(i)))then
            !we are within the deplet. and i-regions
            !integrate gen. rate in this region:
            GTIprime = GTIprime + dx*G_x(ii)
          Else
          End if
          x = x+dx !increment x (indexed by ii)
       End do
       Ji_V(i) = -q*GTIprime !calculate current in this region
       Write(63,*)V,',',GTIprime,',',delxn(i),',',Ji_V(i)
       V = V+dV !increment voltage
    End do
End if

!Calculate minority carrier profiles=============================:
!p-region calculations:
```

```
Term = -Dn*2./(dx*dx) - 1./Tn!Thomas Algorithm(TA) matrix element.
PlusTerm = Dn/(dx*dx)!TA matrix element
MinusTerm = PlusTerm

!TA Decomposition and Forward Substituion steps:
V = Vinitial
Do ii = 1,PointsV
   endPI = endP(ii) +endI(ii) !incremental width of (p+i) region.
   !Set TA solution array:
   Do i = 1,endP(ii)-2 !don't use now: G(0), G(x1).
      G(i) = -G_x_pRegion(i+1) !TA solution array (aka [d]).
   End do

   TermMod(1) = Term !set TA modified 'Term' matrix element array
   GMod(1) = G(1)-MinusTerm*Bcn0 !set TA modified 'G () '

   Do i = 2,endP(ii)-2
      MinusTermMod = MinusTerm/TermMod(i-1)!TA modified term
      TermMod(i) = Term-MinusTermMod*PlusTerm !TA modified term
      If(i==endP(ii)-2)then
          !TA modified term:
          GMod(i)=(G(i)-PlusTerm*BcnX1(ii))-MinusTermMod*GMod(i-1)

      Else
          GMod(i) = G(i)-MinusTermMod*GMod(i-1)! TA modified term
      End if
      If(ii==Check)then
         Write(54,*)i,',',TermMod(i)!to observe sample of results
         Write(52,*)i,',',GMod(i)!to observe sample of results
      Else
      End if
   End do

  !Thomas Algorithm Back Substitution step:
  !(The TempArray() is used to hold the solutions for DeltaN(x=dx)
  !    through DeltaN(x=x1-dx) where DeltaN() refers to the
  !    excess minority carrier electrons (e-) in the p-region.)
  TempArray(endP(ii)-2) = GMod(endP(ii)-2)/TermMod(endP(ii)-2)
  Do i = endP(ii)-3,1,-1
```

```
   TempArray(i) = (GMod(i)-PlusTerm*TempArray(i+1))/TermMod(i)
   If(ii==Check)then !write for specific voltage
      Write(55,*)i,',',TempArray(i)
   Else
   End if
End do

!Put solution in an array including the 2 boundary conditions
!   Delta(x=0) and Delta(x=x1):
DeltaNintegral = 0. !intialize DeltaN integration variable.
Do i = endP(ii),1,-1
   If(i==endP(ii))then
      DeltaN(i)=BcnX1(ii)!excess min. car. electrons at x = x1.
   Else if(i==1)then
      DeltaN(i) = Bcn0 !"" at p-reg. surface (x = 0).
   Else
      DeltaN(i) = TempArray(i-1) !set to TempArray solution.
   End if
   If(ii==Check)then !collect DeltaN() for a specific voltage
        Write(70,*)i,',',V,',',DeltaN(i)
   Else
   End if
   If(i==endP(ii))then
      DeltaNx1V(1,ii) = BcnX1(ii) !used in current density calc.
   Else if(i==endP(ii)-1)then
      DeltaNx1V(2,ii) = TempArray(i-1) !""
   Else
   End if
   If(i==1)then
      DeltaN0(1,ii) = Bcn0 !""
   Else if (i==2)then
      DeltaN0(2,ii) = TempArray(1)!""
   Else
   End if
   !integrate to find total excess min. car. e- in p-region.
   DeltaNintegral = DeltaNintegral + dx*DeltaN(i)
 End do  !end x loop (indexed by i).

 If(ii==Check)then !for specific voltage.
```

```
      !write DeltaN(x) starting with x = 0 instead of x = x1:
      x = 0.
      Do i = 1,endP(ii)
         Write(47,*)V,',',i,',',x,',',DeltaN(i)
         x = x+dx
      End do
    Else
    End if
    !calculate minority carrier electron diffusion current density:
    JnGen(ii)=q*Dn*(DeltaNx1V(1,ii)-DeltaNx1V(2,ii))/dx
    Write(80,*)ii,',',V,',',JnGen(ii)

    V = V+dV !increment voltage
End do !end voltage loop (indexed by ii)

Do i = 1,ii-2
  If(JnGen(i)>0.)then
    !calculate semilong plot current density slope:
    slope = (DLOG(JnGen(i))-DLOG(JnGen(i-1)))/dV
  Else
    slope = 0.!can only calculate slope when JnGen>0.
  End if
  Write(82,*)i,',',slope
End do

!-------------------------------------------------------------------
!n-region calculations:
! (calculations and variables are analogous to those of p-region.)

Term = -Dp*2./(dx*dx) - 1./Tp
PlusTerm = Dp/(dx*dx)!aka g,gamma.
MinusTerm = PlusTerm! can remove this variable if desired.
V = Vinitial !reinitialize V

!Thomas Algorithm Decomposition and Forward Substition steps:
Do ii = 1,PointsV
   endPI = endP(ii)+endI(ii)
   Do i = 1,endN(ii)-2
      G(i) = -G_x_nRegion(endN(ii)-i)!turning the n-region G(x)
```

```
    !    array around to work with and making negative.
    Write(71,*)i,',',G(i)
End do
TermMod(1) = Term !first time only   !aka f,beta.
GMod(1) = G(1)-MinusTerm*Bcp0 !first time only  !aka r,b.
Do i = 2,endN(ii)-2
   MinusTermMod = MinusTerm/TermMod(i-1)
   TermMod(i) = Term-MinusTermMod*PlusTerm
   If(i==endN(ii)-2)then
      GMod(i)=(G(i)-PlusTerm*BcpX2(ii))-MinusTermMod*GMod(i-1)
   Else
      GMod(i) = G(i)-MinusTermMod*GMod(i-1)
   End if
   If(ii==Check)then
     Write(56,*)V,',',i,',',GMod(i)
   Else
   End if
 End do

!Thomas Algorithm Back Substitution step:
!The TempArray() is used to hold the solutions for
!    DeltaP(xprime=dx) through DeltaP(xprime=x2-dx) where DeltaP
!    is the excess min. carrier hole concentration in n-region.
TempArray(endN(ii)-2) = GMod(endN(ii)-2)/TermMod(endN(ii)-2)
Do i = endN(ii)-3,1,-1
   TempArray(i) = (GMod(i)-PlusTerm*TempArray(i+1))/TermMod(i)
   If(ii==Check)then
      Write(53,*)i,',',TempArray(i)
   Else
   End if
End do

!To obtain the entire solution, we also want to include the 2
!  boundary conditions DeltaP(x=x1+xi+x2) and Delta(x=x1+xi):
DeltaPintegral = 0. !intialize
Do i = endN(ii),1,-1
   If(i==endN(ii))then
      DeltaP(i)=BcpX2(ii)
   Else if(i==1)then
```

```
      DeltaP(i) = Bcp0
   Else
      DeltaP(i) = TempArray(i-1)
   End if
   If(ii==Check)then
       Write(72,*)i,',',DeltaP(i)
   Else
   End if
   If(i==endN(ii))then
     DeltaPx2V(1,ii) = BcpX2(ii)
   Else if(i==endN(ii)-1)then
     DeltaPx2V(2,ii) = TempArray(i-1)
   Else
   If(i==1)then
      DeltaP0(1,ii) = Bcp0
   Else if (i==2)then
      DeltaP0(2,ii) = TempArray(1)
   Else
   End if
   End if
   DeltaPintegral = DeltaPintegral + dx*DeltaP(i)

End do  !end x loop (indexed by i).

If(ii==Check)then
   !write DeltaP(x) starting with x = 0 instead of x = x1:
   Do i = 1,endN(ii)
      Write(48,*)V,',',i,',',DeltaP(i)
   End do
Else
End if
JpGen(ii) = q*Dp*(DeltaPx2V(1,ii)-DeltaPx2V(2,ii))/dx
Write(81,*)ii,',',V,',',JpGen(ii)

If(dark==1)then !redudant.
  JTotalPhoto(ii) = JnGen(ii)+Jrg(ii)+JpGen(ii)
  JTotalTotal(ii) = JnGen(ii)+JpGen(ii)
  JTotalDark(ii) = Jrg(ii)
Else !find total current density
```

```
    JTotalPhoto(ii) = JnGen(ii)+Ji_V(ii)+Jrg(ii)+JpGen(ii)
  End if
  Write(87,*)V,',',JTotalPhoto(ii)

  !Calculate power. (JTotalPhoto is total current for
  !  both dark and light conditions that is, for dark conditions
  !  it is actually total dark current and for light conditions it
  !  includes dark current contributions):
  Power(ii) = JTotalPhoto(ii)*V
       Write(95,*)ii,',',V,',',Power(ii)

  V = V+dV
End do !end V loop (indexed by ii).

!Find derivative of power:
V = Vinitial
Do i = 2,PointsV
   dPower(i-1) = (Power(i)-Power(i-1))/dV
   Write(94,*)i-1,',',Power(i-1),',',V,',',dPower(i-1)
   V = V+dV
End do

!Find max power point:
j = 0  !what's this for?
V = Vinitial+dV
Do i = 1,PointsV-1
   If(dPower(i)*dPower(i+1)<0.)then
      MaxPower = ((Power(i+1)-Power(i))/dV)*((V+V+dV)/2.)+
&        Power(i+1)-((Power(i+1)-Power(i))/dV)*(V+dV)
      Print*,'Max Power = ',MaxPower
      Print*,'Max power/hwphiIntegrated*q = '
      Print*,'    ',-MaxPower/(hwPhiIntegrated*q)
      Print*,'hwphiIntegrated*q =',hwphiIntegrated*q
      MaxPowerVoltage = (V+V+dV)/2.
      Print*,' Max Power point voltage = ',MaxPowerVoltage
      MaxPowerCurrent = ((JTotalPhoto(i+1)-JTotalPhoto(i))/dV)*
&       ((V+V+dV)/2.)+ JTotalPhoto(i+1)-((JTotalPhoto(i+1)-
&       JTotalPhoto(i))/dV)*(V+dV)
      Print*,'Max power point current = ',MaxPowerCurrent
```

```
   Else
   End if
   V = V+dV
End do


!Open circuit voltage occurs when total current is zero;
!  estimate this voltage by determining when total current changes
!  from negative to positive and then find an average value
!  between the negative and positive point:
V = Vintitial
Do i = 1,PointsV
   If(JTotalPhoto(i)*JTotalPhoto(i+1)<0.)then
      Voc = (V+V+dV)/2.  ! i.e (V+(V+dV))/2
      Print*,'Open Circuit Voltage = ',Voc
   Else
   End if
   V = V+dV
End do

!Short circuit current density is the current when voltage applied
!  is zero; when initial voltage is zero this current is the first
!  element in the current array:
V = Vinitial
Do i = 1,PointsV
   If(V==0.)then
      Jsc = JTotalPhoto(i)
      Print*,'Jsc = ',Jsc
   Else
   End if
  V = V+dV
End do

!Calculate Fill factor:
FillFactor = MaxPower/(Voc*Jsc)
Print*,'Fill Factor = ',FillFactor
Print*,'Jm*Vm = ',MaxPowerCurrent*MaxPowerVoltage
!compare calculation methods:
FillFactor = (MaxPowerVoltage*MaxPowerCurrent)/(Voc*Jsc)
```

```
Print*,'Fill Factor = ',FillFactor,' Using Jm*Vm'

!Calculate slope of DLOG(J) vs. V:
Do i = 1,ii-1
  If(JpGen(i)>0.)then
    slope = (DLOG(JpGen(i))-DLOG(JpGen(i-1)))/dV
  Else
    slope = 0.
  End if
  Write(83,*)i,',',slope
  slope = (DLOG(JTotalDark(i))-DLOG(JTotalDark(i-1)))/dV
  Write(90,*)i,',',slope
  slope = (DLOG(JTotalPhoto(i))-DLOG(JTotalPhoto(i-1)))/dV
  Write(91,*)i,',',slope
  slope = (DLOG(JTotalTotal(i))-DLOG(JTotalTotal(i-1)))/dV
  Write(93,*)i,',',slope
End do

Print*,'Calculations:'
Print*,'G(x) integrated = ',GtempIntegrated
Print*,'PhotonFlux(x=0) integrated = ',PhotonFluxIntegrated
Print*,'(G(x) integrated)/(PhotonFlux(x=0) integrated) = '
Print*,GtempIntegrated/PhotonFluxIntegrated
Print*,'Integrated PhotonFlux @ end of n-region = ',PFEIntegrated
Print*,'PhotonFlux @x=0 - @end of n-region = '
Print*,PhotonFluxIntegrated - PFEIntegrated
Print*,'Integrated Gp(x) value = ',GTIp
Print*,'Integrated Gi(x) value = ',GTIi
Print*,'Integrated Gn(x) value = ',GTIn
Print*,'Gp(x)+Gi(x)+Gn(x)=G(x)?It should!... = ',GTIp+GTIi+GTIn
Print*,'dx = ',dx

End subroutine

!_________________________________________________________________
Subroutine coefficients

Double precision y,Balpha,Aalpha
```

```
Common /c_y / y
Common /c_Aalpha/ Aalpha
Common /C_Balpha/ Balpha

If(y >= 0. .AND. y <= 0.5)then
  Balpha = 2.25092*y-0.6571
  Aalpha = -6.0169*y+3.52417
Else if(y > 0.5 .AND. y <= 0.57)then
  Aalpha = 1.32486*y-0.14571
  Balpha = 2.19229*y-0.627785
Else if(y > 0.57 .AND. y <= 0.69)then
  Aalpha = -0.2365*y+0.744265
  Balpha = 0.393333*y+0.39762
Else if(y > 0.69 .AND. y <= 0.83)then
  Aalpha = 0.620571*y+0.152886
  Balpha = 0.141714*y+0.571237
Else if(y > 0.83 .AND. y <= 2.)then !2 to be safe
  Aalpha = 0.167412*y+0.529008
  Balpha = -1.343*y+1.80355
Else
End if

End subroutine
```